UNIVERSITY OF VALLADOLID
School of Industrial Engineering
Department of Systems Engineering and Automation

DOCTORAL THESIS

MPC-BASED ENERGY MANAGEMENT SYSTEM FOR HYBRID RENEWABLE ENERGIES

by

Johanna Carolina Salazar Salas

Supervisors:

Dr. Fernando Tadeo
Dr. Cesar de Prada

Thesis submitted to the University of Valladolid in partial fulfillment of the requirements for the doctoral degree.

September 2015

Acknowledgements

La presente tesis doctoral no es más que la suma de la paciencia, dedicación y colaboración de un gran número de personas. Por lo que tratar de enumerar en una página sus nombres resulta difícil si se considera la poca disponibilidad de papel que tenemos para dar con justicia todos los créditos y méritos a quienes se los merecen. Por tanto, quiero agradecerles a todos ellos cuanto han hecho por mí, para que este trabajo saliera adelante de la mejor manera posible.

Primeramente deseo agradecer a mis padres, mi abuela y mi hermano por su apoyo y comprensión, sin los cuales no hubiera podido realizar esta tesis doctoral. En especial agradezco a mi madre por animarme a dar mis primeros pasos en la investigación. Mi definición no es más que aquello que moldearon en mi infancia.

A Reyes, José, Laura y Diego por abrirme las puertas de su hogar. Agradezco los ánimos que me daban cada día para seguir en mi investigación.

A mis supervisores Fernando Tadeo y Cesar de Prada por aceptar la realización de esta tesis doctoral bajo su dirección, por su confianza en mi trabajo, por haberme facilitado siempre los medios suficientes para llevar a cabo todas las actividades propuestas durante el desarrollo de esta tesis, por solventar todas mis dudas referentes al campo de la automática, por su capacidad en guiar mis ideas y prestarme las suyas.

Agradezco a todos mis compañeros y amigos del Departamento de Ingeniería de Sistemas y Automática en la Universidad de Valladolid y del CTA con los cuales he compartido despacho e incontables horas de trabajo: Alvaro Serna, Daniel Navia, Diego Napp, Elena Gomez, Imene Yahyaoui, Ines Zaidi, Luis Palacin, María Pereda, Meriem Nachidi, Mohamed Bolajraf y Ruben Martí. En especial a Miguel Rodríguez y Daniel Sarabia por su disponibilidad y paciencia que hizo que nuestras discusiones redundaran benéficamente tanto a nivel científico como personal.

También me complace reconocer la acogida, el apoyo y los medios recibidos en los distintos centros donde he desarrollado parte de mi Doctorado: el Proyecto Open Gain, el Departamento de Ingeniería de Electrónica y Computación en la Universidad de Limerick, el Departamento de Lenguajes y Computación en la

Universidad de Almería, la Plataforma Solar de Almeria; y el Departamento de Ingeniería de Sistemas y Automática en la Universidad de Sevilla.

Agradezco a todos mis compañeros y amigos del Proyecto Open Gain: Kamilia Ben Youssef y Sami Karaki, del Departamento de Ingeniería de Electrónica y Computación en la Universidad de Limerick: Martin Hayes, Kritchai Witheephanich, Anthony Fee y Juan Manual Escaño; del Departamento de Lenguajes y Computación en la Universidad de Almería: Manuel Pasamontes, Francisco Rodríguez, José Domingo Álvarez, María del Mar Castilla, Sabrina Rosiek, Helton Scherer y Ricardo Silva; de la Plataforma Solar de Almeria: Lidia Roca; del Departamento de Ingeniería de Sistemas y Automática en la Universidad de Sevilla: Carlos Bordons y Luis Valverde.

A las siguientes instituciones que contribuyeron a financiar este trabajo:

- Ministerio de Educación y Ciencia, programa de becas de formación del profesorado universitario (FPU) referencia Nº AP2008-03557.
- Proyecto Singular Estratégico sobre Arquitectura Bio-Climática y Frío Solar, PSE_Arfrisol PS-120000-2005-1.
- Beca de Estancia Breve de la Universidad de Valladolid.

Finalmente, y por encima de todo, tengo que agradecer a Pablo por apoyarme cada día. A él le debo parte de esta tesis, y aunque no pueda incluir su nombre como autor, sinceramente debo confesar su participación.

Abstract

Environmental pollution and the gradual depletion of conventional energy have induced significant research in energy supply systems equipped with renewable and conventional sources. Although wind and solar energy sources emerge as the most promising renewable energies, a supply system comprising two or more sources is recommended to fulfill local loads, as the power generated by renewable sources depends on weather conditions. For this, storage devices are frequently used to store the excess energy generated by the renewable sources and conventional energy sources are used as backup when the production of renewable energies is low and the energy stored is not enough to fulfill the load.

The main idea of any energy supply system is to fulfill the energy demand with the minimum cost, considering the operational constraints related to the components. As a result, some issues, such as security of supply, improvement in the combination of energy sources, efficiency, energy saving, improvement in access to isolated systems, and the development of renewable energy, should all be taken into account.

Up to now, cost reduction and energy saving have been understood almost exclusively as the technological improvement of renewable sources: wind turbines, solar panels, solar collectors, etc. The misconception of "the best system is made with the best components" is still used for the design of energy supply systems. An optimum system is typically more complex than the sum of the components which integrate the system. Technological advances in renewable sources should be coupled with a sophisticated energy management system.

This thesis proposes an energy management system based on control ideas. From a control point of view, the main difficulty is their dynamics, defined according to differential equations and logic rules. Therefore, in this thesis, the design of a hybrid controller based on predictions of energy, estimated from physical models and previous measurements, is considered in order to satisfy the energy supply.

Model Predictive Control (MPC) has been chosen as the main control strategy since it is able to handle variations in the supply of renewable energy; while, in the energy demand, MPC includes a cost function to be minimized and adds the

constraints on the manipulated and controlled variables. The cost function takes into account the value of the energy generated, the cost of storing energy locally, and the aging of the components.

A process model that represents the process dynamic is used to predict the output signal accurately. It is selected to be simple because the future control actions computed by the optimizer take into account the integration of the model along the prediction horizon.

Hybrid process models are then considered in the proposed MPC. Although this gives formulation problems, Mixed Logical Dynamic (MLD) involves continuous variables (involved in linear dynamic equations), discrete variables (specified through propositional logic statements), and the mutual interaction between the two. In this case, the resulting mixed integer quadratic programming (MIQP) could present problems for real time implementation, because the solution is computationally complex and depends exponentially on the number of binary manipulated variables. To simplify the MPC problem, the use of binary manipulated variables is avoided by the parameterization of the binary manipulated variables into continuous variables. This transforms the mixed integer optimization into a nonlinear optimization made up of only by continuous manipulated variables (NMPC).

To illustrate the applicability and effectiveness of the proposed predictive control, four energy supply systems have been considered: a Solar and Wind based Microgrid for Desalination, a Solar Gas Air Conditioning Plant, a Hydrogen based Microgrid, and a Solar Desalination Plant. The study and applicability of these energy supply systems will be carried out throughout the different chapters.

The proposed algorithms are demonstrated in detail using simulations of existing systems, and are partially validated in these systems. The implementation has been done as a modular structure to facilitate changes. Additionally, a library on microsources of renewable energies has been developed in EcosimPro©, as it is a powerful modeling and simulation tool that follows an advanced methodology for modeling and dynamic simulation. The renewable energy library facilitates the training of technicians and engineers in how to operate energy supply systems, how to check different configurations and control strategies, before implementing them, and how to facilitate their design.

Contents

List of Figures

List of Tables

Glossary

ARX	***A**uto**R**egressive Model with e**X**ternal input*
CARIMA	***C**ontrolled **A**uto**R**egressive **I**ntegrated **M**oving **A**verage*
CIESOL	***C**entro Mixto de **I**nvestigación de la **E**nergía **SOL**ar*
CSI	***C**urrent **S**ource **I**nverter*
DER	***D**istributed **E**nergy **R**esource*
DMC	***D**ynamic **M**atrix **C**ontrol*
DTC-GPC	***D**ead-**T**ime **C**ompensator **G**eneralized **P**redictive **C**ontroller*
EPSAC	***E**xtended **P**rediction **S**elf **A**daptive **C**ontrol*
FSP	***F**iltered **S**mith **P**redictor*
GPC	***G**eneralized **P**redictive **C**ontrol*
IDCOM	***M**odel **P**redictive **H**euristic **C**ontrol*
IMC	***I**nternal **M**odel **C**ontrol*
MIPC	***M**ixed **I**nteger **P**redictive **C**ontrol*
MHL	***M**etal **H**ybrid **L**evel*
MPC	***M**odel **P**redictive **C**ontrol*
MPPT	***M**aximum **P**ower **P**oint **T**racking*
NLP	***N**onlinear **P**rogramming*
NMPC	***N**onlinear **M**odel **P**redictive **C**ontrol*
NOCP	***N**onlinear **O**ptimal **C**ontrol **P**roblem*
NOCT	***N**ominal **O**peration **C**ell **T**emperature*
OPC	***O**pen **P**rocess **C**ontrol*
OPEN-GAIN	***Op**en Process Control Optimal **En**gineering Design for Dependable Water and Power **G**eneration in Remote **A**reas using renewable energies and **In**telligent Automation*
PEM	***P**roton **E**xchange **M**embrane*
PFC	***P**redictive **F**unctional **C**ontrol*
PI	***P**roportional **I**ntegral controller*
PMSG	***P**ermanent **M**agnet **S**ynchronous **G**enerator*
PV	*Photovoltaic Panels*
PWM	***P**ulse **W**idth **M**odelation*

RO	***R**everse **O**smosis*
SCADA	***S**upervisory **C**ontrol **A**nd **D**ata **A**cquisition*
SQP	***S**equential **Q**uadratic **P**rogramming*
STC	***S**tandard **T**est **C**onditions*
SVM	***S**pace-**V**ector **M**odulation*
VSI	***V**oltage **S**ource **I**nverter*
WTs	***W**ind **T**urbine **S**ystem*

CHAPTER 1

Introduction

The standard of living is being affected by a variety of far-reaching changes: technological development, globalization, accelerated innovation, new economic order, etc. If the industrial revolution was characterized by significant changes in the production systems and the 20th century was identified by mobility and communications, the coming years will be defined by the development of new technologies and their application to different fields.

Two different visions are present in the interaction between new technologies and the environment: one holds that nature will be destroyed if the interaction between humans and the environment does not change, and it points out that the current development model will lead to the destruction of the environment and, as a consequence, of humanity; the other defends the need of the current model for economic development as a condition of human evolution and believes that if the current model is stopped, it would be the end of the current civilization.

A third point of view arises within this situation of change, where people begin to be aware that scientific knowledge has improved the quality of life through material progress, but that, at the same time, it has brought serious problems related to the environment. In order to avoid this, economic development aims to be compatible with the protection of the environment in what is called sustainable development. Notice that the energy topic plays an important role within sustainable development.

The accelerated development of industrialized societies has been possible due to an intensive use of fossil fuels, which has led to an increase in environmental pollution and the development of dangerous phenomena such as global warming, acid rain, desertification, freshwater pollution or ozone fluctuation, all of which can cause serious damage to humans. For this reason, the world should base its policies on satisfying the energy demand with minimum cost, where conditions are able to ensure the supply and environmental protection. As a result, some issues, such as security of supply, improvement in the combination of energy sources, efficiency,

energy savings, improvement in access to isolated systems and the development of renewable energy, will all be considered in the coming years.

To sum up, a more effective use of fossil fuels and the search for a variety of energy sources is required to avoid dependency on the producing countries, damage to the environment and a quick depletion of fossil fuels. For this, renewable energies are being considered with great interest, looking to increase their efficiency and make them competitive with conventional systems.

Wind and solar sources are two of the most promising renewable power generation technologies. As the power generated by renewable energy sources depends on weather conditions when using them, it is recommended to combine some different renewable sources in the system. Additionally, the extra energy generated by the renewable sources should be stored in storage devices to cover the time periods of low power production by renewable sources.

An energy supply system comprising some renewable and conventional sources, together with a high level of automation, have caught the attention of research worldwide as it has a great potential to provide higher quality and more reliable power to customers than a system based on a single resource. These systems take advantage of the mutual complementarities between sources so that the capacity of the storage device is greatly reduced, while the economic performance and operating reliability of the overall system are improved.

However, the difficulty of combining two or more different energy sources makes the system more difficult to analyze and control due to the fact that their dynamic is defined according to differential equations and logic rules. Additionally, the required capacity of this storage unit progressively increases as more and more energy sources are connected to the system. So an efficient use of the energy stored in storage devices is essential.

In this thesis, the design of a control system has been considered to improve the efficiency of energy supply systems equipped with renewable and conventional energies. For this, a detailed study of some energy supply systems will be carried out over the different chapters.

1.1.- Objective

The objective of this thesis is to design advanced control systems that take full advantage of renewable energy sources and fulfill the operational constraints. For this, some supply systems equipped with conventional and renewable sources, such as diesel generator and wind turbine respectively, will be considered.

First, the thesis proposes a control strategy for Microgrids equipped with conventional energy sources (diesel generator), storage devices (battery banks and

hydride metal storage) and renewable energy sources (photovoltaic panels and wind turbines). The aim is to guarantee electric energy for the local loads by keeping a balance between the consumed power and the produced power in spite of possible disturbances (s. Figure 1.1 and Figure 1.2 for the two systems considered).

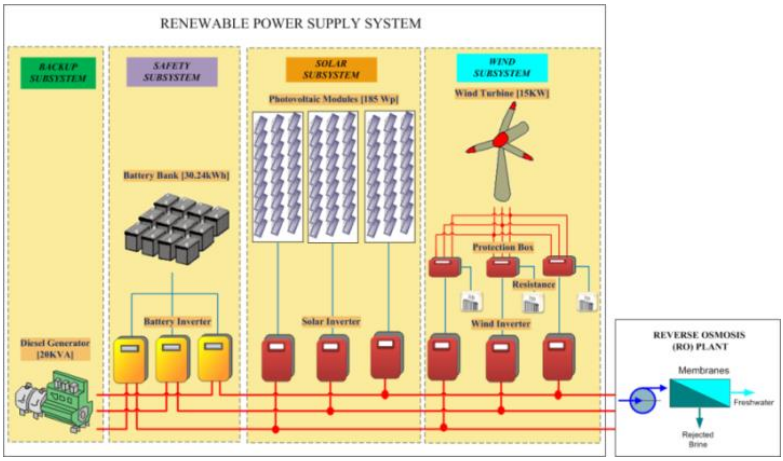

Figure 1.1.- Solar, Wind and battery based Microgrid

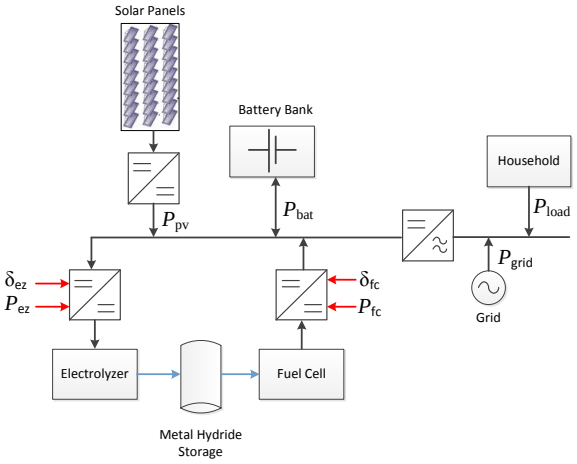

Figure 1.2.- Solar and Hydrogen - based Microgrid

The second system considered focuses on thermal energy with the aim of providing water flow within a specific range of temperatures. The heat supply system comprises solar collectors as the renewable energy source, a gas heater, and storage tanks to store the extra energy generated by the solar collectors (s. Figure 1.3).

In both cases, the main objective of the Energy Management System to be developed is to reduce the energy consumption from conventional energy sources, fulfill the operational constraints, not to decrease the lifetime of the installation, and ensure an efficient use of storage devices.

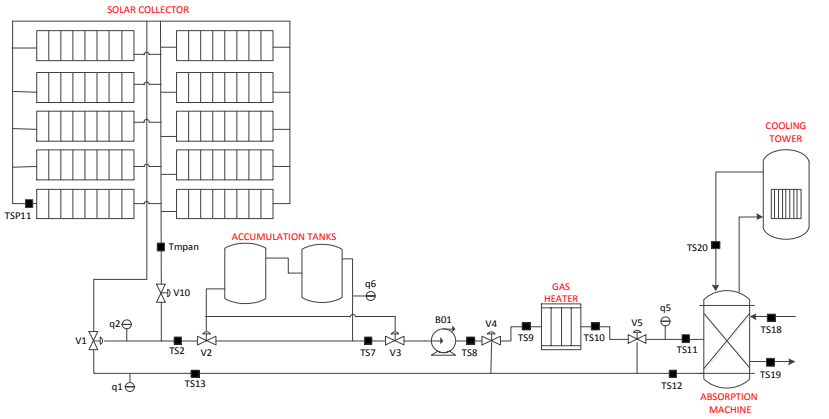

Figure 1.3.- Solar Gas Air Conditioning Plant

As is well known, storage devices are essential for the stable operation of the supply system. Considering traditional control strategy, the required capacity of this storage unit progressively increases as more and more energy sources are connected to the system. However, storage devices are expensive. As a result, one of the aims included in the proposed control is related to the efficient use of the energy stored in storage devices. Thus, the capacity of the storage unit does not depend on the number of energy sources connected to the systems.

Additionally, it is recommended that the proposed controller should be able to predict the dynamic behavior of the system, due to the short-term unreliability of the renewable energy sources, and it should be computationally simple for online implementation.

Model Predictive Control (MPC) has been chosen as it can handle variations in the supply of renewable energy and in the energy demand. It includes a cost function that can be written in economic terms, and operating constraints on the manipulated and controlled variables can be easily included in the control law. The process model must represent the process dynamic; it must predict the output signal with reasonable accuracy as well as being simple, because the future control actions computed by the optimizer take into account the integration of the model along the prediction horizon each sampling time.

For MPC implementation, the main difficulty in the mentioned energy supply systems is in describing their dynamics, as this corresponds to a combination of differential equations and logic rules, in what is called hybrid systems. The usual

approach for dealing with these hybrid process models, considered MPC, is the Mixed Logical Dynamic (MLD) framework, which allows the evolution of continuous variables to be specified through linear dynamic equations, the discrete variables to be specified through propositional logic statements, and the mutual interaction between both of them. As this optimization results in mixed integer quadratic programming (MIQP), it presents some problems for real time implementation, since the solution is computationally complex and depends exponentially on the number of binary manipulated variables. This limits the scope of application of MLD to very slow systems, since, for real time implementation, the sampling time would have to be large enough to allow the worst case computation. Thus, in this thesis, the hybrid MPC problem is transformed into a computationally simple problem which can be applied to the target systems.

1.1.1.- Electrical energy supply system

Most of the results on the control of wind and solar systems have focused on separate wind and solar systems. Specifically, there is a significant body of literature dealing with the control of wind-based energy generation systems (see, for example, Novak et al. [1], Chinchilla et al. [2] and Khan et al. [3] for results and references in this area), while several contributions have been made to the control of solar-based energy generation systems (see, for example, Johansen et al. [4], Camacho et al. [5] and Hamrouni et al. [6]). Currently, significant attention is being given to the development of supervisory control systems for hybrid generation systems that take into account maintenance and optimal operation considerations.

One solution focuses on the design of PI controllers to regulate the output power of each source with the aim of keeping the grid frequency close to the nominal value, considering that the grid frequency deviates for sudden changes in load or generation. However, the use of a conventional PI controller does not meet the requirements of robust performance. For this, a technique has been proposed to tune the controller gains using Particle Swarm Optimization (PSO) in Si et al. [7], or using gain scheduling techniques combined with fuzzy control (Kakigano et al., [8]).

In 2013, Keyrouz et al. presented a multidimensional MPPT controller to search for and maintain operation at the maximum power point for a distributed hybrid energy system based on the irradiance, temperature and wind speed. The controller is based on the fusion of two algorithms, namely the improved PSO and IncCond, using a Bayesian fusion. This novel fusion-based method was proved to be superior to a PSO-based technique and boosted the overall efficiency of the system, even under changing weather conditions (Keyrouz et al., [9]).

Additionally, Weiss presented a fuzzy control to perform the standard power insertion into the line on the principle of maximum tracking (Weiss et al., [10]).

The MPPT controller is only recommended for supply energy systems connected to the main grid, due to the fact that the controller always tries to achieve the maximum power of the renewable source (Hussein et al., [11]). As a result, if the supply energy system is connected to a specific load, the controller is not able to limit the output power of the renewable source when the storage devices are fully charged and an excess energy is presented.

In 2012, Zhang et al. introduced an energy management strategy based on power flow control for off-grid systems, with the aim of maintaining the state of charge (SOC) of the batteries within a certain range and avoiding over-discharge, over-charge and reducing the transitions between charge and discharge through power limitation of sources and loads (Zhand et al., [12]).

In 2011, Qi et al. proposed a supervisor predictive control system which coordinates the renewable sources as well as a storage device to provide enough energy to satisfy the power demand. In the supervisory MPC, a specific cost function is designed to take into account the desired control objective (Qi et al., 2011 [13]). The supervisory MPC optimizes the output power from renewable energy and tries to reduce short term charge and discharge cycles of the storage device. Considering all manipulated variables are continuous, the MPC problem results in a problem of nonlinear optimization with continuous variables (NMPC). Unfortunately, the studied supply energy system does not include a backup subsystem, such as a diesel generator; in consequence, when the renewable energy is not sufficient and the storage devices are empty, the load must be disconnected, which is not recommended.

Once again, in 2013, Qi et al. proposed a supervisory predictive control for a system made up of a wind subsystem, a solar subsystem and a battery bank associated to each renewable source (Qi et al., 2013 [14]). In this case, the energy supply system has the possibility of being connected to the main grid; as a result, it is not necessary to disconnect the load when the renewable energy is not sufficient and the batteries are empty. The centralized supervisory MPC controller, proposed above, is replaced with two distributed supervisory MPC controllers, each of which is responsible for providing optimal reference trajectories to the local controller of each corresponding subsystem. The distributed supervisory controllers are interconnected, so the measurements related to the wind/solar subsystem, the forecast of the future power demand and the weather forecast, are all available to both controllers.

1.1.2.- Thermal energy supply system

For solar thermal systems, most of the proposed control strategies focus on solar collector fields. In this case, the main control requirement is to maintain the outlet temperature of the collector field at a given value. However, this aim can only be achieved through mass flow adjustment, since the solar irradiation cannot be manipulated, and changes substantially during operation. As a result, significant

variations are presented in the dynamic characteristics of the field and a satisfactory performance is difficult to obtain with a linear controller of fixed parameters.

A self-tuning controller for a solar distributed collector field, based on a pole assignment approach which employs serial compensation to cope with measurable external disturbance, was presented by Camacho et al. [15]. Self-tuning control offers an approach by which the controller parameters of the model can be adjusted during operation to compensate for changes in the dynamic characteristics of the field and thereby maintain the desired control performance.

Pickhardt et al. [16] proposed a nonlinear control based on predictive control with a mathematical input-output model of the plant, which was used for the distributed collector field of a solar power plant. The proposed controller is considered an indirect adaptive controller, since the model could change at every sampling instant. The nonlinear model adopted was assumed to be one of a "time invariant" nature.

Henriques et al. [17] proposed a hierarchical control strategy based on a PID with a fuzzy logic switching supervisor. The supervisor was derived to implement the on-line switching between each PID controller, according to the measured conditions. The local PID controllers have been previously tuned off-line, using a neural network approach that combines a dynamic recurrent non-linear neural network model with a pole placement control design. A c-Means clustering technique was applied to reduce the number of local controllers.

Johansen et al. [18] proposed and tested a control strategy based on switching between multiple local linear models/controllers. For this, the application of gain-scheduled control was tested in a pilot-scale solar power plant. It was shown that the gain-scheduling can effectively handle plant nonlinearities, using high-order local linear ARX models that form the basis for the design of local linear controllers using pole placement.

Stirrup et al. [19] proposed a control scheme that employed a fuzzy PI controller with feed forward for the highly nonlinear part of the operating regime, and gain scheduling control over the linear part of the operating envelope.

Johansen et al. [4] proposed a control scheme based on a PID with time varying nonlinear gain, together with a feed forward controller. In this case, the internal energy was used as feedback instead of the outlet temperature of the solar collector. It was shown that the dynamics of the internal energy are simple compared to the dynamics of the outlet temperature.

Stirrup et al. [20] proposed a hybrid controller for a solar thermal power plant using a gain scheduled controller with feed forward to control the more linear operating regimes and a fuzzy PI incremental controller for the highly nonlinear operating region of the plant.

Farkas et al. [21] developed a simplified physically-based model on the basis of energy balances, including solar irradiation as an input, using heat transferred by the flow of the water as a working medium, and overall heat loss from the plant. Average outlet temperature of the collector field is the reference value. A robust internal model-based controller IMC was applied for temperature control.

Another thermal energy supply system considered in the literature comprises renewable and conventional energies, given by a solar collector field and a gas heater. Additionally, difficulties arise from the presence of discretely switched valves and continuous manipulated variables, which make it a hybrid system. The main control goal for this process is to minimize the consumption of auxiliary energy while ensuring a safe and robust operation, even in the face of large disturbances.

Engell [22] presented a supervisory control scheme that switches the discrete inputs of the solar plant according to logic conditions defined over the measurements of process variables. In each mode, the continuous inputs are set to constant values that ensure a safe process operation, while keeping the energy losses to the environment small and minimizing the consumption of auxiliary energy.

Zambrano et al. [23] proposed a hierarchical structure composed of two main levels, namely the configuration and the regulatory control levels. The configuration level selects the operating mode by means of minimizing a linear function with variable weights. The weights assigned depend on the current state of the plant and on the weather conditions, while the regulatory control level adjusts the variables of the process related to each operating point by using model predictive control in several structures of control loops.

Rodríguez et al. [24] developed a model predictive control strategy with the aim of dealing with the mixed discrete-continuous nature of the process. For this, an internal model with embedded logic control is used to transform the hybrid problem into a continuous-nonlinear problem, so NMPC can be applied.

1.2.- Model Predictive Control (MPC)

Predictive Control refers to a set of control methods which use a process model to obtain the sequence of future control signals by minimizing an objective function. These control methods have basically the same structure and the same elements: they use a process model to predict the output signals, computing a control signal sequence by minimizing an objective function, and they use a receding strategy, where the horizon is moved toward the future at each sampling time and only the first control signal of the sequence computed at each step is applied. These control methods differ amongst themselves in the model structure used to represent the process, the noises and the cost function to be minimized.

The methodology of Predictive Control methods is characterized by the following strategy, shown in Figure 1.4, (Camacho et al., [25], Keyser, [26]):

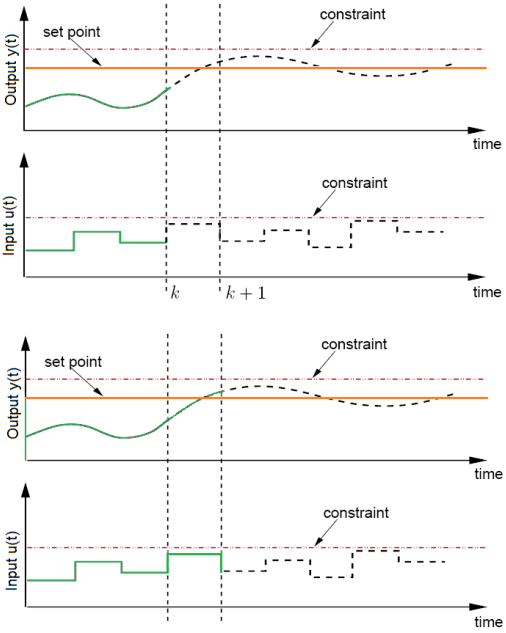

Figure 1.4.- MPC Strategy

1) The future outputs of the process $\hat{y}(t+k|t)$ for a specific horizon N are predicted at each sampling time t, considering the process model, the known inputs and outputs, and the future control signals $u(t+k|t)$.

2) The sequence of future control signals $u(t+k|t)$ is computed by optimizing a cost function defined to keep the process as close as possible to the reference trajectory $\omega(t+k)$. This function usually takes the form of a quadratic function of the differences between the predicted output signal and the reference trajectory. An explicit solution can be obtained if the function cost is quadratic, the model is linear and there are no constraints. An iterative optimization method can alternatively be used.

3) The first control signal of the sequence computed at each sampling time $u(t|t)$ is sent to the process. A new control signal sequence $u(t+1|t+1)$ will be computed at the next instant: the control signal $u(t+1|t+1)$ might be different from the $u(t+1|t)$, as it considers the new information available, such as the measured output $y(t+1)$.

The structure shown in Figure 1.5 is used to implement the algorithm. Notice that a process model is used to predict the future outputs, based on the known past

and current values and the future control actions. These actions are computed by the optimizer based on the cost function and the constraints. To do so, the internal model must adequately represent the process dynamics; it must predict the output signal accurately, as well as being simple.

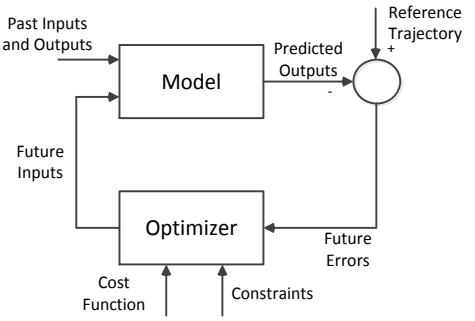

Figure 1.5.- MPC Strategy

Predictive Model

Computing the predicted output at future instants $\hat{y}(t+k|t)$ requires a process model. There are a variety of methodologies to obtain this model. Thus, considering the model structure, some control methods can be distinguished: Dynamic Matrix Control (DMC) (Cutler et al., [27]), Model Predictive Heuristic Control (IDCOM) (Richalet et al., [28]), Predictive Functional Control (PFC) (Richalet et al., [29]), Extended Prediction Self Adaptive Control (EPSAC) (Keyser et al., [30]) and others.

Objective Function

In Predictive Control, the aim is that the future outputs $\hat{y}$ follow a determined reference signal ω during the considered horizon without excessive control efforts $\Delta u = u(i) - u(i-1)$. The general expression is given by (1.1).

$$J(N_1, N_2, N_u) = \sum_{k=N_1}^{N_2} \delta(j)[\hat{y}(t+k|t) - \omega(t+k)]^2 + \sum_{k=1}^{N_u} \lambda(j)[\Delta u(t+k-1)]^2 \quad (1.1)$$

The following parameters can be used as tuning parameters to cover a wide scope of options: (i) N_u is the control horizon. (ii) N_1 and N_2 are the minimum and maximum prediction horizons that indicate the limits in which it is desirable for the prediction of the output to follow the reference. (iii) The coefficients $\delta(j)$ and $\lambda(j)$ are weighting functions (usually constant values or exponential sequences).

Obtaining the Control law

To obtain the sequence of future control signals $u(t+k|t)$, the cost function J is minimized. An explicit solution can be obtained for the future control signal when the cost function is quadratic, the model is linear and there are no constraints;

otherwise, an iterative method of optimization should be used. Whatever the method, obtaining the solution is not easy because there will be N_2-N_1+1 independent variables, a value which can be high. In order to reduce the degrees of freedom, a certain structure may be imposed on the control law by considering that, after a certain interval N_u, there is no variation in the proposed control signals or they are a linear combination of predetermined base functions (Richalet, [31]).

Reference Trajectory

One of the advantages of predictive control is that when the future evolution of the reference is known a priori, the system can react before the change has been applied, thus compensating for delays in the process response.

Constraints

All processes are subject to constraints: the actuators have a limited range of action and a limited slew rate, while the output variables are also limited for safety reasons. For this, the prediction capabilities of the MPC control make it possible to anticipate violations of the constraints and correct them by incorporating constraints into the cost function to be minimized (Maciejowski, [32]).

Thus, bounds in the amplitude and slew rate of the control signal, as well as limits in the output, are all considered in the optimization. However, other types of constraints could be incorporated into the objective function, such as when the output variables are forced to have certain characteristics: band constraints, overshoot constraints, monotonic behavior, non-minimum phase behavior, actuator nonlinearities. Depending on the importance of the constraints, they are classified as hard constraints, relaxable hard constraints or soft constraints.

Feasibility

An optimization problem is infeasible when the region defined in the decision variables by the set of constraints is empty; as a result, the optimization does not have any valid solution. In contrast, it is feasible when there are points in the space of the decision variables that fulfill all the constraints. Notice that feasibility is of great importance for the stability proofs of constrained MPC. Some techniques for improving feasibility can be classified into: disconnection of the controller, constraint elimination, constraint relaxation and changing the constraint horizons.

Predictive controllers present some drawbacks, such as:

a) A process model has to be identified. For this, a significant amount of plant tests are required.

b) The tradeoff between tuning parameters and closed loop behavior is not evident. Tuning in the presence of constraints may be difficult, and even for the nominal case, it is not easy to guarantee closed loop stability, which is why so much effort is spent on simulations.

c) In order to speed up the solution time, several packages provide sub-optimal solutions to the minimization of the cost function. It can be accepted in high speed applications, but is difficult to justify for process control applications unless the suboptimal solution is always very nearly optimal (Scokaert et al. [33]).

d) A systematic analysis of the stability and robustness properties of MPC is not possible in its original finite horizon formulation. The control law is in general time-varying and cannot be represented in the standard closed loop form, especially in the constrained case. For this, some formulations of predictive control have been proposed that ensure closed loop stability (Chen et al. [34]).

1.3.- Nonlinear Predictive Control

Many processes are nonlinear with varying degrees of severity. Sometimes, the process operates within the neighborhood of a steady state, and therefore a linear representation is adequate; although there are some very important situations where the linear representation is not good. On the one hand, there are processes with severe nonlinearities which are crucial to the closed loop stability, where a linear model is not sufficient. On the other hand, there are some processes that experience continuous transitions and spend a great deal of time away from a steady state operating region, or even processes which are never in steady state operation.

For these processes, a linear control law will not be very effective, so nonlinear controllers will be essential for improved performance or simply for stable operation.

Mathematical Formulation of NMPC

A mathematical formulation of NMPC will be described considering a nonlinear continuous model represented by the nonlinear differential equation (1.2) and (1.3).

$$\dot{x}(t) = f(x(t), u(t)), \qquad x(0) = x_o \tag{1.2}$$

$$y(t) = g(x(t), d(t)) \tag{1.3}$$

Here *x(t)*, *y(t)* and *u(t)* denote the vector of states, outputs and inputs, respectively. Additionally, the output and input constraints are given by (1.4), (1.5) and (1.6).

$$Y := \left\{ \underline{y} \le y \le \overline{y} \right\}, \tag{1.4}$$

$$U := \left\{ \underline{u} \le u \le \overline{u} \right\}, \tag{1.5}$$

$$D := \left\{ \underline{\Delta u} \le \Delta u \le \overline{\Delta u} \right\}, \tag{1.6}$$

In NMPC, the input applied to the system is usually given by the solution of the following finite horizon open-loop optimal control problem, which is solved at every sampling instant, as shown in (1.7).

$$J = \int_{N_1}^{N_2} \delta(j)[\hat{y}(t+\tau|t) - \omega(t+\tau)]^2 d\tau + \sum_{k=1}^{N_u} \lambda(j)[\Delta u(t+k-1)]^2 \tag{1.7}$$

Both the vector of states **x** and outputs **y** include continuous variables; as a result, an integral was used instead of the summation for the first term in the cost function, while **u** is considered a discrete variable due to its value being constant at $t \in [k, k+1)$. Finally, the optimization problem at each sampling instant can be expressed as (1.8), subject to (1.9), (1.10), (1.11), (1.12) and (1.13).

$$\min_{\{\Delta u(k),\ldots,\Delta u(k+N_u-1)\}} J = \int_{N_1}^{N_2} \delta(\tau)[\hat{y}(t+\tau|t) - \omega(t+\tau)]^2 d\tau + \sum_{k=1}^{N_u} \lambda(k)[\Delta u(t+k-1)]^2 \tag{1.8}$$

$$\dot{x}(t+\tau|t) = f(\mathbf{x}(t+\tau-1|t), \mathbf{u}(t+\tau|t)) \quad \forall \tau \in [1, N_2] \tag{1.9}$$

$$\hat{y}(t+\tau|t) = g(\mathbf{x}(t+\tau|t), \mathbf{d}(t+\tau|t)) \qquad \forall \tau \in [1, N_2] \tag{1.10}$$

$$\Delta\mathbf{u}(t+k-1|t) \in D \qquad k = 1, \ldots, N_u \tag{1.11}$$

$$\mathbf{u}(t+k|t) \in U \qquad k = 1, \ldots, N_u \tag{1.12}$$

$$\hat{y}(t+\tau|t) \in Y \qquad \forall \tau \in [N_3, N_4] \tag{1.13}$$

The output vector predictions are obtained by solving differential and algebraic equations for different control laws defined in each sampling instant. N_3 and N_4 is the range where output constraints are applied. Notice $1 \le N_3 \le N_4 \le N_2$

If the numerical integration of the differential and algebraic equations is used, it will be necessary to include a new element in the predictive control scheme: a simulation Package. This is known as the direct method for solving dynamic

optimization problems. The optimizer will define a control law $\mathbf{u}(t+k|t)$, $j=1...N_u$ at each sampling instant. The current state of the process, together with the control law, will be used for the simulation package to simulate the model (i.e.: integrate the dynamic equations) and obtain a value for the cost function. Afterwards, the optimizer will define a new control law, the dynamic of the process will be simulated again considering this new control law $\mathbf{u}(t+k+1|t+1)$, a new value for the cost function will be reached, and so on until an optimal control law which minimizes the cost function has been found. This control law will eventually be applied to the process, based on the receding prediction horizon.

Including a simulation package to simulate the dynamic of the process in which the model is programmed allows the use of nonlinear models as complicated and/or detailed as desired, making different formulations of the same models possible. The main drawback is the computational cost associated to the integration of large and complex models.

This predictive control formulation, based on nonlinear and continuous models in which the process model is integrated by means a simulation package, to obtain a value of the cost function at the end of the prediction horizon, together with discrete events, will be the basic idea followed in the following sections.

1.4.- Outline of the Chapter

The remainder of this thesis is organized as follows.

In Chapter 2, the implementation of MPC considering a three blade wind turbine is described. As a result, a review of the dynamic model and the traditional control strategy associated with the wind turbine are also discussed.

The developed predictive control for hybrid systems is implemented considering the energy supply system studied in Chapter 3. The integrated system includes a Reverse Osmosis (RO) desalination unit and a three-phase power supply system comprising PV modules, a wind turbine, a battery bank and a diesel generator. Additionally, a MATLAB simulation platform was built considering the dynamic models of each energy source. Simultaneously, the internal model used for the proposed predictive control will be based on the simulation platform.

Chapter 4 presents the development of a simulation model for a solar gas air-conditioning plant with the aim of providing a suitable temperature inside a building during the hot season with minimum energy consumption. The plant is made up of three main sections: the refrigeration system, the single – effect LiBr-H2O absorption machine and the solar heat supply system. However, the proposed controller is focused on the solar heat supply system, which provides a hot water flow to the generator of the absorption machine and is composed of three main

elements: a solar collector field, an ON/OFF gas heater and two thermally isolated accumulation tanks.

Chapter 5 includes a review of a hydrogen based MicroGrid made up of a PEM electrolyzer, a metal hydride storage, a PEM fuel cell, a battery bank, PV modules and an electronic load. The main objective is to fulfill the local loads by keeping a balance between the consumed and the generated power, in spite of possible ambient disturbances. A central aspect in the optimization of the energy storage is the consideration of its energy requirements. The metal hydride is used to provide energy for long term requirements, while the battery bank is used for the short term. This implies guaranteeing a good behavior of the fuel cell and electrolyzer so as not to reduce the lifetime of the components. Both the aim and the constraint will be taken into account in the proposed MPC control.

The conclusions contain a detailed discussion of the systems' behavior and are made comparing the simulation and experimental results with the theoretical analysis. Finally, potential future work is discussed.

1.5.- Summary of Publications

This thesis is based on submitted articles:

- J. Salazar, F. Tadeo, C. de Prada and M. Chaabane. "Modeling of MicroSource for Microgrid during Island Operation", *2nd Int. Conf. on Communications, Computers and Control Applications (CCCA`12)*, Marseille, France, 6-8 Dec. 2012.

- J. Salazar, F. Tadeo, C. de Prada and L. Palacin. "Modeling and control of a wind turbine equipped with a permanent magnet synchronous generator (PMSG)", *22nd European Modeling & Simulation Symposium*, FES, Morocco, October 13-15, 2010.

- J. Salazar, J. D. Álvarez Hervás, J. L. Guzmán and F. Tadeo, "Control-oriented Modelling of the Solar Climatization of a Public Building in Mediterranean Climate", *Conférence and Exposition Internationales Vehicules Écologiques and Énergies Renouvalables*, Monaco, Monaco, March, 2013.

- J. Salazar, F. Tadeo and C. Prada. "Renewable Energy for Desalinization using Reverse Osmosis", *International Conference on Renewable Energies and Power Quality (ICREPQ'10)*, Granada, Spain, 23th to 25th March, 2010.

- J. Salazar, F. Tadeo, C. de Prada and L. Palacin, "Modeling and control of MicroGrids in Island Operation" *International Renewable Energy Congress*, Sousse, Tunisia, November 5-7, 2009.

- J. Salazar, F. Tadeo, Cesar de Prada and L. Palacin, "Modeling and Simulation of Auxiliary Energy Systems for off-grid Renewable Energy Installations", *The Third International Renewable Energy Congress*, Hammamet, Tunisia, December 20-22, 2011.

- J. Salazar, F. Tadeo, C. Prada and L. Palacin. "Simulation and Control of a PV System connected to a Low Voltage Network", *XXXI Jornadas de Automática*, Jaén, SPAIN, September 08-10, 2010.

- J. Salazar, M. M. Castillo, F. Rodriguez and F. Tadeo. "Minimization of the Operation Costs of a Solar/Gas Air-conditioning System using Duration-based Predictive Control", *The Mediterranean Green Energy Forum 2013, MGEF-13*, Fes, Morocco, 2013.

- J. Salazar, F. Tadeo, K. Witheephanich, M. Hayes and C. de Prada. "Control for a Variable Speed Wind Turbine equipped with a Permanent Magnet Synchronous Generator (PMSG)", *Sustainability in Energy and Buildings (SEB`11)*, Marseille, France, 1-3 June 2011.

- J. Salazar, L. Valverde, C. Bordons and F. Tadeo, "Predictive Control of a photovoltaic system with mixed battery and hydrogen storage". *39th Annual Conference of the IEEE Industrial Electronics Society (IECON)*, 2013.

- J. Salazar, F. Tadeo, C. de Prada. "A Microgrid Library in a General Simulation Language". *The International Federation of Automatic Control*, Cape Town, South Africa, Volume 19, August 2014, Pages 3599-3604.

- J. Salazar, F. Tadeo, C. de Prada. "Modelling of Diesel Generator Sets that assist Off-Grid Renewable Energy Microgrid". *Journal of Renewable Energy and Sustainable Development (RESD)*, Volume 1, Issue 1, June 2015, Pages 85-91.

- Palacín, L. G., Tadeo, F., de Prada, C., and Salazar, J. "Operation of desalination plants using hybrid control". *Desalination and Water Treatment*, 25:119-126. IF: 0.614, 2011.

- Palacín, L. G., Tadeo, F., Salazar, J., and de Prada, C. "Operation of medium-size reverse osmosis plants with optimal energy consumption". *In 9th International Symposium on Dynamics and Control of Process Systems*, Leuven, Belgium, 2010.

- Palacín, L. G., Tadeo, F., Salazar, J., and de Prada, C. “Initial validation of a reverse osmosis simulator”. *In Emerging Technologies and Factory Automation*, Bilbao, Spain, 2010.

- Tadeo, F., Palacín, L. G., Salazar, J., and de Prada, C. “Desalination in remote areas: A prediction-based approach”. *In IDA World Congress*, Perth, Australia, 2011.

- Tadeo, F., Val, R., Palacín, L. G., Salazar, J., and de Prada, C. “Control of reverse osmosis plants using renewable energies”. *In International Conference on Control and Applications*, Cambridge, UK, 2009.

CHAPTER 2

Wind Turbine Control

The usual approach in the design of traditional controllers comprised a set of proportional-integrated (PI) controllers whose gain depends on the operating mode. Thus, switches between controllers cannot be avoided. Additionally, the tuning of control parameters is based on the linearization of nonlinear aeroelastic codes. As a result, some dynamics may be lost after linearizing an original nonlinear process. However, the need to satisfy the increasing energy demand requires the design of new controllers for wind turbines. The real main objective for the controller will be to optimize the energy provided by the turbine as well as to satisfy the real operational constraints from the equipment, considering the short-term unreliability of the wind speed.

Model Predictive Control (MPC) emerges as a control strategy able to handle variations in the wind speed which includes, in the control law formulation, a cost function in economic terms to be minimized and the constraints related to the manipulated and controlled variables.

In this chapter, the application of the proposed controller for a wind turbine will be taken into account. For this, a wind turbine model is given in detail, to be used as the internal model in the MPC formulation. Then, a comparison between the traditional control strategy based on PID and the proposed nonlinear predictive control is presented.

2.1.- Process Description

The main components of a three blade wind turbine are tower, rotor, end nacelle. The tower carries the nacelle and the rotor. Since the wind speed increases with the height, a taller tower generally enables a wind turbine to capture more energy from the wind and generate more electric power. The rotor is consisting of the blades and the supporting hub. Finally, the nacelle houses the drive train and the generator (s. Figure 2.1 and Figure 2.2).

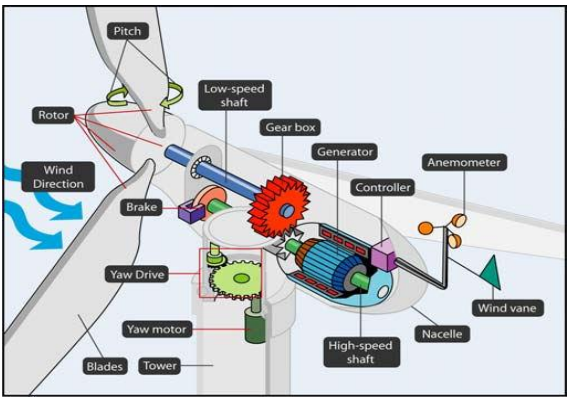

Figure 2.1.- Wind Turbine Components

Figure 2.2.- Wind Turbine components into nacelle

The drive train includes the rotating parts of the wind turbine. It is usually consists of a low-speed shaft (on the rotor side), a high-speed shaft (on the generator side), a gearbox and a mechanical brake. The purpose of the gearbox is to speed the rate of rotation of the rotor from a low value (tens of rpm) to a rate suitable for driving a standard generator (hundreds of thousands of rpm). However, the elimination of gearbox can be reached using a permanent magnet synchronous generator.

The yaw mechanism is used to turn the wind turbine rotor against the wind as the wind direction changes. The pitch actuator controls the pitch of the blades by rotating the blades. The anemometer and the wind vane are used to measure the speed and direction of the wind.

The description and modeling of a three-blade, variable speed wind turbine equipped with PMSG are described throughout this section. The mechanical components of the Wind Turbine System (wind turbine rotor and drive train) as well as the electrical components (synchronous generator) will be presented (s. Figure 2.3). These models can be used to test different configurations, as well as control strategies and fault detection and accommodation algorithms.

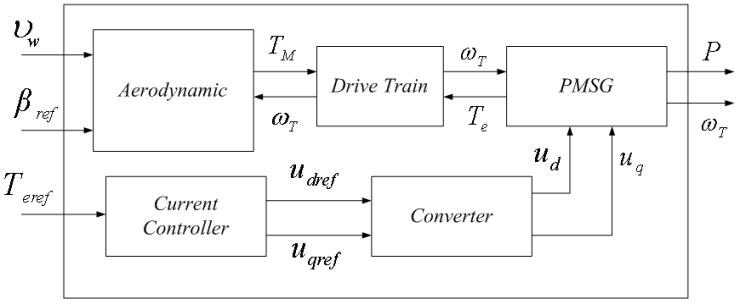

Figure 2.3.- Wind Turbine Model

The measured variables are related to the nomenclature used in the modeling and they are expressed as:

- The rotor rotational speed: ω_T
- The output power provided by the wind turbine: P
- The blade pitch angle: β
- The wind speed: υ_w
- The mechanical torque of the turbine: T_M
- The generator electromagnetic torque: T_e
- The current and voltage of the Permanent Magnet Generator: i_A, i_B, i_C, v_A, v_B and v_C.

The wind turbine system has the following manipulated variables that allow the control of the whole system:

- A reference blade pitch angle (β_{ref}) which defines the desired angle for the blade associated to the rotor.
- A reference generator electromagnetic torque (T_{eref}).

The strategy of the traditional controller is given by two controllers cross-coupled for a variable speed wind turbine (s. Figure 2.4): below-rated power and above-rated power. Below rated value (Region I), the speed controller continuously adjusts the speed of the rotor to maintain the tip speed ratio constant at the level that gives the maximum power coefficient (s. Figure 2.5). Generator torque provides the control input to vary the rotor speed, and blade pitch angle is held constant. Above-rated value (Region III), the main objective is to keep a constant power output. This

is generally achieved by keeping generator torque constant and varying blade pitch angle. Finally, Region II is a transition region mainly concerned with keeping rotor torque and noise low (Rasila, [35]). Outside these regions (when the wind speed is either lower than cut-in speed or higher than the cut-out speed), the turbine does not generate power, and the pitch angle is usually set to 90°.

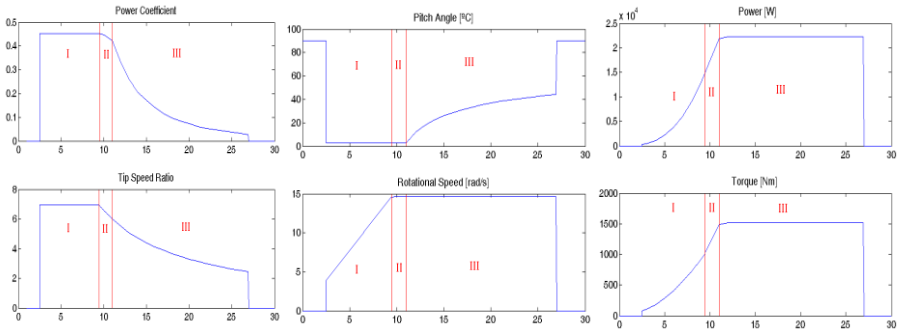

Figure 2.4.- Operation Region of Wind Turbine

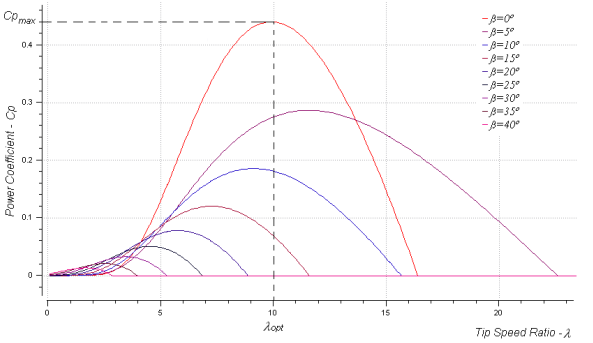

Figure 2.5.- Power Coefficient vs. Tip-Speed Ratio

Some constraints are necessary to define for the operation of wind turbine which are related to the cut in and cut out velocity; and the rated speed as is shown in Figure 2.6. The cut-in-wind speed is defined as the lowest wind speed at which the turbine starts to generate power. Below this speed, it is not efficient to turn on the turbine. The rated speed is the wind speed at which the turbine reaches its rated power. The cut-out velocity is the maximum wind speed at which the turbine can still operate. Beyond this wind speed, the rotor has to be blocked to keep the blades, the electrical generator and other components from reaching damage.

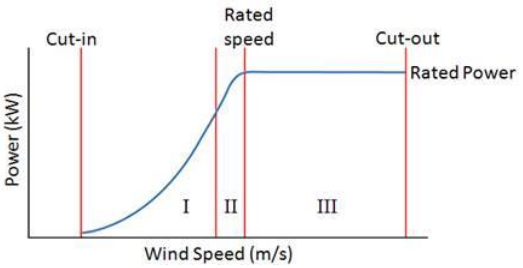

Figure 2.6.- Operational Constraints of a variable speed Wind Turbine

2.2.- Wind Turbine Model

The design of a traditional strategy controller integrated by a set of proportional-integral (PI) controller require the linearization at a specific operating point of the non-linear dynamic model. Additionally, the proposed model predictive control is based on an internal model which is used to predict how performance depends on present and future control actions, which are then selected to optimize the performance of the process. For this, a reliable model of the wind turbine must be provided. However, in the model predictive control formulation, the model must be evaluated by the optimizer several times and this must happen in every sampling period until a feasible solution is found, as a result, the model must be simple with very good reliability to obtain trustworthy results of the optimization.

2.2.1.- Aerodynamic Model

The power in the wind is known to be proportional to the cube of the wind speed, so it may be expressed as (2.1), where ρ is the air density, A is the area swept by the blades and v_w is the wind speed. However, a wind turbine can only extract a fraction of the power, which is limited by the Betz limit (maximum 59%). This fraction is described by a power coefficient, C_p, which is a function of the blade pitch angle β and the tip speed ratio λ. Therefore the mechanical power extracted from the wind by the turbine is given by (2.2), where the tip speed ratio λ is defined as the ratio between the blade tip speed and the wind speed v_w. ω_T is the turbine rotor speed and R is the radius of the blades (2.3).

$$P = \frac{1}{2}\rho A v_w^3 \tag{2.1}$$

$$P_{mec} = \frac{1}{2} C_p(\beta, \lambda) \rho A v_w^3 \tag{2.2}$$

$$\lambda = \frac{\omega_T R}{v_w} \tag{2.3}$$

The power coefficient is defined by (2.4) and (2.5) (Raiambal et al., [36]).

$$C_p(\lambda,\beta) = Pa\left(\frac{P_b}{\sigma} - P_c\beta - P_d\right)exp\left(\frac{P_e}{\sigma}\right) + P_f\lambda \tag{2.4}$$

$$\sigma = \left[\frac{1}{\lambda + P_g\beta} - \frac{P_h}{\beta^3 + 1}\right]^{-1} \tag{2.5}$$

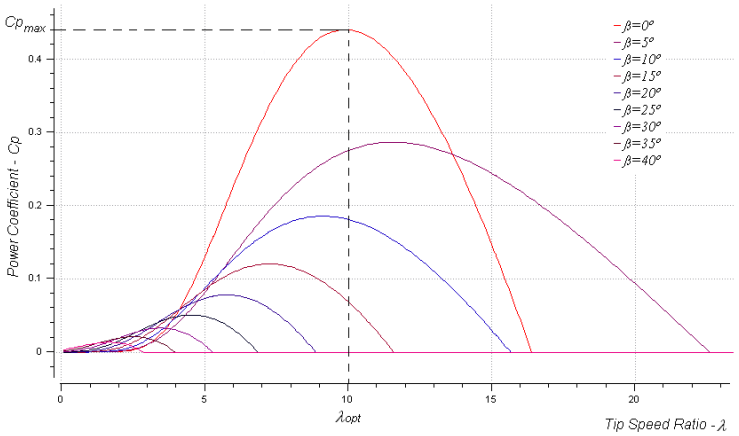

Figure 2.7.- Power Coefficient vs. Tip-Speed Ratio

Thus, changes in the rotor or wind speeds induce changes in the tip speed ratio, leading to power coefficient variation. In this way, the generated power is affected. Figure 2.7 shows a typical *CP* -λ curve for a wind turbine that follows equation (2.4). The wind turbine power coefficient is maximized C_{pmax} for an optimum tip-speed ratio of λ_{opt} and an optimum pitch angle β_{opt}.

2.2.2.- Hydraulic Actuator Model

The hydraulic actuator of the pitch angle β can be modeled as a first order system, as shown in Figure 2.8. The signal β_{ref} is taken from Torque and Pitch Angle Control, as it is described in (2.6), where T_{servo} is the time constant of the Pitch actuator (s), β_{ref} is the reference of the pitch angle (degree) and β is the actual pitch angle (degree).

$$\frac{\beta}{\beta_{ref}} = \frac{1}{(\tau_{servo}s + 1)} \tag{2.6}$$

In order to respect the dynamic of the system, the time constant of the pitch actuator has to be bigger than the time constant of the generator and smaller than the response of the plant.

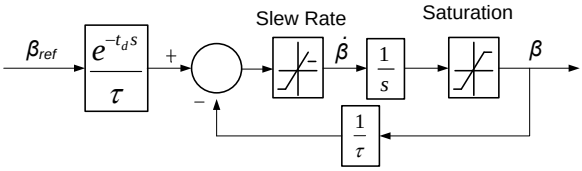

Figure 2.8.- Hydraulic Actuator Model

2.2.3.- Drive Train Model

The mechanical system of the wind turbine can be simply modeled (Mei et al., [37]) with the one-mass model given by (2.7), where $J_{total}=J_T+J_g$ is the inertia constant of the whole drive train, with J_T and J_g the inertia constants of the turbine and the generator ($k_g m^2$) , respectively; ω_T is the rotor speed (rad/s); F_r is the friction coefficient ($K_g m^2 s$); T_e is the generator electromagnetic torque (Nm) and the mechanical torque of the turbine T_M (Nm) is given by (2.8).

$$J_{total}\frac{d\omega_T}{dt} = T_M - T_e - F_r\omega_T \tag{2.7}$$

$$T_M = \frac{P_{mec}}{\omega_T} = \frac{1}{2}\frac{C_p(\beta,\lambda)\rho A v_w^3}{\omega_T} \tag{2.8}$$

2.2.4.- Permanent Magnet Synchronous Generator Model

The rotor excitation of the Permanent Magnet Synchronous Generator (PMSG) is assumed to be constant, so its electrical model in the synchronous reference frame is given (Wua et al., [38]) (Svechkarenko, [39]) by (2.9) and (2.10), where subscripts d and q refer to the physical quantities that have been transformed into the (d,q) synchronous rotating reference frame; R_s is the stator resistance; L_s is the inductances of the stator; u_d and u_q are, respectively, the d- and q- axis components of stator voltage; i_d and i_q are, respectively, the d and q axis components of stator current; ψ_f is the permanent magnetic flux and the electrical rotating speed ω_e is given by (2.11), where n_p is the number of pole pairs.

$$L_s\frac{di_d}{dt} = u_d - R_s i_d + L_s\omega_e i_q \tag{2.9}$$

$$L_s \frac{di_q}{dt} = u_q - R_s i_q - L_s \omega_e i_d + \omega_e \psi_f \tag{2.10}$$

$$\omega_e = n_p \omega_T \tag{2.11}$$

The power equations are given by (2.12) and (2.13), where P and Q are the output active and reactive powers, respectively. The electromagnetic torque T_e can be derived from (2.14).

$$P = \frac{3}{2}\left(u_d i_d + u_q i_q\right) \tag{2.12}$$

$$Q = \frac{3}{2}\left(u_q i_d - u_d i_q\right) \tag{2.13}$$

$$T_e = -\frac{3}{2} n_p \psi_f i_q \tag{2.14}$$

Current Controller

The current control scheme of the generator side converter is show in Figure 2.9. This control is based on projections which transform a three phase time and speed dependent system into a two co-ordinate (d and q co-ordinates) time invariant system. These projections lead to a structure similar to that of a DC control that makes easier AC control (Mahdi et al., [40]). Notice the output variable are given by the 'd' and 'q' current (i_d and i_q, respectively) while the manipulated variables are represented by the 'd' and 'q' voltages $\hat{u}_d$ and $\hat{u}_q$.

In order to design independent controllers for the two coordinates, the influences of the q-axis on the d-axis component, and vice versa, must be eliminated (s. Figure 2.10). For this the decoupling voltages u_{dref} and u_{qref} are given (Chinchilla et al. [2]) by (2.15) and (2.16):

$$u_{dref} = \hat{u}_d - L_s \omega_e i_q \tag{2.15}$$

$$u_{qref} = \hat{u}_q + L_s \omega_e i_d - \omega_e \psi_f \tag{2.16}$$

These decoupling voltages are added to the current controller outputs, resulting in the control signal for the PWM-rectifier as is shown in Figure 2.10. In order to combine a fast response of the controlled variable to a change of the set point with zero steady state deviation, proportional integral (PI) current controllers are chosen. Control equations are given by (2.17), (2.18), (2.19) and (2.20).

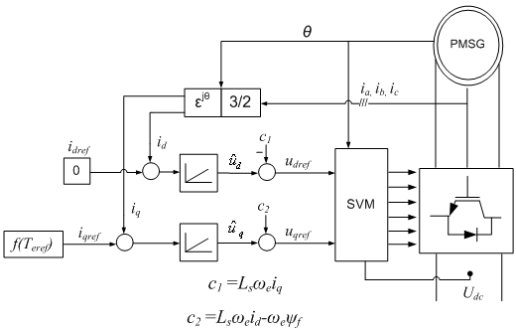

Figure 2.9.- Current Controller Model

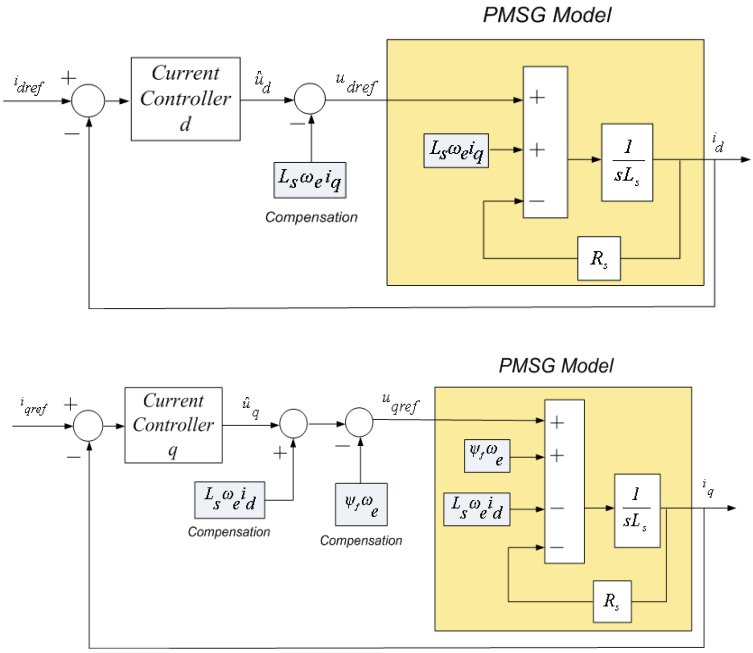

Figure 2.10.- Decoupling between |d| and |q| axis

$$\frac{dx_1}{dt} = i_{dref} - i_d \tag{2.17}$$

$$\frac{dx_2}{dt} = i_{qref} - i_q \tag{2.18}$$

$$\hat{U}_d = K_{p1} \Delta i_d + K_{i1} x_1 \tag{2.19}$$

$$\hat{U}_q = K_{p2}\Delta i_q + K_{i2}x_2 \tag{2.20}$$

The required d-q components of the rectifier voltage vector are given by (2.21) and (2.22).

$$u_{dref} = K_{p1}\Delta i_d + K_{i1}x_1 - L_s\omega_e i_{qs} \tag{2.21}$$

$$u_{qref} = K_{p2}\Delta i_q + K_{i2}x_2 + L_s\omega_e i_d - \omega_e\psi_f \tag{2.22}$$

The stator current reference in d-axis i_{dref} is maintained at zero, for producing maximum torque, due to the non-saliency of the generator. The stator current reference in q-axis i_{qref} is calculated from the reference torque T_{eref} as shows in (2.23).

$$i_{qref} = \left(\frac{2}{3n_p\psi_f}\right)T_{eref} \tag{2.23}$$

The dynamic response of power converter with space-vector modulation (SVM) is not included in the current controller considering its dynamic response is faster than the rest of the system. From equation (2.9), (2.10), (2.15) and (2.16) results the transfer function of the stator winding (s. (2.24) and Figure 2.11).

$$\frac{i_d}{\hat{u}_d} = \frac{i_q}{\hat{u}_q} = \frac{1}{(sL_s + R_s)} \tag{2.24}$$

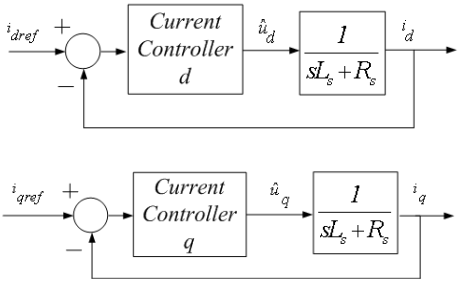

Figure 2.11.- Current controller scheme considering |d| and |q| axis

2.3.- Simulations Platform

A simulation platform under the MatLab® Simulink® environment was developed in order to evaluate the dynamic of a three blade - variable speed wind turbine equipped with permanent magnet synchronous generator as is shown in Figure 2.12. The implementation has been done as a modular structure to make easy the change and the improvements of the model.

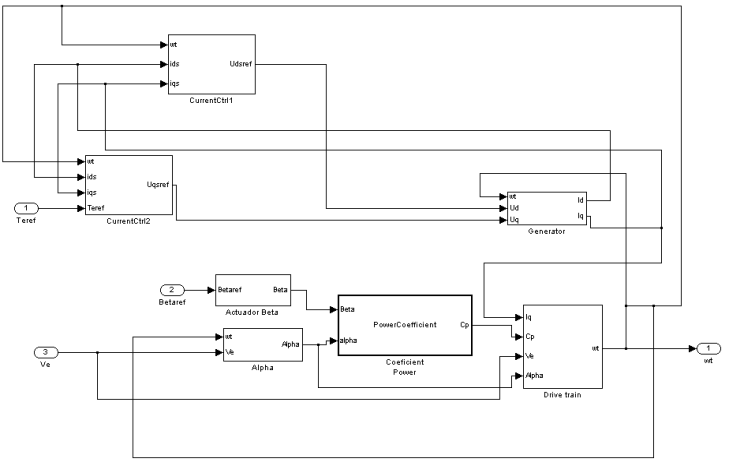

Figure 2.12.- Simulink boxes of the Wind Turbine

The mechanical model of the Wind Turbine Model is given by equations from (2.1) to (2.8), considering the parameters given in Table 2.1, while the electrical components including the current controller and the synchronous generator are defined thorugh equations from (2.9) to (2.24) with the parameters given in Table 2.2.

Unfortunately, the model could not be validated since a real wind turbine system was not available. As a result, the value of the parameters was taken in the literature in (Raiambal et al., [36]), (Cataña et al., [41]), (Solsona et al., [42]). However, the proportional integral (PI) current controller connected directly to the synchronous generator was designed considering a Pole Placement method with a damping factor ξ= 0.7448 and ωn= 134.26. Thus, the resulting controller is Kp= 9.6 and Ki= 1334.4, considering the equation (2.24).

Parameter		**Value**	**Unit**
Radio of Blade	R	4.5	M
Parameters for WTs Model	P_a	0.71	-------
Parameters for WTs Model	P_b	230	-------
Parameters for WTs Model	Pc	0.4	-------

Parameters for WTs Model	P_d	20	-------
Parameters for WTs Model	P_e	-21	-------
Parameters for WTs Model	P_f	0.00571	-------
Parameters for WTs Model	P_q	0.08	-------
Parameters for WTs Model	P_h	0.035	-------
Maximum Power Coefficient	C_{pmax}	0.44	-------
Optimum Tip-Speed Ratio	λ_{opt}	6.96	rad/s
Optimum Pitch Angle	β_{opt}	3º	Degree
Time constant of the Pitch actuator	τ_{servo}	1.5	S
Inertia Constant of the whole drive train	J_{total}	156.95	$k_g m^2$
Friction Coefficient	F_r	2.79	$K_g m^2 s$
Cut-in Wind SpeedVelocity			
Cut-out Wind Speed Velocity			

Table 2.1.- Parameters for mechanical model of the WTs

Parameter		**Value**	**Unit**
Stator Resistance	R_s	5.2	Ω
Stator Inductances	L_s	0.074	H
Permanent Magnetic Flux	ψ_f	0.1	Wb
Number of poles	n_p	18	-------

Table 2.2.- Parameters for electrical model of the WTs

2.4.- Traditional Wind Turbine Control

Most control strategies for torque and pitch angle control are based on a linear model of wind turbine which can be obtained by linearizing the nonlinear model at a specific operating point (Hand et al., [43]). In Abdin et al. [44], a proportional-integral (PI) controller based on the linearized model of wind turbine was designed. However, the controller does not provide a good performance when the working point deviates from operating point (Chedid et al., [45]), because the numbers of pitch gains are usually the partial derivatives of the rotor aerodynamic torque respect to blade pitch and these gains will change with different wind speeds and pitch angles. In Lescher et al. [46], a gain scheduling controller was designed, which gains change with the wind speed or other parameters. The author reported satisfactory simulation results, but the controller was not verified on the nonlinear model. In Yilmaz et al. [47], a neural network controller was proposed and the experiments shows a convincing performance, but it seems too complicated to be implemented in real WTs.

In this section, a proportional-integral (PI) controller for below-rated power and a gain scheduling controller for above-rated power are proposed and verified on the nonlinear model.

Low Wind Speed Operation (Region I)

The main objective is to capture as much power as possible from the wind. The speed controller is used to keep the turbine at its most effective operation, keeping the blade pitch constant at an optimal value β_{opt}. The reference speed is set such that the tip speed ratio, λ is maintained at its optimal value, λ_{opt} according to equation (2.25). The basic scheme is shown in Figure 2.13.

$$\omega_{Tref} = \frac{\lambda_{opt} \upsilon_w}{R} \tag{2.25}$$

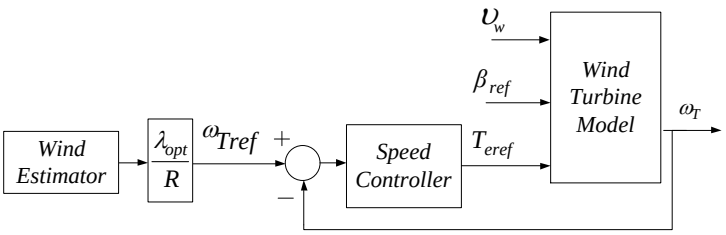

Figure 2.13.- Operational regions of Wind Turbines

For this a good estimation of the wind speed is required. Wind measurements by an anemometer do not sense the same turbulence as the wind turbine.

Middle Wind Speed Operation (Region II)

The generator is controlled to keep nominal rotational speed considering an optimal value for the pitch angle β_{opt}. The reference speed will be the nominal rotational speed of the generator. Usually this interval ends when nominal generator power is reach so in this region turbine operate below rated power. The basic scheme is shown in Figure 2.14.

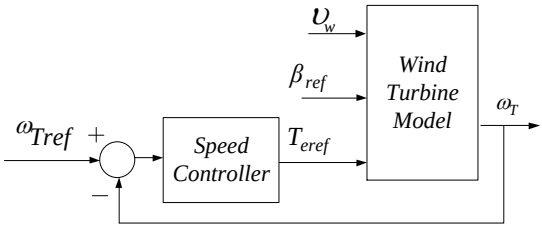

Figure 2.14.- Control scheme in Middle Wind Speed

The Transfer function in low and middle wind speed is given by (2.26).

$$\frac{\Delta\omega_T}{\Delta T_{eref}} = \frac{sK_p + K_I}{\left(L_s s^2 + \left(R_s + K_p\right)s + K_I\right)\left(J_T s - \gamma + F_r\right)} \tag{2.26}$$

Selection of the operating point is critical to ensure stability in the system. The stability depends on the torque coefficient which is defined by (2.27).

$$C_q = \frac{C_P}{\lambda} \tag{2.27}$$

Considering the derivative of the torque coefficient C_q respect to λ, the typical C_p-λ curve can be divided into two regions: stable and unstable as shown in Figure 2.15. The controller has to be designed to keep inside the stable region.

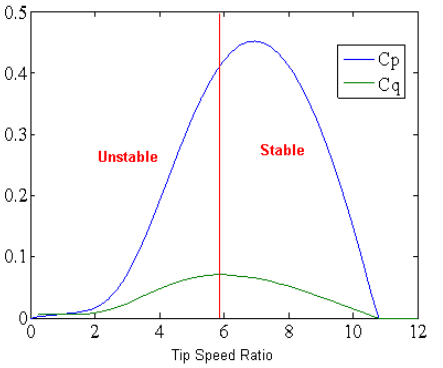

Figure 2.15.- Unstable and stable regions over Cp-λ and Cq-λ curve

High Wind Speed Operation (Region III)

The purpose of the pitch angle control should be to maintain the rotor speed and the output power as close as possible to the rated value in order to regulate the aerodynamic power for keeping safe operation. The electric torque is defined as production of constant rated electric power $\left(T_e = T_e^{rated}\right)$. The basic scheme is shown in Figure 2.16.

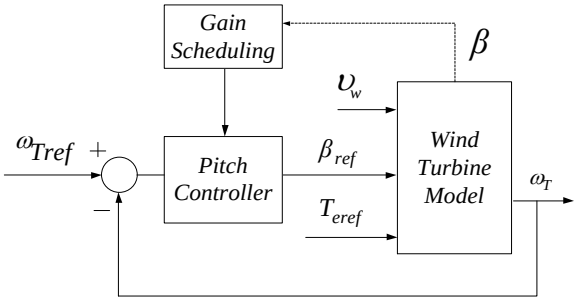

Figure 2.16.- Control scheme in High Wind Speed

The Transfer function is given by (2.28).

$$\frac{\Delta\omega_T}{\Delta\beta_{ref}} = \frac{\varsigma}{(\tau_{servo}s+1)(J_T s-\gamma+F_r)} \tag{2.28}$$

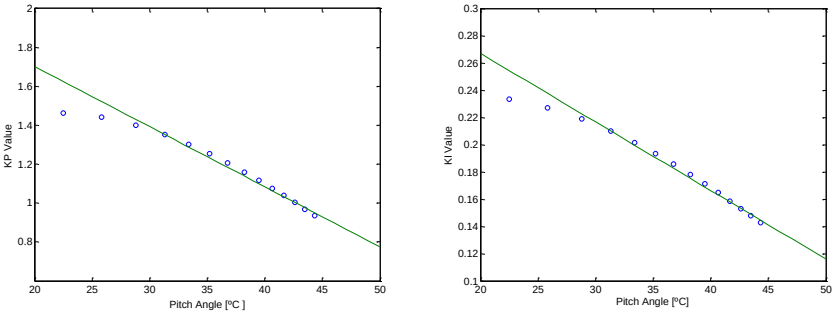

Figure 2.17.- Lineal interpolation of the pitch controller gains

Considering the highly nonlinear aerodynamics of variable speed wind turbine, the whole speed area is not able to operate using only one Proportional Integrator (PI) controller. The controller can only work well in the neighborhood of the operating point. However, the controller fails to provide acceptable performance when the working point deviates from the operating point. In consequence, the pitch controller is implemented as a gain scheduling controller, where the controller gains are scheduled depending on blade pitch angle. The transfer function (2.29), (2.30) and (2.31) are used to determine the proportional gain (s. Figure 2.17).

$$Controller = K_p(\beta) + \frac{K_i(\beta)}{s} \tag{2.29}$$

$$K_p(\beta) = -0{,}028\beta + 2{,}1158 \tag{2.30}$$

$$K_i(\beta) = -0{,}0048\beta + 0{,}3542 \tag{2.31}$$

Operating points take into account during controller design are shown in Figure 2.18.

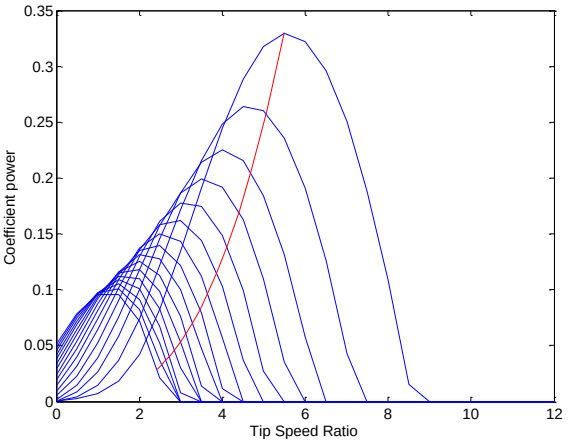

Figure 2.18.- Operating points proper of zone III

The control overview scheme is shown in Figure 2.19. It is not possible to operate in the whole speed area using only one controller and due to this the final controller is a combination of the controllers from the various wind speed intervals. Finally, after modeling and analyzing those three different controllers, the whole control scheme is obtained (Kulka, [48]).

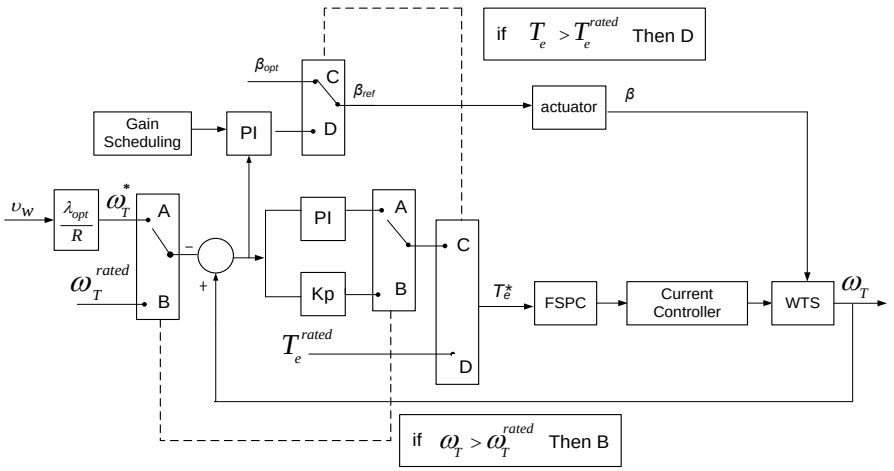

Figure 2.19.- Overview of the whole control scheme

2.4.1.- Linearized Wind Turbine Model

The approach to design a traditional proportional-integral (PI) controller requires that the non-linear turbine dynamics are linearized at a specified operating point.

The linearization of the pitch actuator equation (2.6) results in (2.32), whereas the linearization of the turbine equation (2.7) gives the differential equation in (2.33), with the linearization coefficients are given by (2.34), (2.35) and (2.36). Here, $\Delta\omega_T$, $\Delta\beta$ and $\Delta\upsilon_w$ represent the deviations of $\overline{\omega}_T$, $\overline{\beta}$ and $\overline{\upsilon}_w$ respectively.

$$\tau_{servo}\,\Delta\dot{\beta} = \Delta\beta_{ref} - \Delta\beta \tag{2.32}$$

$$J\Delta\dot{\omega}_T = \varsigma\Delta\beta + \alpha\Delta\upsilon_w + \gamma\Delta\omega_T - \left(\frac{3n_p\psi_f}{2}\right)\Delta i_q - F_r\Delta\omega_T \tag{2.33}$$

$$\gamma = \frac{1}{2}\rho\pi R^4\overline{\upsilon}_w\left.\frac{dc_q}{d\lambda}\right|_{OP} \tag{2.34}$$

$$\alpha = \frac{1}{2}\rho\pi R^3\overline{\upsilon}_w\left(2\overline{c}_q - \overline{\lambda}\left.\frac{dc_q}{d\lambda}\right|_{OP}\right) \tag{2.35}$$

$$\varsigma = \frac{1}{2}\rho\pi R^3\overline{\upsilon}_w^2\left.\frac{dC_q}{d\beta}\right|_{OP} \tag{2.36}$$

The linearization of the PMSG equations (2.9) and (2.10) results in (2.37), (2.38), (2.39) and (2.40).

$$L_s\Delta\dot{i}_d = -\left(R_s + K_p\right)\Delta i_d + K_i\Delta x_1 \tag{2.37}$$

$$L_s\Delta\dot{i}_q = \left(\frac{2K_p}{3n_p\psi_f}\right)\Delta T_{eref} - \left(R_s + K_p\right)\Delta i_q + K_i\Delta x_2 \tag{2.38}$$

$$\Delta\dot{x}_1 = -\Delta i_d \tag{2.39}$$

$$\Delta\dot{x}_2 = \left(\frac{2}{3n_p\psi_f}\right)\Delta T_{eref} - \Delta i_q \tag{2.40}$$

Using the linearization of the pitch actuator (2.32), the turbine (2.33) and the generator (2.37) and (2.38) equations give the continuous-time linear system in (2.41) and (2.42), where *x* and *u* are defined in (2.43) and (2.44), respectively, considering A, B, C and D defined as (2.45), (2.46), (2.47) and (2.48).

$$\dot{x} = Ax + Bu \tag{2.41}$$

$$y = Cx + Du \tag{2.42}$$

$$x = \begin{bmatrix} \Delta\omega_T \\ \Delta\beta \\ \Delta i_q \\ \Delta i_d \\ \Delta x_1 \\ \Delta x_2 \end{bmatrix} \tag{2.43}$$

$$u = \begin{bmatrix} \Delta T_{eref} \\ \Delta\beta_{ref} \\ \Delta v_w \end{bmatrix} \tag{2.44}$$

$$A = \begin{bmatrix} \frac{\gamma - F_r}{J_t} & \frac{\varsigma}{J_t} & -\frac{3n_p\psi_f}{2J_T} & 0 & 0 & 0 \\ 0 & -\frac{1}{\tau_{servo}} & 0 & 0 & 0 & 0 \\ 0 & 0 & \frac{-K_p - R_s}{L_s} & 0 & 0 & \frac{K_i}{L_s} \\ 0 & 0 & 0 & \frac{-K_p - R_s}{L_s} & \frac{K_i}{L_s} & 0 \\ 0 & 0 & 0 & -1 & 0 & 0 \\ 0 & 0 & -1 & 0 & 0 & 0 \end{bmatrix} \tag{2.45}$$

$$B = \begin{bmatrix} 0 & 0 & \frac{\alpha}{J_T} \\ 0 & \frac{1}{\tau_{servo}} & 0 \\ \frac{2K_p}{3n_p\psi_f L_s} & 0 & 0 \\ 0 & 0 & 0 \\ 0 & 0 & 0 \\ \frac{2}{3n_p\psi_f} & 0 & 0 \end{bmatrix} \tag{2.46}$$

$$C = \begin{bmatrix} 1 & 0 & 0 & 0 & 0 & 0 \end{bmatrix} \tag{2.47}$$

$$D = \begin{bmatrix} 0 & 0 & 0 \end{bmatrix} \tag{2.48}$$

2.5.- Simulation Results for Traditional Control

Considering the designed controller for each area, low, middle and high speed in section classical control, together with the overall control scheme shown in Figure 2.19 and the realistic wind speed values taken in Borj Cedria, Tunis, where the plant we are focused on is installed. The obtained results are presented in Figure 2.20.

The first shows wind speed over time. The second and third plots shown rotational speed and torque, its values depend on wind speed. Notice that both variables never exceed its rated values. The fourth plot shown power coefficient which depend on blade pitch angle and tip speed ratio value. Both variable are shown in figure fifth and sixth plots respectively.

The cut in wind speed defined as the lowest wind speed at which the wind turbine starts to produce power is around 2.5m/seg. Below this speed, it is not efficient to turn on the turbine. Consequently, when the wind speed is lower that the cut in speed, the pitch angle is set to 90º which means full feathering of the blades while the tip speed ratio is set close to 0 so that the resulting power coefficient is null.

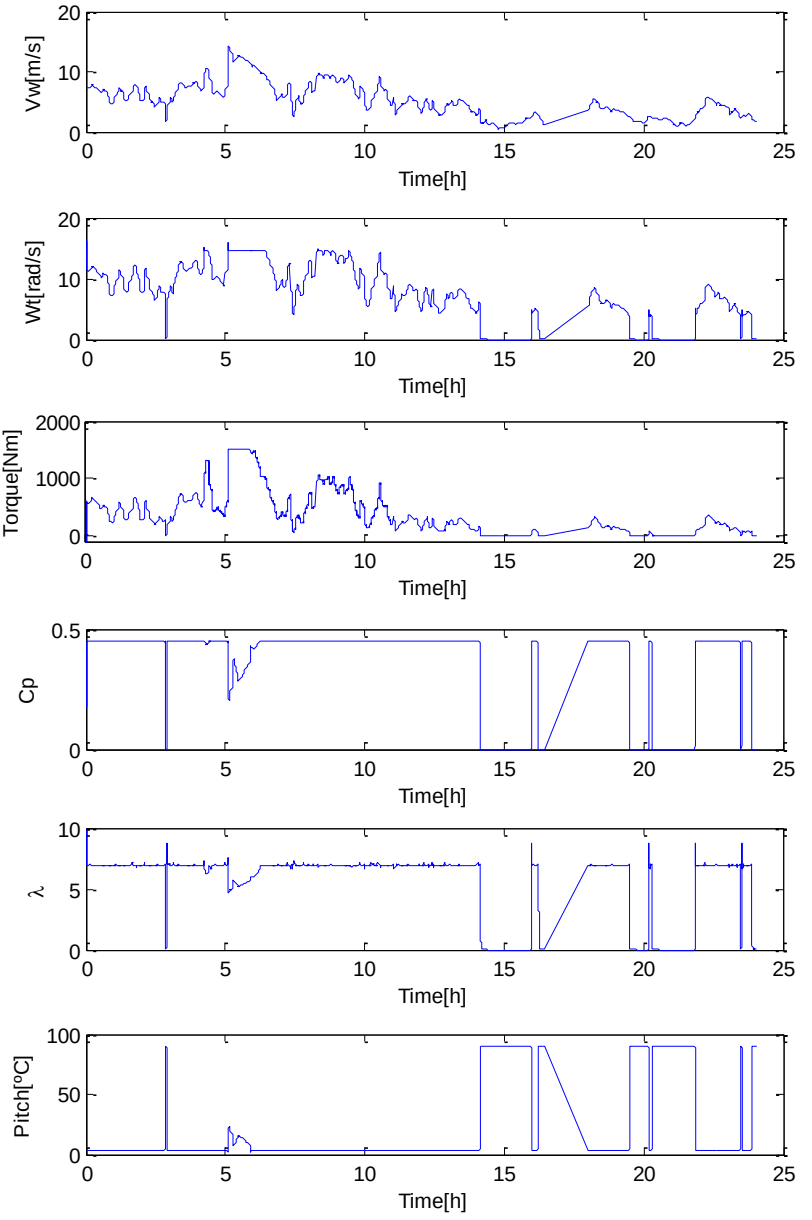

Figure 2.20.- System Response considering traditional PID control

Futhermore, when the wind speed is higher than 2.5m/s and less than the nominal wind speed 10m/s, the objective is to extract the maximum power from the wind. For this, the tip speed ratio and the pitch angle are set at its optimum values

6.96 and 3º respectively. As a result, the power coefficient obtained is close to 0.44. Notice, a wind turbine can extract at most 59% from wind power.

Finally, when the wind speed is higher than the nominal wind speed, the pitch angle starts to increase while the tip speed ratio starts to decrease with the aim to limit the power extracted from wind. In this case, the resulting power coefficiente is below its optimum value 0.44. The higher the wind speed gets, the smaller the power coefficient results. At this point, both the rotational speed and torque are limit to its rated value.

2.6.- Nonlinear Predictive Control

Nonlinear Predictive Control (NMPC) is an advanced control tool which predicts the future behavior of a system using a nonlinear internal model and the current measurements. With this information, the control actions necessary to regulate the plant are computed by solving an optimal control problem over a given time horizon. Part of the solution trajectory for the control inputs is transferred to the system, new measurements are obtained, and the optimal control problem is solved again at the next time step. Feedback is incorporated, since the current state of the turbine is implemented as the initial condition of the optimal control problem at the next time step. Multivariable control and constrains on actuator and states are incorporated in the optimization. The control overview scheme is shown in Figure 2.21.

The internal model must represent the process dynamic; predict the output signal quite accurately as well as being simple because the future control actions computed by the optimizer takes into account the integration of the model along the prediction horizon each sampling time. The dynamic model correspond to the wind turbine is given by equations from (2.1) to (2.24).

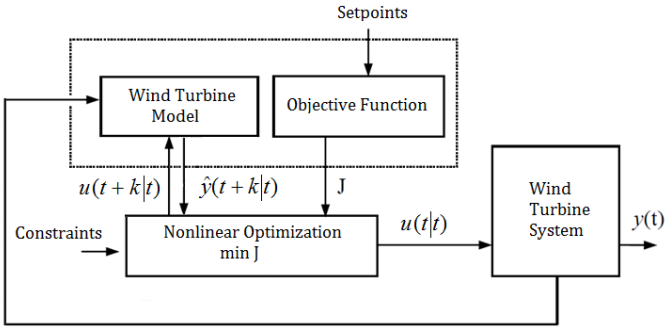

Figure 2.21.- Nonlinear Predictive Control scheme

The formulation of the wind turbine control problem can be described by (2.49) where the proposed optimization problem is to maximize the output power extracted by the wind turbine.

$$\max\ J = \sum_{N_1}^{N_2} \alpha_1(\tau)[\hat{P}_{el}(t+\tau|t)]^2 d\tau \tag{2.49}$$

Additionally, some constraints which have to be fulfilled are defined as follows:

- The rotational speed of the rotor ω is limited by a maximum value ω_{rated} considering specifications for the wind turbine, as shown in (2.50).

$$\hat{\omega}(t+\tau|t) \le 1.2\,\omega_{rated} \qquad \forall \tau \in [N_3, N_4] \tag{2.50}$$

- The pitch angle β is limited by a minimum $\underline{\beta}$ and a maximum $\overline{\beta}$ value, as presented in (2.51).

$$\underline{\beta} \le \beta(t+k|t) \le \overline{\beta} \qquad k = 1, \ldots, N_u \tag{2.51}$$

The advantage of this control strategy in reducing the variance of the output error will imply economic benefits and allow work close to constraints and optimal operating conditions, reducing the number of constraint violation and the number of costly emergency shut downs, ensuring maximize the energy extract from the wind turbine through the optimization of a cost function formulated with energy efficiency implications.

2.7.- Simulations Results for NMPC

An illustrate example performed under turbulent wind conditions in Matlab Simulink is given in Figure 2.22. A prediction horizon and a sampling time of 10 and 1 minute have been chosen respectively. As the optimizer takes into account the integration of the model along the prediction horizon each sampling time is necessary to use a complete and simplified process model able to compute the predicted outputs at future instants.

Similar to the traditional control, two areas can be identified: a limitation area when the wind speed is above the nominal value and an optimization area when the wind speed is below the nominal value.

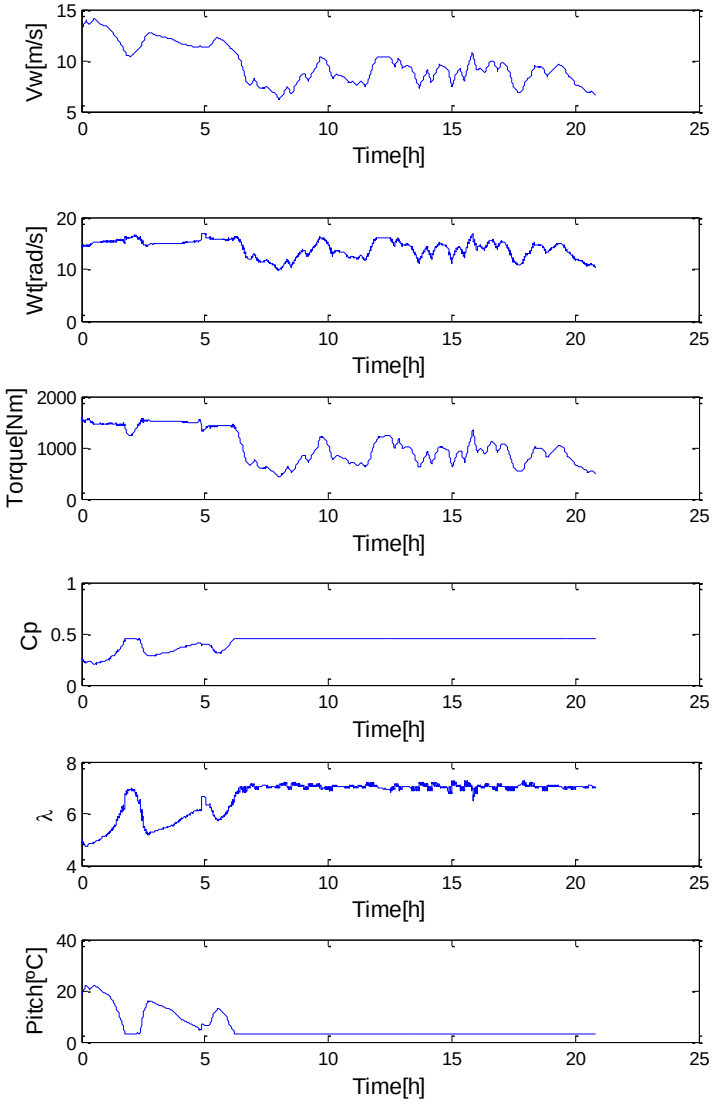

Figure 2.22.- System Response considering Nonlinear Predictive Control

From time t=0 until t=6 hours, the wind speed is above the nominal value, the pitch angle is a manipulated variables which is used for the controller to limit the amount of power taken from the wind and its value keeps inside the range [0º, 90º], the rotor rotational speed and the electromagnetic torque keeps close to its rated value 15.5 rad/s and 1400 Nm respectively.

From time t=6 hours, the wind speed is below the nominal value, the pitch angle is 0º, the power coefficient is close to its maximum value 0.5, the value of the rotor rotational speed and the generator electromagnetic torque depends on the

value of the wind and keep inside the ranges [0,16] rad/s and [0,1500] Nm respectively.

In both case, the NMPC controller is seen to be faster and overshoot less than the traditional controller.

2.8.- Conclusions

This work has presented the dynamic model of a wind turbine system equipped with a Permanent Magnet Synchronous Generator (PMSG) for simulation and controller design. A standard controller is designed, based on PI controllers at three operating regions. Some simulation results show that the expected responses are obtained. Furthermore, an advanced controller MPC have been designed and compared with the classical control strategy.

Controller tuning is a relatively well solved problem in the wind sector, since linear models based on linearization of nonlinear model are used. Although, the adequacy of the linearized models can be criticized since in many occasions the control parameters obtained by means of such procedure are not subsequently used in the real Wind turbine. Most of the times, control parameters are turned in real WTs based on the experience of the control engineer who proceeds according to rules of thumb or on a trial and error basis. Therefore, there is a need for obtaining relevant and accurate models which can effectively be used for controller tuning. The basic idea will be obtained a trustworthy model based on parameter estimation process and dynamic model for wind turbine.

Once a trustworthy model is build, validation test should be performed in order that the model will be qualified. The validation test helps to decide among several validated models which one is the best. At the end of the parameter estimation process, there will be one model which will be better in terms of the validation test applied to the set of proposed models. The objective is to find what plant model combined with torque and pitch controller provides the best prediction of the behavior of the true closed loop system.

CHAPTER 3

Solar and Wind Based Microgrid for Desalination

In order to combat water scarcity, intensive desalination activities are being carried out in arid and semi-arid regions (Postel, [49]). The main disadvantage of desalination plants is the intensive energy consumption (Fritzmann et al., [50]) (Wilf et al., [51]).

Desalination efforts now concentrate mainly on big desalination facilities, connected directly to a high-voltage electrical grid, and frequently placed near energy plants. However, this is not adequate for areas where population is sparse and infrastructures (pipelines, electrical grid) are inadequate or nonexistent. Thus, a more cost-effective solution is the local production of energy for the desalination facilities (normally in an off-grid structure, with no external transmission lines). This is especially relevant in remote areas, where power grid connections do not have sufficient excess capacity to power a desalination plant (Seibert et al., [52]) (Amer et al., [53]).

Nowadays, the usual approach for remote areas is to power the plants through big diesel generators. This approach is not sustainable from an environmental point of view and depends on the constant supply of cheap fuel (Kalogirou, [54]). Unfortunately, fossil fuel resources are limited, cause greenhouse emissions, and are expected to increase in costs due to an increase in demand. In consequence, the design of an integrated system that combines water and electricity generation with a high degree of automation has been considered in order to make more efficient use of energy: Reverse Osmosis (RO) emerges as a feasible desalination technology, while renewable energy sources also emerge as a necessary complement, and the decentralization of water and electricity supplies emerges as a solution to this particular problem (Setiawan et al., [55]).

In this chapter, the application of hybrid predictive control to a solar and wind based microgrid for desalination is described and the results are shown.

3.1.- Process Description

A central aspect is the design of an integrated system (s. Figure 3.1) that supplies energy to small Reverse Osmosis plants through local renewable energies.

The Reverse Osmosis (RO) technology is at present the most versatile desalination method. It is known to be a cost-effective solution to produce drinkable water from underground and sea water. Currently, RO plants need less energy, investment cost, space requirements and maintenance than other desalination processes (Gambier et al., [56]), so they are being extensively implanted in fresh-water depleted areas (Baker, [57]).

Thus, the approach presented here is based on adapting the water production along the day, adjusting water production and water consumption. This significantly reduces the tank sizes and decreases the loss of drinkable water by evaporation.

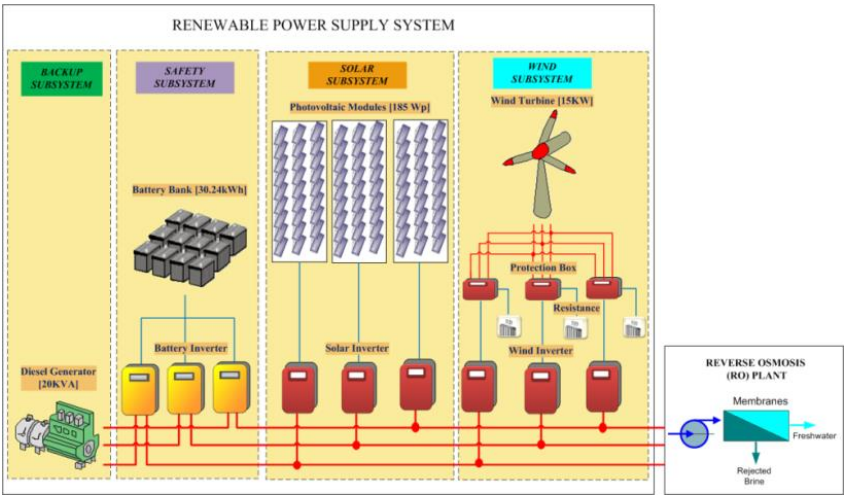

Figure 3.1.- Microgrid for desalination in remote areas

As the target regions are arid, solar energy should be the preferred energy source. Although water demand is usually higher when the solar radiance is higher, most of the day no energy is provided by the solar panels, so they are complemented with a small wind turbine, that provides the minimal energy required when solar energy is not available. Unfortunately, the short-term unreliability of these renewable energy sources is well-known (in the presence of clouds, wind gusts, etc.). Thus, as the water demand must always be fulfilled, a backup system is

needed. The most logical approach is to use a diesel generator to keep the RO plant running when the production of renewable energies is low. Nevertheless, big diesel generators are expensive, noisy, and not environment-friendly.

Additionally, some batteries will be used to temporally store the extra energy generated by the renewable sources. However, batteries need special care of their charge/discharge cycles, due to the fact that they reduce their capacity and lifetime.

In the past, power supplies were based on a mixed DC- and AC-coupled concept (s. Figure 3.2), where PV and wind turbine are coupled on the DC-side with the battery as central component. In these systems, AC-loads are supplied by battery inverters which, in some cases, also act as battery chargers supplied by AC-generators (e.g. Diesel). These systems are not usually extendable and show a complicated DC system design and therefore high system costs (Hammerstrom, [58]). The power from the DC-side sources coupled power generator (e.g. PV, wind turbine) is limited by the rated power of the battery inverter.

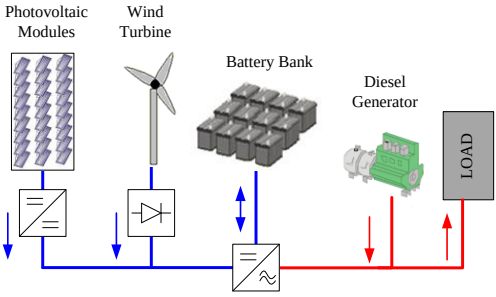

Figure 3.2.- Mixed DC and AC coupled concept

To overcome the problems associated with the use of DC-Technology in off-grid systems, the concept of (Pure) AC coupling (s. Figure 3.3) is used here (Kleinkauf, [59]). "Pure AC coupled" systems, where all consumers and generators are coupled independently and equitably on a common AC-bus, are currently evolving as a standard due to numerous advantages (Cramer et al. 2003, 2004 [60][61]):

- Expandability of the system to any size at any time
- Simplified design and operation of island grids
- Standardized coupling of different components (ACcoupling)
- Off-the-shelf components can be used.

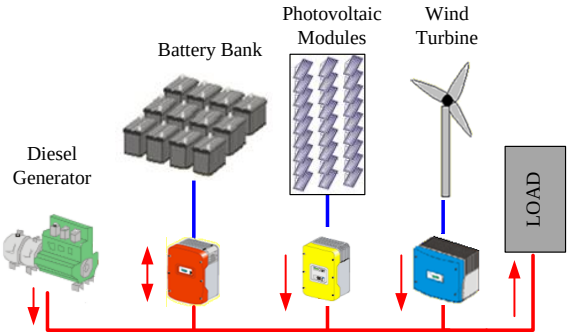

Figure 3.3.- Pure AC coupled concept

Figure 3.4.- Prototype built at Borj Cedria by Open-Gain Workgroup

In order to gain real experience with the new system concept, a prototype was built at Bordj Cedria in Tunis (Salazar et al., [62]) by the Open-Gain Workgroup as is shown in Figure 3.4. The workgroup was integrated by professors and PhD students coming from Germany, Greece, Spain, Tunisia, Lebanon, Jordan and Algeria. All members are specialized in desalination, renewable energy or automation. The main Open-Gain objective was to offer a solution to cost optimal co-production of energy and water using renewable energy besides conventional sources. The optimization of water and electricity production using renewable

energy (wind and solar) made possible to reduce the variability in energy production. The components prototype will be given in the following sections.

The first proposed control strategy based on the prototype built by the Open Gain workgroup was developed in Palacin et al [63] (s. Figure 3.5).

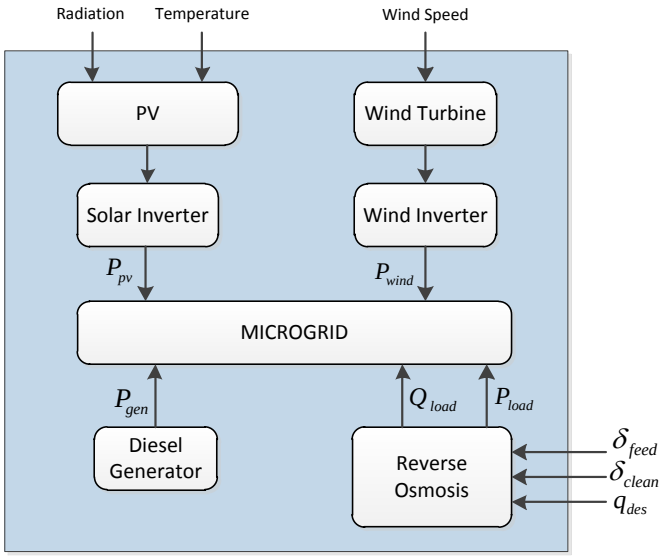

Figure 3.5.- Control strategy proposed by Open Gain workgroup [63].

The integrated system was comprised by some solar panel arrays, a wind turbine, a conventional energy source (diesel generator) with a controllable output power and the reverse osmosis desalination plant. Notice that a battery bank was not available in the energy supply system. In this case, the manipulated variables taken into account are:

- The binary variable (δ_{feed}) associated to the supply pump
- The binary variable (δ_{clean}) related to periodic cleanings of the membranes
- The water flow through membranes when the plant is producing drinkable water (q_{des}).

The measured variables related to the nomenclature used in the modeling are described below:

- The electric power consumed or generated by the battery bank: P_{bat}
- The electric power generated by the solar panels: P_{pv}

- The electric power generated by the wind turbine: P_{wind}
- The electric power consumed by the load: P_{load}
- The state of charge of the battery bank: SOC
- The electric power generated by the diesel generator: P_{gen}
- The solar radiation, ambient temperature and wind speed: G, T_{env}, v_{wind}

The main objective of the control problem is to fulfill the water demand, make an effective use of the available renewable energies and avoid underflows or overflows of the water storage tanks during a given time horizon 48h. For this, a model predictive control in combination with hourly predictions of renewable energies and water demand are used to schedule adequately the amount of energy takes from the conventional energy source, the cleaning periods and the switching ON/OFF of the supply pump. The conventional energy source is used only when the energy consumption of the desalination is greater than the available renewable energy. The main difficulty founded in this control strategy is when the available renewable energy exceeds the energy consumption and the water storage tanks are filled, so that there are no storage devices available to save the extra energy. In this case, the disconnection of one or all renewable energy sources is proposed as a possible solution.

In this thesis, a model predictive control is proposed for the system shown in Figure 3.6.

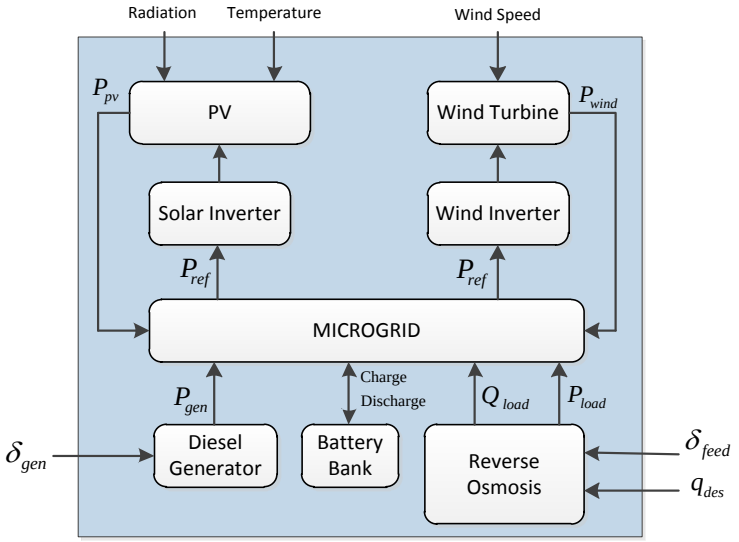

Figure 3.6.- Wind and solar based microgrid used in this thesis

The system is comprised by some solar panel arrays, a wind turbine, a battery bank, a diesel generator and a reverse osmosis desalination plant. Notice that each renewable source is connected to an inverter which controls the injection to the microgrid, considering weather and demand conditions. The battery inverter is responsible for charging and discharging of the battery and the quality of the power supply (voltage and frequency regulation). Thus, the manipulated variables taken into account are:

- The binary variable (δ_{gen}) of the diesel generator controller. When the value of the variable δ_{gen} is 1, the diesel generator is active, and when it is 0, energy is produced by diesel generator.
- The binary variable (δ_{feed}) of the feed pump controller. When the value of the variable δ_{feed} is 1, the PLC fills the primary tank (T1).
- The water flow through membranes when the plant is producing drinkable water (q_{des}).

The main objectives of the proposed controller

- Fulfill the water demand
- Minimize the use of the diesel generator
- Make an effective use of the available renewable energies and the stored energy without reducing the lifetime of the components due to excessive intermittent operation.

Predictions of renewable energies, state of charge of battery and water demand per second are used to calculate the manipulated variable. It must be pointed out that the time instant when the desalination plant should start the cleaning task has not been considered as the sample time required in the proposed predictive controller is much lower than one defined in Palacin et al. [63].

Additionally, a library on microsources of renewable and conventional energies has been developed in Ecosimpro based on the real experience obtained from the prototype built by the Open Gain Workgroup. The mathematical models include in the library will be given in the following sections. Some additional information could be found in Appendix A. The results have been presented in (Salazar et al., [64]).

3.2.- Renewable Energy Source Model

As it has mentioned before, the proposed Energy Management System is based on an internal model which is used to predict how performance depends on present and future control actions, which are then selected to optimize the performance of the process.

To obtain trustworthy results of the optimization, we must provide a reliable model of the plant at the optimizer, but at the same time it must be simple, due to the fact that the model must be evaluated by the optimizer several times, and this must happen in every sampling period.

3.2.1.- Wind Turbine

The main components of the wind turbine system includes the blades, which take a part of the wind energy available, a drive train, where energy is transferred from the blades to a synchronous generator (PMSG), and a synchronous generator which converts mechanical to electrical energy. An electronic power interface comprised by a microsource side converter (AC/DC), a grid side converter (DC/AC), an AC filter and a transformer is required for connecting the wind turbine to main grid as shown in Figure 3.7 (Salazar et al., [65]). Both the microsource and grid side converter are implemented using Pulse Width Modulation (PWM). The microsource side converter works as a rectifier, while the grid side converter works as an inverter and includes a local secondary control which will be explained later.

In order to transfer all the energy available in the microsource side to the grid side, the main objective is to reduce the energy stored in the capacitor of the DC link maintaining its voltage. Notice that the difference between the instantaneous power from the microsource side converter and the one taken by the grid side converter is equal to the variation of the energy stored in the capacitor time.

The AC filter in Figure 3.7 reduces the high frequency harmonic content of the current caused by the PWM converter. Finally, the low frequency transformer provides a galvanic isolation between the wind turbine and main grid.

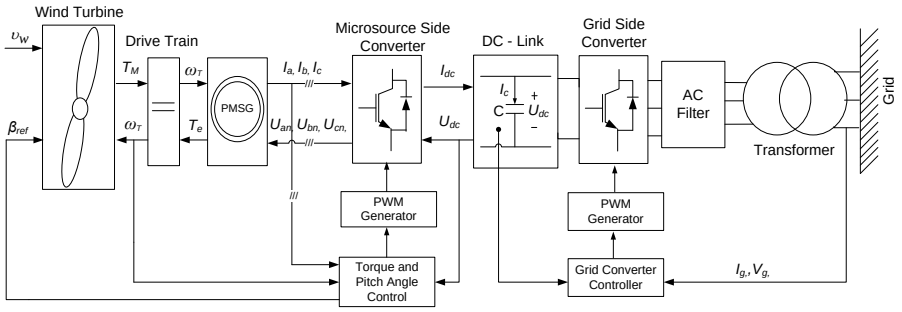

Figure 3.7.- Wind Turbine control diagram

To obtain an adequate model for the Energy Management System, the fast transients related to the commutation of solid state switches, due to the Pulse Width Modulation used, are not considered, detailed modeling of the inverters is avoided and the long-term dynamical models of the inverters are ignored. Furthermore, a

simple model is assumed for the wind turbine, by using the fact that the time constants of the pitch actuator and the generator are smaller than the response time of the plant.

The controllers designed and implemented in this thesis for a variable speed wind turbine considering a normal operation with the absence of grid voltaje dips. However, when a grid voltage dips occurs, the DC link voltages increase rapidly to avoid the flow of active power coming from the generator to the grid (Ibrahim et al., [66]). In (Ibrahim et al., [67]) a novel topology based on series voltage compensation using magnetic amplifiers is proposed to reduce the DC link voltage rise as well as limiting the stresses on the power electronics converters in case of grid voltage dips.

As mentioned in Chapter II, the control strategy for the wind generator is based on dividing the operation into three distinct regions (s. Figure 3.8) based on wind speed:

- Region I consists of low wind speeds: the turbine runs at the maximum efficiency to extract all power.
- Region II is a transition region, to keep rotor torque low.
- Region III consists of high wind speeds: the turbine speed is limited to keep the generated power at the rated value.

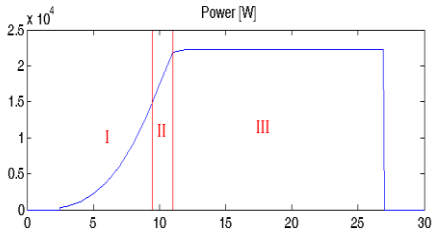

Figure 3.8.- Operating Regions of Wind Turbine

The power in the wind is known to be proportional to the cube of the wind speed υ_w, so it may be expressed as (3.1), where A is the area swept by the blades, ρ is the air density. Moreover, the wind output power is limited by a maximum value P_{max} which will be taken into account.

$$P_{wind} = \frac{1}{2} C_p \rho A \upsilon_w^3 \tag{3.1}$$

The fraction of the power that can be extracted by the wind turbine (limited by the Betz limit of 59%) is described by the power coefficient, C_p, which is a function of the blade pitch angle β and the tip speed ratio λ, which depends on the rotational

speed, as shown in (3.2). Therefore, the power coefficient is given by (3.3), where P_a, P_b, P_c, P_d and P_e are unknown parameters that are experimentally estimated, and σ can be expressed as (3.4), where P_h and P_g are unknown parameters, which also are experimentally estimated.

$$\lambda = \frac{\omega_T R}{\upsilon_w} \tag{3.2}$$

$$C_p(\lambda,\beta) = P_a\left(\frac{P_b}{\sigma} - P_c\beta - P_d\right)exp\left(\frac{P_e}{\sigma}\right) + P_f\lambda \tag{3.3}$$

$$\sigma = \left[\frac{1}{\lambda + P_g\beta} - \frac{P_h}{\beta^3 + 1}\right]^{-1} \tag{3.4}$$

Finally, the operational rotational speed ω_T can be expressed as (3.5), where λ_{opt} is the optimum tip-speed ratio which combines with the optimum pitch angle β_{opt}, giving the maximum power coefficient C_{pmax}. It must be pointed out that the rotational speed is limited by a maximum $\overline{\omega_T}$ and a minimum $\underline{\omega_T}$ value.

$$\omega_T = \frac{\lambda_{opt}\upsilon_w}{R} \tag{3.5}$$

3.2.2.- Solar Panels Model

The photovoltaic system shown in Figure 3.9 comprises a PV array, a microsource side converter (DC/DC) represented by a boost circuit, a grid side converter (DC/AC), an AC line filter and a transformer. The boost controller chose the solar array operating point, while the grid side converter controls the DC-link capacitor voltage to guarantee that energy generated by the solar panels will be transferred to the grid (or microgrid). The grid converter also includes a local secondary control which will be explained later. Both microsource and grid side converters are implemented using Pulse Width Modulation (PWM). The line filter reduces the high frequency harmonic content of the line current caused by the PWM converter. Finally, the low frequency transformer provides a galvanic isolation between the solar panels and the grid.

Again, to simplify the model used by the Energy Management System, the fast transients due to the solid state switches are not considered, detailed modeling of the inverters is avoided and the microsource side converter model is a first order transfer function.

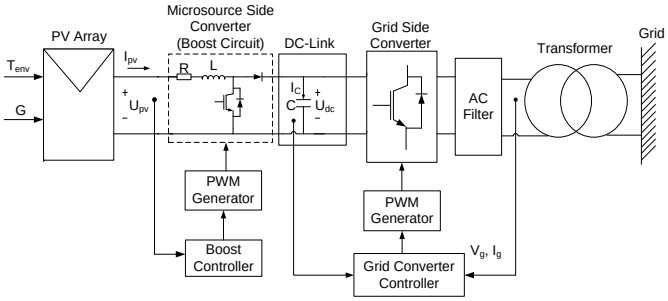

Figure 3.9.- Photovoltaic Panels control diagram

Photovoltaic Arrays Model

The building block of PV arrays is the solar cell, which is basically a p-n semiconductor junction that directly converts solar irradiation into DC current using the photovoltaic effect. As a starting point the simple equivalent circuit of a solar cell shown in Figure 3.10 is used here: a current source in parallel with a diode (Chouder et al., [68]).

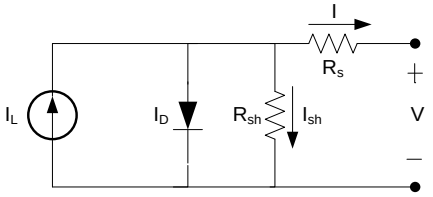

Figure 3.10.- Circuit diagram of a solar cell

The series resistance R_s represents the internal losses due to the current flow, the shunt resistance R_{sh} corresponds to the leakage current and V_t is the thermal voltage. The characteristic equation is then (3.6).

$$I = I_L - I_{sc}\left(\exp\left(\frac{V + R_s I}{v_t}\right) - 1\right) - \frac{(V + R_s I)}{R_{sh}} \tag{3.6}$$

As further simplification, the shunt resistance R_{sh} is neglected, I_L is assumed to be equal to I_{sc} and $\exp((V+R_sI)/v_t)$ is assumed to be much greater than 1. The open circuit voltage is then included in the characteristic equation to comply with the boundary conditions $I(V_{oc})=0$ and $I(V=0)=I_{sc}$. Then, the resulting characteristic equation is (3.7).

$$I = I_{sc}\left[1 - \exp\left(\frac{V + R_s I - V_{oc}}{v_t}\right)\right] \tag{3.7}$$

PV cells are grouped together in larger units known as PV modules or arrays, which are combined in series and parallel to provide the desired output voltage and current. The mathematical model that predicts the power production of the PV array is then (3.8), where V_{pv} and I_{pv} are the output voltage and current of the PV array, respectively, R_{sg} is the series resistance of the PV array, I_{scg} is the short circuit current, V_{ocg} is the open circuit voltage, N_{sc} is the number of cells in series within the PV module and N_{sm} is the number of modules in series within the PV array (Salazar et al., [69]).

$$I_{pv} = I_{scg}\left[1 - \exp\left(\frac{V_{pv} + R_{sg} I_{pv} - V_{ocg}}{v_t N_{sm} N_{sc}}\right)\right] \tag{3.8}$$

Temperature and solar irradiation effects

If the temperature and solar irradiation levels change, the voltage and current outputs of the PV array will change. Hence, the effects of the changes in temperature and solar irradiation levels should also be included in the final PV array model. A method to include these effects in the PV array modeling is described now.

The characteristic equation to define the module operating temperature T_C [ºC] as a function of the ambient temperature T_{amb} [ºC] and the solar irradiation G [W/m^2] is described in (3.9), where *NOCT* is the Nominal Operation Cell Temperature (ºC) at standard test conditions (STC). The test conditions are an irradiance level of 1000 W/m^2, with the reference air mass 1.5 solar spectral irradiance distribution and module junction temperature T_{ref} of 25°C.

$$T_C = T_{amb} + G\left(\frac{NOCT - 20}{800}\right) \tag{3.9}$$

The cell temperature T_C affects the module open circuit voltage V_{ocm} and the module short circuit current I_{scm}. These effects are represented in the model by the temperature coefficients β and α for V_{ocm} and I_{scm}, respectively, as shown in (3.10) and (3.11), where $I_{scm,stc}$ and $V_{ocm,stc}$ are short circuit current and open circuit voltage for the solar module at STC, respectively.

$$V_{ocm} = V_{ocm,stc}\left(1 + \frac{\beta(T_C - T_{ref})}{100}\right) \tag{3.10}$$

$$I_{scm} = \frac{I_{scm,stc}G}{G_{stc}}\left(1 + \frac{\alpha(T_C - T_{ref})}{100}\right) \tag{3.11}$$

Normalized Resistance Model

The normalized resistance R_{sm} taken into account to compute the series resistance within the solar module r_s is described in (3.12).

$$R_{sm} = \frac{V_{ocm,stc}}{I_{scm,stc}} r_s \tag{3.12}$$

Similarly, the form factor for a solar cell under standard conditions, and the form factor for an ideal cell without the resistance in series are considered to compute the normalized resistance as shown in (3.13).

$$r_s = 1 - \frac{FF}{FF_o} \tag{3.13}$$

The form factor for a solar cell under standard conditions is defined as (3.14), while the form factor for an ideal cell without the resistance in series is given by (3.15). V_{ocn} is known as the normalized open circuit voltage for a solar cell, described as (3.16), where V_{oc}, I_{sc} and P_{max} are the open circuit voltage (V), the short circuit current (A) and the maximum power (W) for a solar cell, and can be expressed as is presented in (3.17), (3.18) and (3.19).

$$FF = \frac{P_{\max}}{I_{sc}V_{oc}} \tag{3.14}$$

$$FF_o = \frac{V_{ocn} - \log(V_{ocn} + 0.72)}{V_{ocn} + 1} \tag{3.15}$$

$$V_{ocn} = \frac{V_{oc}}{v_t} \tag{3.16}$$

$$V_{oc} = \frac{V_{ocm,stc}}{N_{sc}} \tag{3.17}$$

$$I_{sc} = \frac{I_{scm,stc}}{N_{pc}} \tag{3.18}$$

$$P_{\max} = \frac{P_{\max m,stc}}{N_{pc} N_{sc}} \tag{3.19}$$

Maximum Power Point Tracking (MPPT)

PV systems normally use a maximum power point tracking (MPPT) technique to continuously deliver the highest possible power when variations in the irradiance and temperature occur. In consequence, the maximum power point tracking (MPPT) control is critical for the success of a PV system. MPPT algorithms, ranging from simple hill-climbing algorithms to fuzzy logic and neural network algorithms, have been considered extensively in the literature (Esram et al., [70]) (Yahyaoui, [71]) (M'Sirdi et al., [72]).

As the maximum power point tracking (MPPT) control is faster than the dynamic of the plant, the derivative of the power with respect to the voltage was used instead of an algorithm. For this purpose, the equations are shown in (3.20), (3.21), (3.22), (3.23), (3.24), (3.25) and (3.26), where P_{solar} is the solar output power (W), I_{max} and V_{max} are the current and the voltage at maximum power, N_{sm} and N_{pm} are the number of modules in series and in parallel within the PV array, N_{sc} is the number of cells in series within the PV module, I_{scg} and V_{ocg} are the short circuit current (A) and the open circuit voltage (V) for the PV array, v_t is the thermal voltage (V) and R_{sg} is the series resistance within the PV array. The variables R_{sm}, I_{scg} and V_{ocg} are defined above in (3.12), (3.25) and (3.24), respectively.

$$V_{\max} = \left(v_t N_{sm} N_{sc}\right) \log\left(1 - \frac{I_{\max}}{I_{scg}}\right) + V_{ocg} - I_{\max} R_{sg} \tag{3.20}$$

$$\frac{dI}{dV} = \frac{-\frac{I_{scg}}{v_t N_{sm} N_{sc}} \exp\left(\frac{V_{\max} + I_{\max} R_{sg} - V_{ocg}}{v_t N_{sm} N_{sc}}\right)}{1 + \frac{I_{scg}}{v_t N_{sm} N_{sc}} \exp\left(\frac{V_{\max} + I_{\max} R_{sg} - V_{ocg}}{v_t N_{sm} N_{sc}}\right) R_{sg}} \tag{3.21}$$

$$I_{\max} = -V_{\max} \frac{dI}{dV} \tag{3.22}$$

$$P_{solar} = I_{\max} V_{\max} \tag{3.23}$$

$$V_{ocg} = N_{sm} V_{ocm} \tag{3.24}$$

$$I_{scg} = N_{pm} I_{scm} \tag{3.25}$$

$$R_{sg} = R_{sm} \frac{N_{sm}}{N_{pm}} \tag{3.26}$$

The simulated I-V and P-V characteristics of such a system, deduced from equation (3.8), are represented in Figure 3.11 considering the parameters given in Table 3.1 which have been defined considering datasheet specifications of the solar panels used in the Open-Gain plant. Notice the MPP, short circuit current I_{scg} and open circuit voltage V_{ocg} of the PV array (Zegaoui et al., [73]).

Variable		Unit	Value
Open Circuit Voltage	$V_{ocm,stc}$	Volts	44.8
Short Circuit Current	$I_{scm,stc}$	Amps	5.51
Normal Operating Cell Temperature	$NOCT$	ºC	46
Voltage at maximum power	$V_{mpm,stc}$	Volts	36.2
Current at maximum power	$I_{mpm,stc}$	Amps	5.11
Maximum Power	$P_{maxm,stc}$	Wp	185
Reference Temperature	T_{ref}	ºC	25
Standard Solar Radiation	G_{stc}	Wm^{-2}	1000
Sensitivity of Open Circuit voltage to temperature	B	% $ºC^{-1}$	-0.38
Sensitivity of Short Circuit Current to temperature	A	% $ºC^{-1}$	0.10
Sensitivity of Maximum Power to temperature	Γ	% $ºC^{-1}$	-0.47
Module Surface	S_{urface}	m^2	1.277
Number of cells in series within PV module	N_{SC}	-	12
Number of cells in parallel within PV module	N_{pc}	-	6
Modules efficiency	$E_{fficiency}$	%	14.8
Number of modules in parallel within the PV array	N_{pm}	-	3
Number of modules in series within PV array	N_{sm}	-	9
Thermal voltage	V_t	Volts	0.0248

Table 3.1.- Solar Panel Parameters

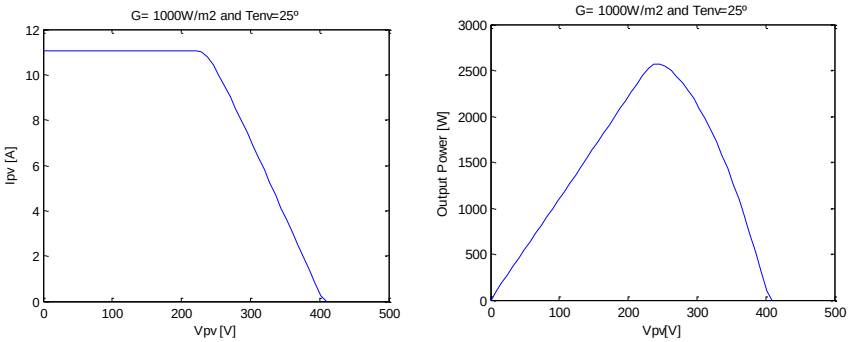

Figure 3.11.- I-V and P-V photovoltaic array characteristic

The change of irradiance results in vertical shifting of the IV curve of the PV array, as shown in Figure 3.12. This change can be implemented as the shifting of the maximum operating current and the short-circuited current values. Figure 3.13 shows how the MPP moves with the irradiation on a constant voltage.

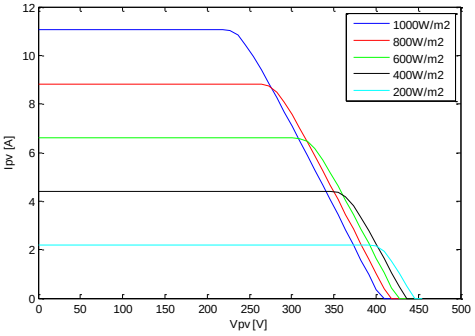

Figure 3.12.- Irradiation influence on PV array characteristics I-V curves

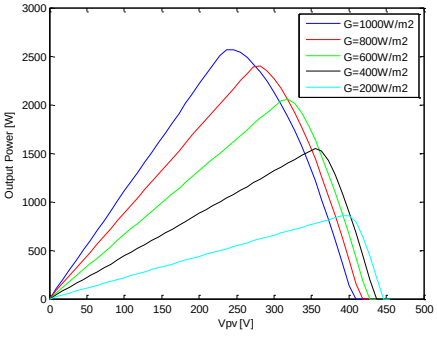

Figure 3.13.- Irradiation influence on PV array characteristics P-V curves

The influence of the temperature at constant irradiation is shown in Figure 3.14. The change results in shifting the IV curve horizontally. Figure 3.15 shows how the MPP moves with the temperature on a constant voltage.

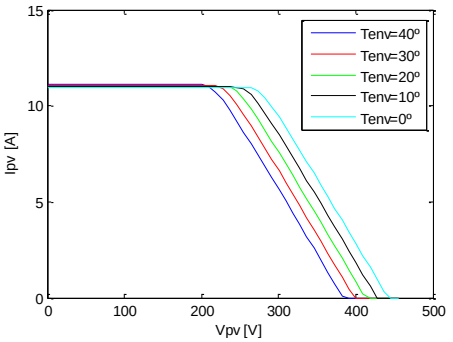

Figure 3.14.- Temperature influence on PV array characteristics I-V curves

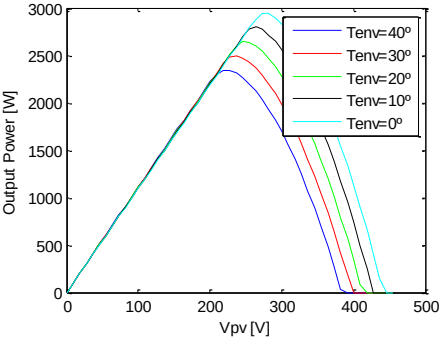

Figure 3.15.- Temperature influence on PV array characteristics P-V curves

3.2.3.- Battery Bank Model

Nowadays, many dynamic models are available for batteries (Barsali et al., [74]), (Manwell et al., [75]). These models are mainly concerned with stationary working point conditions as a result of the complex response of this element.

The simple battery model used in an application is shown in Figure 3.16. It consists of a variable voltage source V_g and a variable resistor R_g. This first generic model includes the main variables of the system: the battery state of charge SOC and the current flowing to the battery I_{bat}:

$$V_{bat}(SOC, I_{bat}) = V_g(SOC) + R_g(SOC, I_{bat}) * I_{bat}(SOC, I_{bat}) \tag{3.27}$$

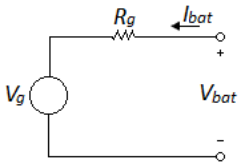

Figure 3.16.- Circuit diagram of a battery

The voltage source $V_g(SOC)$ represents the voltage at open circuit between the battery terminals. This voltage is due to energy stored in the battery through the electrochemical reactions, so it depends directly on the energy stored, expressed using the SOC. On the other hand, $R_g(SOC, I_{bat})$ represents the resistance that the battery offers to the energy flow producing energy lossed during charging and discharging. This value includes the effects of working point (SOC, I_{bat}) and the health of the battery (as an effect of aging due to charging/discharging the battery).

For the Energy Management System, on input is the battery power P_{bat}, which is positive when power is demanded from the battery bank and negative when power is supplied to the battery bank. The battery current is calculated as defined in (3.28), where N_b is the number of batteries in series that constitute the battery bank.

$$I_{bat} = \frac{P_{bat}}{V_{bat} N_b} \tag{3.28}$$

An essential term is the state of charge of the battery, which is the relation between the energy accepted and the rated capacity. Th expression is given by (3.29), where the integral models the energy accepted over the battery's working life, and the term outside the integral SOC models the battery capacity. C_{nom} is the rated battery capacity, η(t) is the charging efficiency and I_{bat}(t) the current flowing through it. The state of charge (SOC) ranges from 0 when the batteries are completely discharged to 1 when the batteries are completely charged.

$$SOC(t_i) = \frac{\int_0^t \eta(\tau) I_{bat}(\tau) d\tau}{C_{nom}} \tag{3.29}$$

In practice, due to the ample dependence of V_g and R_g with SOC and I_{bat}, an experimental model is used, using two working zones depending on the sign of the battery current: charges and discharges. This model is now presented:

a) Charge Model

If power is applied to the battery, energy is absorbed and causes the voltage to increase. A charge efficiency factor, η(t), must be considered in order to reflect that

only a fraction of the theoretical energy is really stored, as described in (3.30) and (3.31) (Guasch et al., [76]).

$$V_{bat}(t) = \left[V_{boc} - K_{boc} SOC(t)\right] - \frac{I_{bat}(t)}{C_{10}} \left(\frac{P_{1c}}{1 + I_{bat}(t)^{P_{2c}}} + \frac{P_{3c}}{\left(1 - SOC(t)\right)^{P_{4c}}} + P_{5c} \right) \tag{3.30}$$

$$\eta(t) = 1 - \exp\left(\frac{\alpha_{cmt}}{\left(\frac{I_{bat}(t)}{I_{10}} + b_{cmt} \right)} \left(SOC(t) - 1\right) \right) \tag{3.31}$$

b) Discharge Model

In this area the battery is delivering energy to the system. The battery voltage is determined by the following equations:

$$V_{bat}(t) = \left[V_{bodc} - K_{bodc}\left(1 - SOC(t)\right)\right] - \frac{\left|I_{bat}(t)\right|}{C_{10}} \left(\frac{P_{1dc}}{1 + \left|I_{bat}(t)\right|^{P_{2dc}}} + \frac{P_{3dc}}{SOC(t)^{P_{4dc}}} + P_{5dc} \right) \tag{3.32}$$

As an example, the parameters given by the Table 3.2 correspond to the battery used in the Open-Gain plant.

Variable		Unit	Value
N_b	Number of batteries in series	-	24
C_{nom}	Rated Battery Capacity	Ah	5000
V_{boc}	Extra voltage when the battery is charged	Volts	2
K_{boc}	Constant which relates open circuit voltage to state of charge	Volts	0.16
P_{1c}	Loss coefficients associated with the internal resistance	Vah	6
P_{2c}	Loss coefficients associated with the internal resistance	-	0.86
P_{3c}	Loss coefficients associated with the internal resistance	Vh	0.48
P_{4c}	Loss coefficients associated with the internal resistance	-	1.2
P_{5c}	Loss coefficients associated with the internal resistance	Vh	0.036
α_{cmt}	Model Parameter to be estimated	-	20.73
b_{cmt}	Model Parameter to be estimated	-	0.55
V_{bodc}	Residual voltage when the battery is discharged	Volts	2.085
K_{bodc}	Constant which relates open circuit voltage to state of charge	Volts	0.12
P_{1dc}	Loss coefficients associated with the internal resistance	Vah	4

P_{2dc}	Loss coefficients associated with the internal resistance	-	1.3
P_{3dc}	Loss coefficients associated with the internal resistance	Vh	0.27
P_{4dc}	Loss coefficients associated with the internal resistance	-	1.5
P_{5dc}	Loss coefficients associated with the internal resistance	Vh	0.02

Table 3.2.- Battery Bank Parameters

3.2.4.- Diesel Generator Model

The diesel generator is considered to have three main components: the diesel engine, the synchronous generator and the excitation system (s. Figure 3.17). A complete model of the diesel generator is detailed in Wellstead et al. [77]. As the dynamics of all those components are several orders of magnitude faster than the dynamics of the rest of the system, a first order system will be used here.

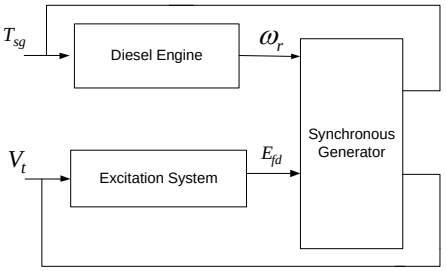

Figure 3.17.- The overall block diagram of diesel generator

3.3.- Microgrid Operation Model

A MicroGrid (MG) can be defined as the set formed by a Low Voltage network, its loads and the modular generation units (called here MicroSources - MS). Most MicroSources installed in a MG are connected through power electronics interfaces (DC/AC or AC/DC/AC inverters are required). Thus, inverter control is a central concern in MicroGrids.

The MG is intended to operate in two different operating conditions:

- *Connected mode:* The MicroGrid is connected to a small diesel generator, so frequency and voltage are provided by the diesel generator controller. All inverters act as current sources (slaves), following the reference from the diesel generator controller.

- *Island mode:* The MicroGrid is not connected to a diesel generator, so frequency and voltage references are provided by one inverter which acts as a voltage source (VSI – Voltage Source Inverter). In this case, one inverter connected to the battery bank acts as a voltage source (master) and the other inverters act as current sources (slaves), following the reference from the VSI.

In both cases, wind and solar inverters act as current source (slaves), without any participation in the voltage or frequency regulation, following the reference frequency and voltage fixed by the diesel generator (in connected mode) or battery inverter (in island mode). The battery inverter acts as a voltage or current source inverter depending on MicroGrid operation: In connected mode, it acts as current source inverter (slave), following the reference defined by the diesel generator whereas in island mode, it acts as voltage source inverter to guarantee stable power by defining the references for voltage and frequency.

Additionally, the battery inverter is responsible for the control of charging and discharging the battery bank, providing the reference for the charging voltage. The battery inverter functions as inverter or rectifier charger mode: In the inverter mode, it converts direct current (DC) from the battery bank into alternating current (AC), which is injected into the AC bus. When the total power generated by the PV generator and the wind turbine exceeds the load needs, it will act as rectifier charger to charge the battery bank.

The control of a Microgrid does not use external communication channels, using droop control methods. A small droop is acceptable as long as it remains within predefined limits. The droop control methods can be related to an inductive coupling (called conventional), or a resistive coupling (called oppositive). Low voltage grids are characterized by a resistive coupling, so an opposite droop control is used. However, an inductive coupling is frequently used, as it is compatible with high voltage, and allows power sharing with rotating generators and a precise power dispatch. The applicability of the conventional droops in low-voltage grids is studied in Engler [79].

For the conventional droops, the variation in the grid's frequency f depends on its current active power supply P, (see Figure 3.18), and the variation of the grid's voltage U depends on its current reactive power supply Q, (see Figure 3.19), as described in (3.33) and (3.34), where S_{t1} and S_{t2} are the droop slopes (positive quantities), f_o and U_o are the nominal frequency and nominal grid voltage respectively, and P_o and Q_o are the nominal active and reactive powers of the inverter.

$$f = f_o + S_{t1}(P - P_o) \tag{3.33}$$

$$\left|U_{ref}\right| = U_o + S_{t2}(Q - Q_o) \tag{3.34}$$

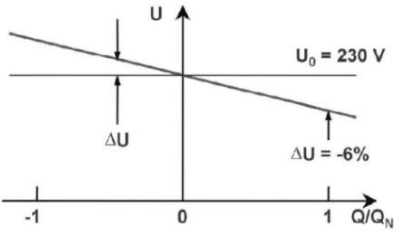

Figure 3.18.- Droop Mode: Active Power/Frequency-relation

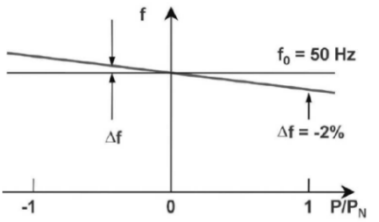

Figure 3.19.- Droop Mode: Reactive Power/Voltage-relation

The main principle of the voltage and frequency droop control is to use the active and reactive power exchanged between a generator or storage unit and the grid to control the grid voltage magnitude and frequency. The droop algorithm operates as follows:

- When the active power supply rises, the frequency is reduced, from the nominal frequency f_o. This reduction Δf is -2 % of the nominal frequency (1 Hz) when the active power supply is the nominal active power P_N.
- When the reactive power supply rises, the voltage is reduced, starting from the nominal RMS voltage U_o. This droop is 6 % of the nominal RMS when the reactive power supply is the nominal reactive power Q_N.

The available power on the AC bus is higher than the power demanded; the battery inverters will charge their batteries and let the idle frequency rise slightly, proportionally to the amount of energy stored in the batteries. If the available power is less than the one demanded, the missing amount will be fed into the AC bus by the battery inverter, reducing the AC frequency. The maximum deviation is around 0.5Hz.

3.3.1.- Current Source Inverter Model (CSI)

Most microsources such as photovoltaic arrays and wind turbine require power electronics interfaces for connecting to the microgrid, as was shown in Figure 3.7 and Figure 3.9. These interfaces are comprised by a microsource side converter, a DC-Link, a grid side converter, a line AC filter and a transformer (s. Figure 3.20). These microsources work in current source configuration; they are designed to inject the power available into the grid, the active and reactive powers injected aim to follow at pre-specified values P_{ref} and Q_{ref} (In order to operate with a unit power factor, the pre-specified value Q_{ref} is normally set to zero).

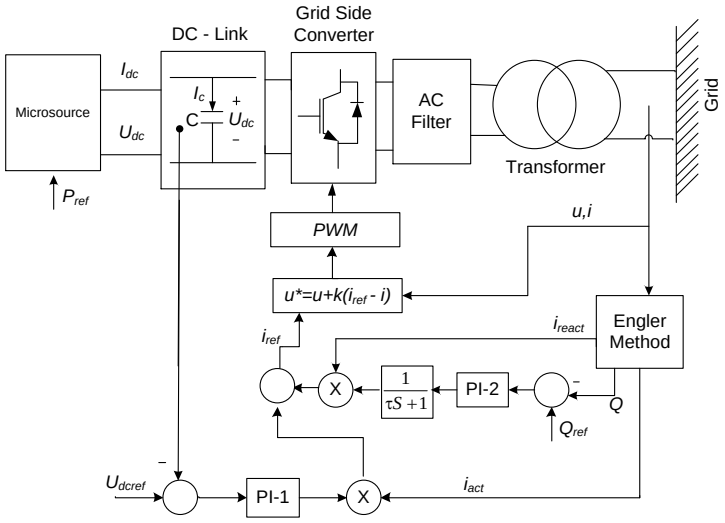

Figure 3.20.- Current Source Inverter Control

The grid side converter is implemented as a current controlled voltage source. The components of the current in phase (i_{act}) and quadrature (i_{react}) with the inverter terminal voltage are computed based on the Engler Method, which is presented in Burger et al. [80].

Power variations in the microsource induce dc-link voltage errors, which are corrected via the PI-1 regulator, by adjusting the magnitude of the active current delivered to the grid (i_{act}). The reactive power Q is controlled via the PI-2 regulator by adjusting the magnitude of the output reactive current (i_{react}).

Additionally, a local secondary controller is included into the microsource side converter which has the purpose of returning the grid frequency to the nominal value. This is due to the fact that if the MicroGrid frequency stabilizes at a value different from the nominal one, storage devices would keep on injecting or absorbing active power whenever the frequency deviation differs from zero. This should only be admissible during transient situations, where storage devices are

responsible for the primary load frequency control. Storage devices have a finite storage capacity and can be loaded mainly by absorbing power from the LV grid.

Therefore, correcting permanent frequency deviation during islanded operation should be a key objective in any control strategies in order to avoid storage devices injecting (or absorbing) active power whenever the MicroGrid frequency deviation differs from zero. Combining the primary frequency regulation provided by the storage device and a secondary load frequency control are the key features for successful MG islanded operation (Lopes et al., [81]).

In order to promote adequate secondary control, to restore frequency to the nominal value after a disturbance, a local secondary control is proposed by using a PI controller at each microsource converter controller. This PI controller in the MicroSource computes the reference output power P_{ref}, which should be injected into the grid so that the frequency will return to the nominal value (s. Figure 3.21) (Madureira et al., [82]).The pre-specified value P_{ref} depends on the grid's frequency as shown in the equation (3.33). The secondary local control forces the MicroSources to produce the right amount of power so the storage device will not contribute to the overall generation.

In the solar microsouces, the maximum power point tracking control (MPPT) works together with the secondary load control: Both controllers can regulate the amount of power generated by the photovoltaic arrays. The aim of the MPPT is to provide the highest possible power when variations in the irradiance and temperature occur, while the aim of the secondary control is to limit the output power. For wind turbine microsources, the unused power is redirected to a load resistor.

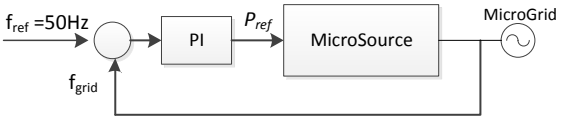

Figure 3.21.- Local Secondary Load-Frequency Control

3.3.2.- Voltage Source Inverter Model (VSI)

When the microgrid works in island mode, the grid side converter connected to the storage devices (known as battery inverter) works as a voltage controlled current source, defining a reference AC voltage source. For this, storage devices will be used as a buffer to balance the generation and demand of energy.

The grid terminal voltage and current are measured and used by the *selfsync* control to define the reference of AC voltage. The difference between reference and the grid side converter terminal voltage, with a voltage controller and a

subordinated current controller, are though for define the reference signals that control the grid side converter switching sequence, using a PWM modulation technique (s. Figure 3.22).

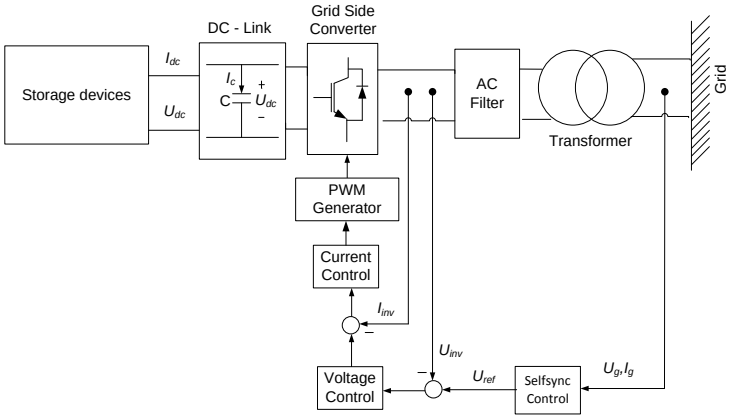

Figure 3.22.- Voltage Source Inverter Control

The *selfsync* control is used to define the reference AC voltage source. It is divided into four parts (s. Figure 3.23):

- The active and reactive powers are estimated from the grid terminal voltage and current.
- The active and reactive power controls are decoupled by using a first order system with the time constants: T_{mech} and $T_{excited}$.
- The droops influence the frequency, phase and amplitude of the voltage reference.
- The reference AC voltage source is defined by (3.35).

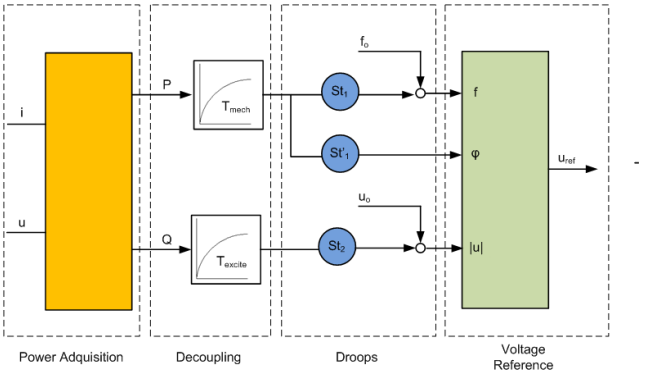

Figure 3.23.- Control approach *selfsync* by ISET (Engler, [83])

$$U_{ref} = |U_{grid}| \sin(2\pi f_{grid} t + \varphi) \tag{3.35}$$

Since the available microsources cannot generate reactive power, the battery inverter includes an additional capacitor to compensate the reactive power. The droop method related to the reactive power will not be considered. As a result, a constant value has been considered for the grid's voltage U_{grid}.

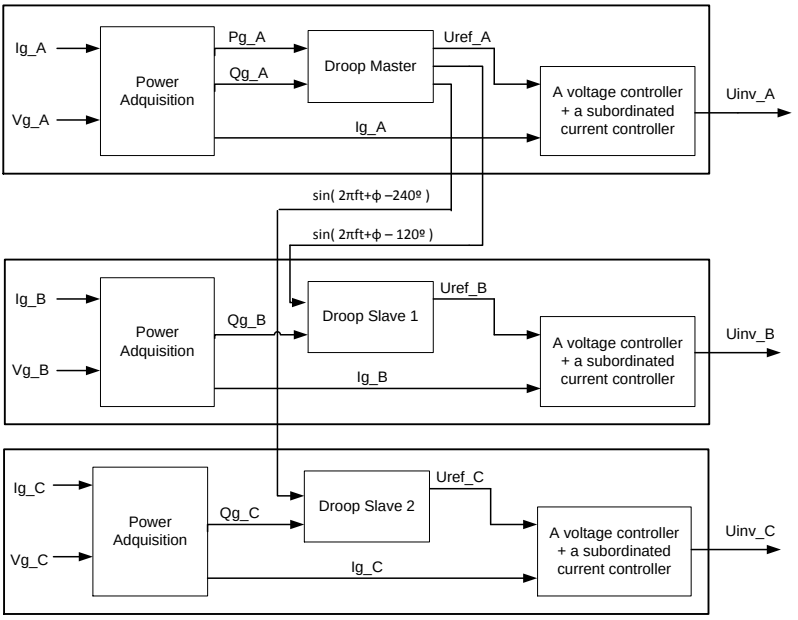

Figure 3.24.- Three phase *selfsync* control algorithm

The *selfsync* control structure uses the droop control to regulate the frequency, phase and amplitude of the reference AC voltage source. For this, fast computing of active and reactive powers is required. In three phase systems, the active and reactive powers can be computed instantaneously using space vectors, but in single phase systems there is no space vector. To overcome this problem, a simple filter was proposed by Engler in Burger et al. [80].

In the three phase *selfsync* control algorithm, a droop controller is available for each phase: a 'Droop Master' for phase A and a 'Droop Slave' for phase B and phase C (s. Figure 3.24). The droop master is the one which defines the phase and the frequency for the three phases. The reference voltage source for phase A is directly given by the droop master, while the reference voltage for phases B and C is derived from the instant frequency and the phase (120º, 240° respectively) given by the droop master and the voltage magnitude given by the droop slave.

3.4.- Reverse Osmosis Desalination Model

Nowadays, revese osmosis (RO) is known as the most versatile desalination method to produce drinkable water since it needs less investment cost, energy and maintenance than other desalination method.

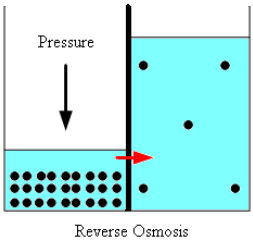

Figure 3.25.- Direct and Reverse Osmosis Process

Reverse Osmosis (RO) uses pressure to force water flowing across a semipermeable membrane from a salty solution, the salts are retained and the water molecules pass to the other side. The water flow is called "permeate" and needs a remineralization before being consumed. The rejected salty water flow is called "retentate". Process is shown in Figure 3.25.

A reverse osmosis plant consists of four major processes (s. Figure 3.26):

- *Pre-Treatment*: The incoming salty water is pretreated to be compatible with the membranes, by removing suspended solids, adjusting the pH, and adding an inhibitor to control scaling on the membranes.
- *Pressurization:* A high pressure pump raises the pressure of the pretreated salty water to an operating pressure appropriate for the membrane and the salinity.
- *Separation*: The permeable membranes inhibit the passage of dissolved salts while permitting water to pass through. Because no membrane is perfect in its rejection of dissolved salts, a small percentage of salt passes through the membrane and remains in the product water.
- *Post-Treatment:* The water that passed through the membrane usually requires pH adjustment and remineralization before being used as drinking water.

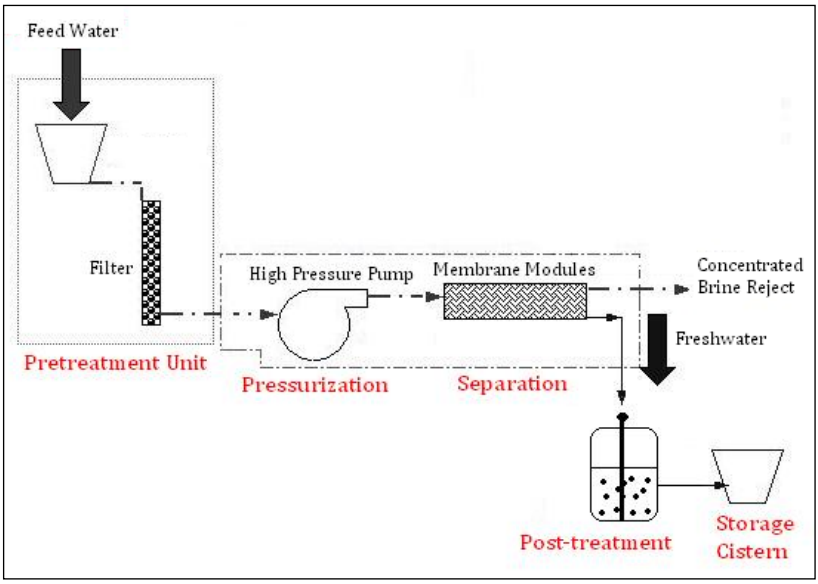

Figure 3.26.- Reverse Osmosis Plant

For testing the controllers developed a detailed and simplified model of the process was developed. The desalination plant model is based on a set of components (s. Figure 3.27) representing the different units such as pumps, RO membranes and storage tanks. Every component has been modeled using first principles and correlations from literature: mass balances, energy balances, and physic-chemical equations are in the core of the models.

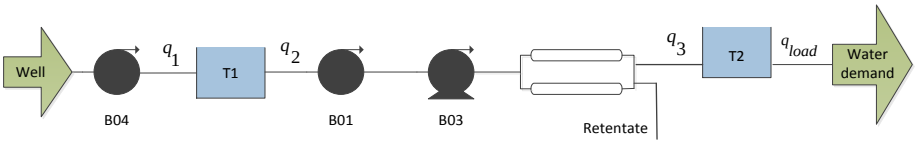

Figure 3.27.- Desalination Plant Model

In order to produce drinkable water, the following general process is assumed: First, a pump (B04) injects water to a primary tank (T1). Afterwards, water from this tank is pumped through (B01) pump to receive the pretreatment where the water is made compatible with the membranes by removing suspended solids, adjusting the pH, and adding a threshold inhibitor to control scaling. Then, the pretreated feedwater is pumped through a high pressure pump (B03) that increases its pressure to a value above the osmotic pressure. Next, the pressurized water goes to the RO membrane rack. The clean water produced is stored in the secondary tank (T2) that supplies water to the consumers.

Pumps Model

The pump performance curves used (shown in Figure 3.28) provides the value of the differential head *H* for each water flow *q*.

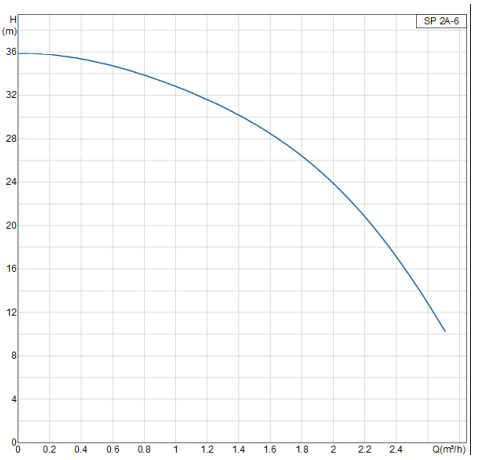

Figure 3.28.- Pump performance curves

The curves can be identified through a polynomial as proposed in the following equation. The parameters P_a, P_b and P_c were identified considering some experimental results (3.36).

$$H(q) = P_a q^2 + P_b q + P_c \tag{3.36}$$

The ideal hydraulic power to drive a pump depends on the mass flow rate *q*, the liquid density ρ and the differential head *H* and is presented in (3.37), where P_{hyd} is the ideal hydraulic power (W), *q* is the water flow through the pump (m^3/s), ρ is the density of the fluid (kg/m^3), *g* is the gravity (m/s^2) and *H* is the differential head (m).

$$P_{hyd} = \rho g H q \tag{3.37}$$

Additionally, the shaft power - the necessary power transfer from the motor to the shaft of the pump - depends on the efficiency of the pump η_{pump} and the motor η_{motor}. The shaft power P_1 can be calculated as is shown in (3.38).

$$P_1 = \frac{P_{hyd}}{\eta_{pump}\eta_{motor}} \tag{3.38}$$

Finally, the pressure difference through the pump is given by the equation (3.39).

$$P_1 = \frac{P_{hyd}}{\eta_{pump}\eta_{motor}} \tag{3.39}$$

Tanks Model

A mass balance is used to compute the level of the liquid. Consequently, two mass balances have been defined: one over each tank. The equations are given in (3.40) and (3.41), where A_1 and A_2 are the areas while H_{T1} and H_{T2} are the level of the liquids in each tank T1 and T2, q_1 is the outlet flow of the pump B04, q_2 is the inlet flow of the pump B01, q_3 is the permeate flow of the membranes and q_{load} is the water demand.

$$A_1 \frac{dH_{T1}}{dt} = q_1 - q_2 \tag{3.40}$$

$$A_2 \frac{dH_{T2}}{dt} = q_3 - q_{load} \tag{3.41}$$

Considering q_2 as the inlet flow to the membranes, the pressure at the nozzle of the tank T1 is an essential parameter to develop the dynamic models of the membrane modules. This pressure P_{T1out} can be expressed in (3.42) and (3.43), where V_e is the velocity at the nozzle of the tank T1 and P_{atm} is the atmospheric pressure.

$$P_{T1out} = P_{atm} + \frac{\rho g H_{T1}}{100000} + \frac{\rho V_e^2}{2(100000)} \tag{3.42}$$

$$V_e = \frac{q_2}{A_1} \tag{3.43}$$

RO Membranes

The RO membrane model used was proposed in Palacin et al. [78]. The model is based on a finite volume method and includes a stratified model with *n* sections, affecting concentration and pressure (s. Figure 3.29). The variables on both sides of

the membranes are assumed to be constant in each section, considering that in each section the input pressure is *P(i)* and the pressure at the permeate side is $P_{permeate}$.

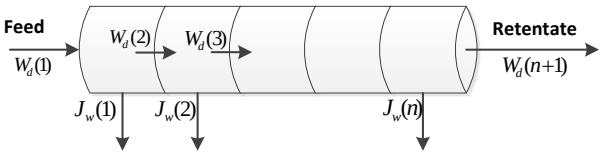

Figure 3.29.- Stratified modeling of the RO membranes

The water flows J_w are related with the pressure gradients by the equation (3.44), where A is the water permeability constant, $\Delta\pi$ is the osmotic pressure at each section, $P_{permeate}$ is the pressure on the permeate side ($P_{permeate}$ is about 1.5 bar), and P(i) is the pressure across the section (i), calculated as is shown in (3.45). P_{feed} is the inlet pressure to the membrane and ΔP is the pressure difference across the membrane which can be expressed in (3.46), where $W_d(1)$ is the feed water flow and k_{pd} is a proportional constant which depends on the characteristics of the membranes (typically k_{pd} is about 1.3).

$$J_w(i) = \frac{A}{2}\left[P(i) - P_{permeate} - \Delta\pi(i)\right] \tag{3.44}$$

$$P(i) = P_{feed} - \frac{i}{(n+1)}\Delta P \tag{3.45}$$

$$\Delta P = k_{pd}\sqrt{W_d(1)} \tag{3.46}$$

Additionally, the equation defining the osmotic pressure is presented in (3.47), where α is the osmotic coefficient and T is the temperature (ºK).

$$\Delta\pi(i) = \alpha\left(C(i) - C_{permeate}\right)T \tag{3.47}$$

The salt concentration on the (i) section is given by a mass balance defined in (3.48), where W_d(i) is the inlet water flow for each section (i), which is given by the equation (3.49).

$$V_i\frac{dC(i)}{dt} = W_d(i)C(i-1) - W_d(i+1)C(i) - J_s(i)\rho \tag{3.48}$$

$$W_d(i) = W_d(i-1) - J_w(i-1) \tag{3.49}$$

$W_d(1)$ is the feed water flow, $W_d(n+1)$ is the retentate flow. Finally, the permeate flow is represented by (3.50).

$$q_3 = \sum_{i=1}^{n} J_w(i) \tag{3.50}$$

Similarly, the flow of salt across a section of the RO membrane J_s, is described in (3.51), where B is the salt permeability constant, C(i) the salt concentration on the (i) section, and $C_{permeate}$ is the salt concentration on the permeate sides of the membrane, calculated in (3.52).

$$J_s(i) = B\left(C(i) - C_{permeate}\right) \tag{3.51}$$

$$C_{permeate} = \frac{\sum_{i=1}^{n} J_s(i)}{\sum_{i=1}^{n} J_w(i)} \rho_w \tag{3.52}$$

3.5.- Simulation Platform

A simulation platform under the MATLAB® Simulink® environment was developed considering the specification of the prototype built by the Open-Gain workgroup in order to evaluate the dynamic behavior of the MicroGrid considering a three-phase balanced operation.

The prototype includes a Reverse Osmosis (RO) desalination unit and a three-phase power supply system. The reverse osmosis desalination plant was designed to produce up to 24 m^3/day of drinking water from brackish water with salinity close to 18g/L, using six membrane modules and a 35 bar high pressure pump. The power supply system comprises mainly the following components: 80 silicon mono-crystalline PV modules with a total capacity of 185 Wp, a wind turbine with 22 kW as maximum power installed on a 25m high tower, a battery bank with a capacity of 5000Ah and voltage of 48 V, and a Diesel Generator with rated power of 16kW and 20KVA. The platform includes models and controls for a wind turbine, PV panels and storage devices (batteries), as well as controllable loads (available for load shedding purposes).

The principles described in section 3.3 for power limitation through a local secondary control in current source can be seen in Figure 3.30. For this, a constant impedance load of 3kW per line was taken into account.

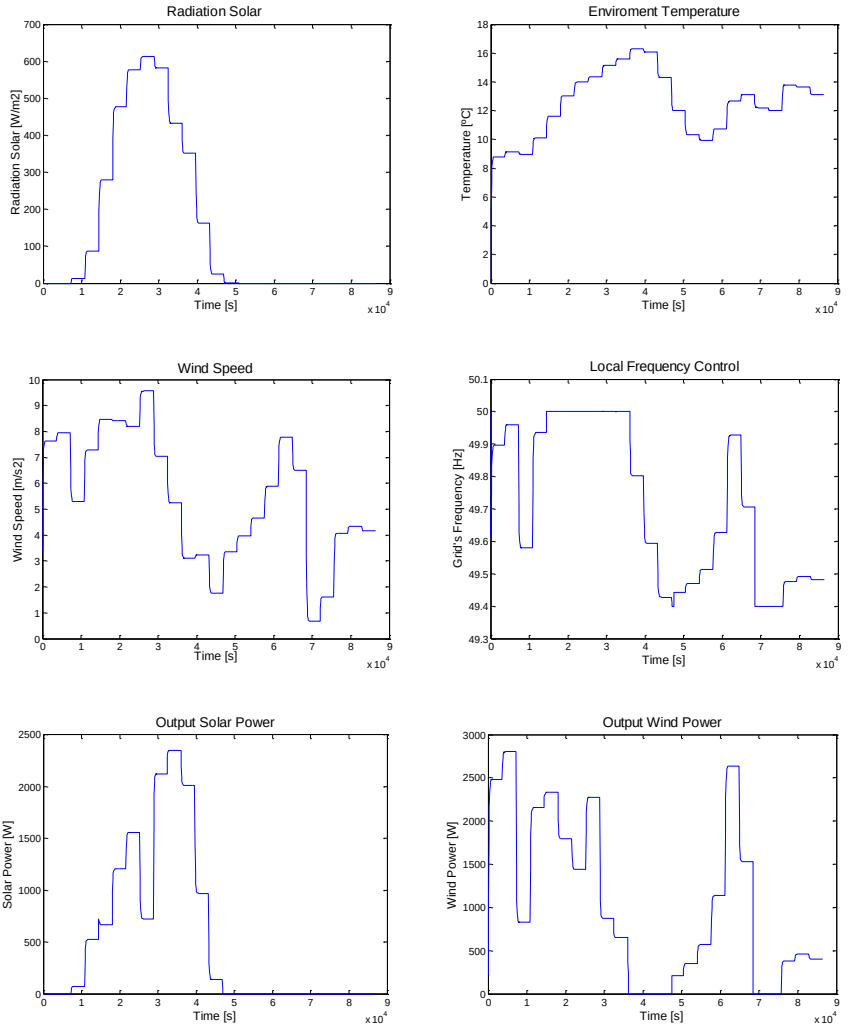

Figure 3.30.- Experimental results for a constant load of 3kW per line

3.6.- Renewable Ecosimpro Library

A library on microsources of renewable energies integrated to form low voltage microgrids has been developed in EcosimPro to supply electrical power to remote areas that the main or national grid cannot reach on account of the typology or weather (s. Figure 3.31). EcosimPro© is a powerful modeling and simulation tool that follows an advanced methodology for modeling and dynamic simulation. It provides an object oriented and non-causal approach that allows new simulations to be created that interconnect reusable component libraries.

Generally, the generators and microsources that make up a microgrid are renewable/non-conventional distributed energy resource (DER) systems. In this library, the microsources are represented by photovoltaic sets and a wind turbine, and they are equipped with power electronic interfaces (DC/AC or AC/DC/ AC) and a local controller to regulate production levels of active and reactive power. In addition, the library contains a number of different elements of power electronics as needed to control the facilities, as well as diesel motors and generators, sources of wind or sunlight, pumps, tanks, etc. that are found in those facilities.

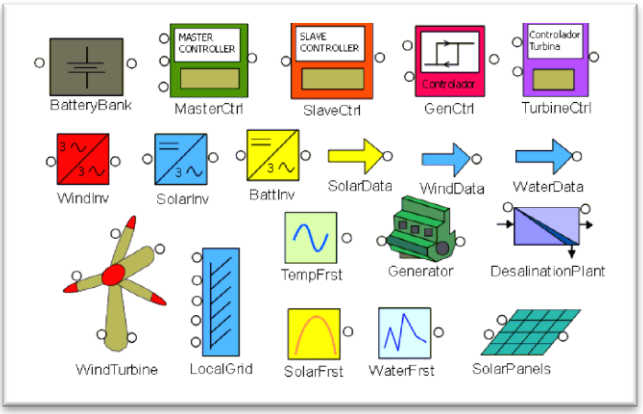

Figure 3.31.- Some elements for Renewable Energy Library

The model of the photovoltaic set is based on an equivalent circuit from a solar cell depicted by a source of current in parallel with a diode. It includes the effects of changes in temperature and levels of sunlight, as well as considering the specification sheets. The component was made to be general, so that it can be used in other simulation projects considering the technical specifications of the solar panels but without having to modify the existing component.

A model was run on a conventional, three-blade, variable speed wind turbine equipped with a permanent magnet generator. The control strategy basically consists of controllers that work in different operating areas. The first controller is active when the wind speed is below the rated speed, and its aim is to maximize the output power by adjusting the speed of the rotor. Other control systems activate when the wind speed rises above the rated speed, and their purpose is to limit the power generated by varying the pitch angle. A number of different control strategies were used to improve the quality of the power output.

The system was modeled modularly, so that the dynamic response of a wind turbine can be obtained even after modification of the mechanical structure, the electronic configuration, or the control strategy. For example, the permanent magnet generator may be replaced with a dual-power induction generator joined to a multiplier. Notice, changes in the mechanical structure and the electronic configuration may also require changes in the control strategy.

In general, the microgrids essentially have two operating modes: connected and isolated. Connected mode occurs when the microgrid is connected to the main grid or to a diesel generator in order to take/ inject an amount of energy from/to the main grid. In contrast, in isolated mode, the microgrid is disconnected from the main grid or generator, so the microsources and storage elements must cooperate with each other to keep the integrity of the microgrid steady.

The renewable energy library facilitates the training of technicians and engineers in how to operate microgrids, how to check different configurations and control strategies before implementing them and how to facilitate their design. Additionally, it is also easy to integrate new components into the library.

3.7.- Disturbance Prediction Models

The main difficulty found when a controller is proposed for energy supplied system equipped with renewable energies is the short-term unreliability of the power supply (in the presence of clouds, wind gusts, etc.). There is often an excess of energy for some hours, whereas at other times the provided renewable energy is not enough to supply the instantaneous demand. Thus, the proposed controller is based on predictions of energy and water demand, estimated from physical models and previous measurements.

3.7.1.- Water Demand Prediction Model

The estimation of the water demand is a central aspect during the design and operation of the desalination plant. The estimation is based on historical measures of water demand in a given population. The water demand can be modeled as a periodic curve which is repeated every 24 hours, moving vertically due to seasonal variations. Notice that seasonal variations (more water is consumed when the weather is hot), daily variations (the demand in holidays is different from on labor days) and hourly variations (very low demand during the night, high demand in the mornings) should be taken into account. The model will be used to make predictions in the control algorithm during a short interval of time (3.53), where Q(d,w,h) is the estimation of the water demand at day d (from 1 to 365), weekly w (from Sunday w=1 to Saturday w=7) and hour h (1 to 24). Q_d(d) is the average daily water demand at Julian date d, Δw(w) and Δh(h) are correction factors that represent daily and hourly variations of the water demand.

$$Q(d,w,h) = Q_d(d) + \Delta_w(w) + \Delta_h(h) \tag{3.53}$$

A Fourier series is used to estimate the average daily water demand, as shown in (3.54), where d_o represents the initial day of the year in climate terms. Parameters are obtained from experimental results.

$$Q(d) = a_o + \sum_{k=1}^{N}\left(\alpha_k \cos\frac{2\pi k(d-d_o)}{365} + b_k \sin\frac{2\pi k(d-d_o)}{365}\right) \quad (3.54)$$

3.7.2.- Wind Speed Prediction Model

The prediction of the wind speed for long-term scale performs more difficulties than the short-term prediction. Although, a short-term prediction (up to 1h) is required to obtain a prediction model for the nonlinear model predictive control (NMPC) strategy proposed for the solar/wind based microgrid.

To start with, the filtered wind speed will be taken into account to design the prediction model, thus the ineffective frequency components will be removed from the spectrum with the objective to provide a better prediction. For this, a low pass filter will be used in order to make the wind speed smoother and more predictable for short term (Riahy, 2008 [84]).

The filtered wind speed is calculated as a function of the measured wind speed in the previous sample time, as is shown in equation (3.55).

$$\hat{v}_n = (1-r)v_{n-1} + r\hat{v}_{n-1} \quad (3.55)$$

Where $\hat{\boldsymbol{v}}_n$ is the estimated wind speed at time *n*, $\boldsymbol{v}_{n-1}$ is the wind speed measured at the moment before, $\hat{\boldsymbol{v}}_{n-1}$ is the wind speed computed at the moment before, *r* is a parameter that represents the correlation before two consecutive wind speeds.

3.8.- Hybrid Systems

The mathematical model of a system is traditionally associated with differential or difference equations, typically derived from physical laws governing the dynamics of the system under consideration. Consequently, most of the control theory and tools have been developed for such systems. On the other hand, in many applications the system to be controlled comprises also parts described by logic, such as ON/OFF switches or valves, gears or speed selectors, and evolutions dependent on if-then-else rules. Often, the control of these systems is left to schemes based on heuristic rules inferred from practical plant operation.

Recently, researchers started dealing with hybrid systems, namely processes which evolve according to dynamic equations and logic rules. One example of hybrid system is a switching system where the dynamic behavior of the system is described by a finite number of dynamic models that are typically sets of

differential or difference equations, together with a set of rules for switching among these models. The switching rules are described by logic expressions or a discrete event system.

The interest in hybrid systems has grown over the last few years not only because of the theoretical challenges, but also because of their impact on applications. Hybrid systems arise in a large number of application areas and are attracting increasing attention in both academic theory-oriented circles as well as in industry.

3.8.1.- Model Predictive Control for Hybrid Systems

The proposed nonlinear optimization problem described in equation (3.56) subject to (3.57), (3.58) and (3.59), is solved each sampling instant. $\mathbf{x}, \mathbf{y} \in R^n$ are the inputs and output vectors respectively, **u** is the binary manipulated vector, T_p is the prediction horizon, $F(\cdot)$ is a cost function whose integral must be minimized, $f(\cdot)$ and $g(\cdot)$ are the differential and algebraic equations which integrate the internal dynamic model. Moreover, inputs and output constraints could be included as penalty functions in $F(\cdot)$. In this problem, only binary manipulated variables have been taken into account, although, continues manipulated variables may incorporate in an extended version.

The cost function J is calculated by integrating the internal model along the prediction horizon T_p, considering the current state of the process as initial conditions and evaluating the cost function at the end of integration. The first control signal of the sequence computed at each sampling time is sent to the process while the rest control signals are rejected because the procedure will be repeated in the next sampling instant.

$$\min_{\{u_i\}} J = \int_0^{T_p} F(\mathbf{y}, u, t)dt \tag{3.56}$$

$$\dot{\mathbf{x}}(t) = f(\mathbf{x}, u_i, t) \tag{3.57}$$

$$\mathbf{y}(t) = g(\mathbf{x}, u_i, t) \tag{3.58}$$

$$u_i(t) \in \{0,1\} \qquad \forall i = 1, \ldots, n_{bv} \tag{3.59}$$

The periodic operation proper from the binary variables, such as ON/OFF valves, fixed speed pumps and so on, will be considered to transform a MIQP optimization problem into a NLP problem. For this, a parameterization is proposed in which the binary variables are transformed into continues variables by considering the duration of the activation/deactivation of the ON/OFF actuator. This control strategy reduces the number of manipulated variables and uses

nonlinear optimization problem instead of mixed integer optimization, so that the computational cost is reduced.

A variety of numerical strategies are available to solve continuous dynamic optimization such as: dynamic programming, direct methods and indirect methods.

- Dynamic programming was proposed by Bellman [85] and is based on the optimal principle: "In a sequence of optimal decisions, all subsequence must also be optimal".
- Indirect methods (Bryson et al., [86]) focus on a numerical solution to the classic conditions of optimality
- Direct methods transform the infinite dynamic optimization problem in one of nonlinear finite dynamic programming (NLP). Within this class, there are three strategies methods: sequential simulation and optimization or control parameterization (Sargent et al., [87]), simultaneous simulation and optimization (Neuman et al., [88]) and multiple shooting (Bock et al., [89]) that combines ideas from last two.

In the control parameterization, the control signal *u(t)* approximates a finite family of basic functions, where the duration of the periods in which each function is applied are considered as continuous manipulated variables in the optimization problem. This control strategy will be used to solve the optimization problem described in (3.56) and will be the core of the hybrid predictive control developed.

In the proposed parameterization, two new real variables are defined $T_{on,i}^{k}(t)$ and $T_{off,i}^{k}(t)$ for each binary manipulated variable u_i (i = 1,…, n_{bv}). $T_{on,i}^{k}$ and $T_{off,i}^{k}$ denote the duration of the binary variable u_i when its value is equal to one and zero respectively for each pulse k, as is shown in Figure 3.32. $T_{on,i}^{k}$ and $T_{off,i}^{k}$ are unknown manipulated variables along the prediction horizon and the optimizer must find its value. This parameterization is related with the assumption that during the "normal operation of the system", once the transient due to a disturbance or a change reference has happened, follows a periodic behavior. Notice, a "stable operation" cannot be achieved with a constant value in the actuators.

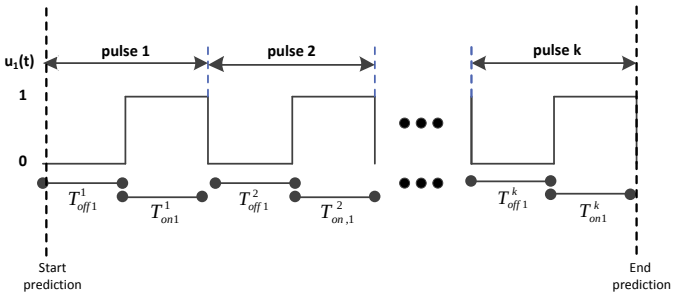

Figure 3.32.- Binary Variable parameterization u_i

A converter between the process and the controller is recommended. The hybrid controller computes the durations $T_{on,i}^{k}$ and $T_{off,i}^{k}$ for each binary manipulated variable u_i while the converter transform these times into the corresponding binary variable 0-1 when the different events take place, s. Figure 3.33. Additionally, the decoupled between the applying of the values of these binary variables and the sampling instants of the hybrid controller is achieved.

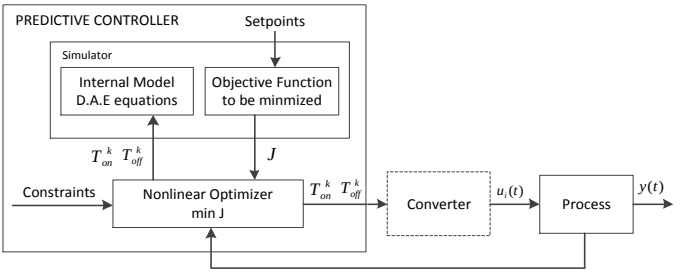

Figure 3.33.- Nonlinear Predictive Control Implementation

3.8.2.- Predictive and Control Horizon

The predictive horizon refers to the time required for computing the future and current control signals. After, N_u sampling instants, the controller maintains the last control signal obtained at N_u until the end of the prediction horizon N_2 for computing predicted outputs. Considering the binary manipulated variables, it is recommended to formulate the control horizon $N_{b,i}$ as the number of pulse for each manipulated variable u_i for which the controller computes the manipulated variables $T_{on,i}^{k}$ and $T_{off,i}^{k}$, (The duration of activation and deactivation for each pulse $k \forall k = 1,2,3, \ldots$).

From the pulse $N_{b,i}$ to the end of the prediction horizon $T_p=N_2T_s$, the value of the manipulated variables $T_{on,i}^{k}$ and $T_{off,i}^{k}$ ($k > N_{b,i}$) are fixed at the values obtained for the pulse $N_{b,i}$. Thus, the control signal u_i will be forced to follow a pattern defined by the pulse $N_{b,i}$, assuming that the system will reach a stationary state.

The prediction horizon N_2 is related to the future number of sampling instants, with duration T_s, used for computing the internal model predictions. In the traditional predictive control, this value is chosen much longer than the time constant of the process. Although, process which includes binary manipulated variables never stabilize at a stationary point and oscillate around a value, eventually reaching a stable pattern of operation. Therefore, it is recommended to define the prediction horizon N_2 as the number of pulses N_p of the slower variable in changing u_i required to achieve a stable operation pattern. To obtain the cost function J, the internal model will be integrated until the slower pulse train has exactly completed N_p pulse. Notice, each manipulated variables could make different numbers of pulses during the same prediction horizon T_s.

Figure 3.34 shows an example which includes two binary variables u_1 and u_2. The prediction horizon N_2 is defined as the time required making exactly four pulses by the variable u_2. Notice, the variable u_1 makes more number of pulses than u_2. The control horizon for the variable u_1 is $N_{b,1}$=1, therefore, only the durations $T^1_{on,i}$ and $T^1_{off,i}$ related to the first pulse will be computed and the same pattern is applied for future pulses, ie, $T^k_{on,i} = T^1_{on,i}$ and $T^k_{off,i} = T^1_{off,i} \quad \forall k > N_{b,1}$. The control horizon for the variable u_2 is $N_{b,2}$=2, therefore, the controller will compute the durations $T^1_{on,2}$, $T^1_{off,2}$, $T^2_{on,2}$ and $T^2_{off,2}$. The next pulses will follow the pattern defined by the second pulse $T^2_{on,2}$ and $T^2_{off,2}$. Thus, $T^k_{on,2} = T^2_{on,2}$ and $T^k_{off,2} = T^2_{off,2}$ $\forall k > N_{b,2}$.

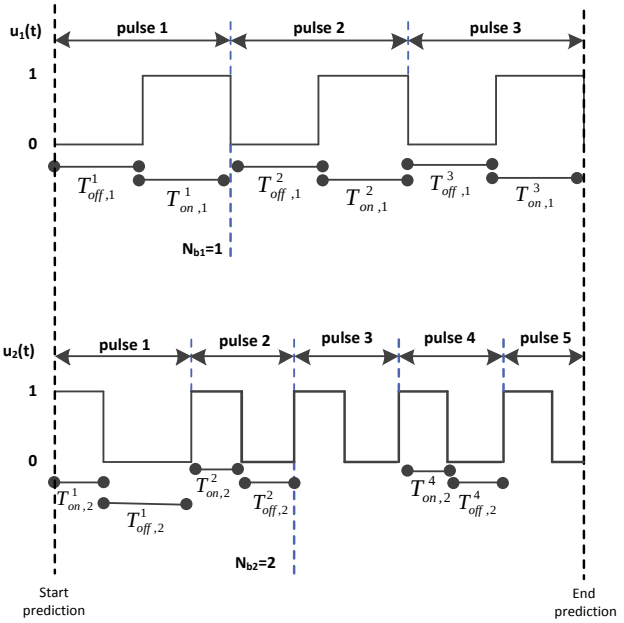

Figure 3.34.- Prediction and Control Horizon

3.8.3.- Mathematical Formulation

Using the proposed parameterization, the mathematical formulation can be expressed as described in (3.60), subject to (3.61), (3.62), (3.63), (3.64), (3.65) and (3.66), where $T^k_{on,i}$ and $T^k_{off,i}$ (i = 1,…,n_{bv}) are the new continuous manipulated variables defined for each binary manipulated variable (u_i) and pulse $N_{b,i}$. n_{bv} is the total number of binary manipulated variable and $h_i(\cdot)$ is the function which defines the control signal considering the continuous manipulated variables ($T^k_{on,i}$ and $T^k_{off,i}$). The total number of binary manipulated variables is shown in (3.67).

$$\min_{\{T_{on,i}^k, T_{on,j}^k\}} J = \int_0^{T_p} F(\mathbf{y}, u, t)dt \tag{3.60}$$

$$\dot{\mathbf{x}}(t) = f(\mathbf{x}, u_i, t) \tag{3.61}$$

$$\mathbf{y}(t) = g(\mathbf{x}, u_i, t) \tag{3.62}$$

$$u_i(t) = h_i(T_{on,i}^k, T_{off,i}^k, t) \tag{3.63}$$

$$T_{on,i}^k, T_{off,i}^k \in R \tag{3.64}$$

$$T_{on,i}^{\min} \leq T_{on,i}^k \leq T_{on,i}^{\max} \qquad \forall k = 1, \ldots, N_{b,i},\ \forall i = 1, \ldots, n_{bv} \tag{3.65}$$

$$T_{off,i}^{\min} \leq T_{off,i}^k \leq T_{off,i}^{\max} \tag{3.66}$$

$$\sum_{i=1}^{n_{bv}} 2N_{B,i} \tag{3.67}$$

Using optimization methods based on gradients, such as SQP, could cause difficulties relate to the discontinuities in the model what could promote discontinuities in the derivatives of the cost function. However, the manipulated variables which integrate the cost function are continuous and represent the duration of the binary variable when its value is equal to one and zero respectively. Additionally, the cost function considering for computing the gradients is the integral of the state variables, such as tank level, temperature, etc., which usually present a continuous behavior considering the changes in the binary manipulated variables.

The computing of gradients in hybrid dynamic systems; and the sufficient and existence conditions are shown in Galán et al. [90], while a variety of problems where the gradient based methods can be applied is given in Barton et al. [91].The main idea is that the sensitivities of hybrid systems can exist, therefore, the optimization problem NLP can be used if the timing sequence of the switches in the internal model is fixed even the duration of such switches change. Thus, the sequence of events is clearly fixed in the proposed optimization problem (s. Figure 3.34) and numerical difficulties have not been found in optimization.

In contrast, if the timing sequence of the switches depends on the manipulated variable, the optimization problem NLP can lead to problems. In such cases, it is recommended to use other options as those shown in Barton et al. [92].

3.9.- Hybrid Model Predictive Control

A central aspect in the optimization of water production in remote areas, using renewable energy, is the use of a high degree of automation that integrates the operation of the water production facilities and the energy storage systems. This makes it possible to adapt to the working conditions: variations in the supply of renewable energy and water demand and the necessary maintenance operations of desalination plants. For this reason, a control system is necessary to ensure efficient use of resources.

Energy consumption comes mainly from the operation of the pumps located in the desalination plant. Unfortunately, the short-term unreliability of renewable energy sources is well-known. Thus, as shutting down Reverse Osmosis plants is not recommended and the water demand must always be fulfilled, a backup system is needed (diesel generator).

Regarding the diesel generator, the typical approach is to define the ON/OFF switching of the diesel engine based on the battery SOC using a hysteresis band with a specific width. This control algorithm is known as "hysteresis band control". Although a new strategy has been considered for ON/OFF switching of the diesel engine since the "hysteresis band control" algorithm, this is not recommended for microgrids integrated by a variety of components.

In general, the control objective is to fulfill the water demand of the desalination plant, reduce the energy consumption from the diesel engine and the pumps, and maximize the energy stored in the batteries. Additionally, it is recommended to fulfill the operational constraints related to the battery bank, the diesel generator and the desalination plant; to avoid excessive intermittent operation in the battery, the diesel generator and the feed pump B04; and to left the accumulation tanks with a level of water as high as possible to ensure the water demand is fulfilled.

The proposed optimization problem is to minimize the cost function J in each sampling time, considering the manipulated variables and the control objectives mentioned in (3.68), where P_{gen} is the output power of the diesel generator (W), P_{bat} refers to the energy consumed or generated by the batteries (W), SOC is the state of charge of batteries and L_{T1}, L_{T2} are the levels of the primary and secondary tank respectively. Finally, T_p is the total time prediction.

$$\begin{aligned} J = {} & \gamma_{gen} \sum_{k=0}^{T_p} P_{gen}(k) - \gamma_{bat} \sum_{k=0}^{T_p} \min\left(P_{bat}(k), 0\right) + \\ & \gamma_{T1} \sum_{k=0}^{T_p} \left(L_{T1}^{ref} - L_{T1}(k) \right) + \gamma_{T2} \sum_{k=0}^{T_p} \left(L_{T2}^{ref} - L_{T2}(k) \right) + \\ & \gamma_{soc} \sum_{k=0}^{T_p} \left(SOC^{ref} - SOC(k) \right) \end{aligned} \tag{3.68}$$

Some constraints which have to be fulfilled are defined as follows:

- The water level of both tanks (T1 and T2) is limited by a minimum and a maximum value considering specifications for the tank storage, as shown in (3.69).

$$\begin{aligned} \underline{L_{T1}} \le L_{T1}(k) \le \overline{L_{T1}} \\ \underline{L_{T2}} \le L_{T2}(k) \le \overline{L_{T2}} \end{aligned} \tag{3.69}$$

- Time limitations between feed pump startups and shutdowns to avoid fast switching, as presented in (3.70).

$$\begin{aligned} T^{k}_{on,\,feed} \ge \underline{T_{on,\,feed}} \\ T^{k}_{off,\,feed} \ge \underline{T_{off,\,feed}} \end{aligned} \tag{3.70}$$

- The water flow through the pumps B01 and B03 when the plant is producing drinkable water is limited by a minimum $\underline{q_{des}}$ and a maximum $\overline{q_{des}}$ value in order to protect the high pressure pump from intensive use, as described in (3.71).

$$\underline{q_{des}} \le q_{des} \le \overline{q_{des}} \tag{3.71}$$

- Time limitations between generator startups and shutdowns to avoid excessive intermittent operation, as described in (3.72).

$$\begin{aligned} T^{k}_{on,\,gen} \ge \underline{T_{on,\,gen}} \\ T^{k}_{off,\,gen} \ge \underline{T_{off,\,gen}} \end{aligned} \tag{3.72}$$

- The state of charge for the battery is also limited by a minimum $\underline{SOC}$ value to avoid undercharging, which can reduce the capacity and lifetime of the batteries, as expressed in (3.73).

$$\underline{SOC} \le SOC \tag{3.73}$$

As the proposed model predictive control includes some binary and manipulated variables, the MPC problem corresponds to a problem of mixed integer optimization which is computationally complex. To overcome this problem, the MPC problem of mixed integer optimization was turned into a problem of nonlinear optimization with continuous variables (NMPC). For this, two new continuous

manipulated variables are defined for each binary manipulated variable $T_{on,i}^{k}$ and $T_{off,i}^{k}$ which correspond to the duration of the activation/deactivation of the binary variable δ at each pulse k. In our case, four new continuous manipulated variables are defined $T_{on,feed}^{k}$, $T_{off,feed}^{k}$, $T_{on,gen}^{k}$ and $T_{off,gen}^{k}$ which correspond to the binary variable δ_{feed}, and δ_{gen} respectively.

Regarding the MPC tuning parameters, the control horizons N_c and prediction horizons N_p are usually related to the sampling time of the controller, but in this case, the prediction horizon will depend on the number of pulses N_{pb} required by the binary variables. To compute the cost function *J*, the internal model will be integrated until the binary variable δ_{feed} and δ_{gen} has made at least N_{pb} pulses (each manipulated variable can make different numbers of pulses in the same prediction period T_p).

As shown in Figure 3.35, the prediction horizon is defined by the time required for the binary variable δ_{feed} and δ_{gen} to make at least two pulses (N_{pb}=2). Both binary variables have a prediction control of N_b=1; therefore, the times corresponding to the first pulse will be calculated $T_{on,feed}^{1}$, $T_{off,feed}^{1}$, $T_{on,gen}^{1}$ and $T_{off,gen}^{1}$, and the same pattern is applied for future pulses, i.e., $T_{on,feed}^{k} = T_{on,feed}^{1}$, $T_{off,feed}^{k} = T_{off,feed}^{1}$, $T_{on,gen}^{k} = T_{on,gen}^{1}$ and $T_{off,gen}^{k} = T_{off,gen}^{1}$.

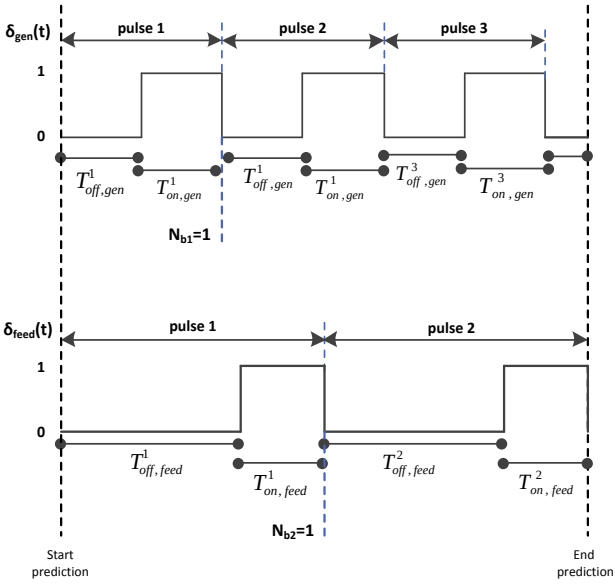

Figure 3.35.- Prediction and Control Horizons of the variables δ_{gen} and δ_{feed}

Regarding the continuous manipulated variable q_{des}, not only the control actions applied in each sampling period, but also the duration of each action must be computed. Considering a control horizon of 3, the optimization algorithm will

provide three values for manipulating the desalination flow ($q_{des}(1)$, $q_{des}(2)$, $q_{des}(3)$) and two values for the time ($Tq_{des}(1)$ and $Tq_{des}(2)$) that must be applied to the first two predictions $q_{des}(1)$ and $q_{des}(2)$. The last prediction $q_{des}(3)$ is not necessary, since the sign is held until the end of the prediction horizon. Therefore, the optimizer will provide five optimal signs for the control of the desalination flow (s. Figure 3.36).

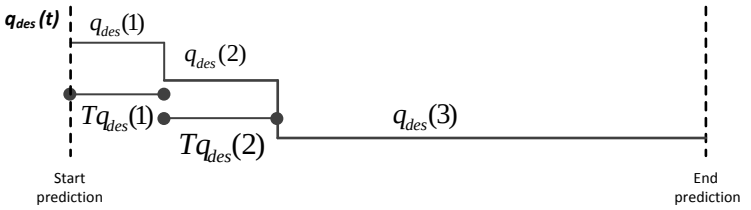

Figure 3.36.- Parameterization of the desalination flow q_{des}

3.10.- Simulation Results

This section shows the dynamic of the solar and wind based microgrid once the NMPC controller proposed in Section 3.9 is applied. The prediction horizon (T_p) taken to integrate the internal model is 30 minutes. The sampling period at which the proposed optimization problem has to be solved is one minute.

The amount of energy provided by the solar panels and the wind turbine is controlled by the battery inverter considering the grid frequency. In the plot third and fourth of the Figure 3.37, the renewable energy available (red line) is compared with the renewable energy results from the droop control (blue line). The resulting grid frequency defined by the battery inverter guarantees the state of charge (SOC) will not be greater than 0.8 and the power consumed or generated by the battery will not be higher than 5000W. Both situations can be seen in the second and fourteenth plot of the next figure.

The NMPC controller proposed guarantees a balance between the consumed and the generated power in spite of possible ambient disturbances. As the short-term unreliability of renewable energy source is well-known, the diesel generator is activated when the production of renewable energy is not enough to fulfill the load, some extra energy is not available inside the battery bank and the level of water of the tank (HT_1, HT_2) are close to their lower limit. The activation of the diesel generator should be avoided since the diesel generators are expensive, noisy, and not environment-friendly. In case the activation of the diesel generator is unavoidable, the proposed controller maximizes the power generated by the diesel engine by means of the energy storage in water tanks and batteries. The activation/deactivation and the generated power of the diesel engine is shown in the sixth and eighth plot.

Energy consumption of the Reverse Osmosis plant comes mainly from the operation of the pumps. However, the level of water inside the tanks (HT_1, HT_2) depends on the activation/deactivation of the feed pump. Thus, the proposed controller increase the level of water in the tanks, by the activation of the feed pump, when there is some extra renewable energy available. Additional, the proposed controller ensure the level of the tanks keep inside the ranges [0.3, 3.2] m and [0.3, 2.7] m respectively.

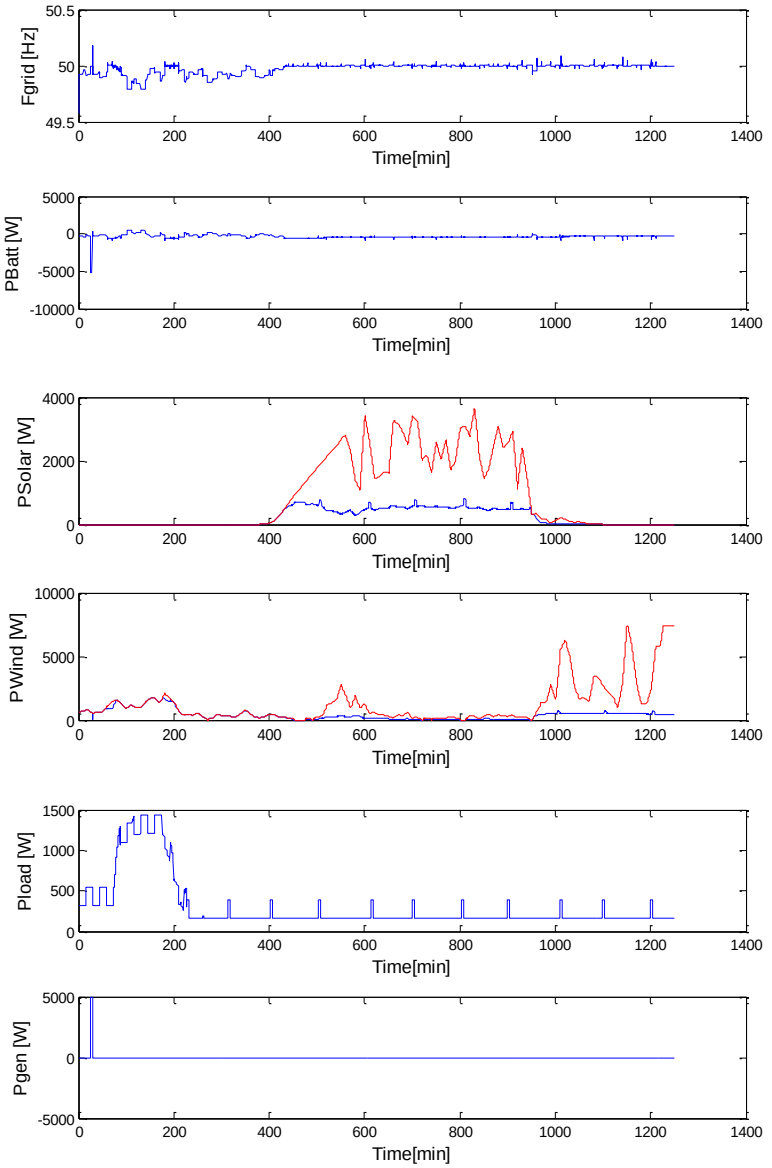

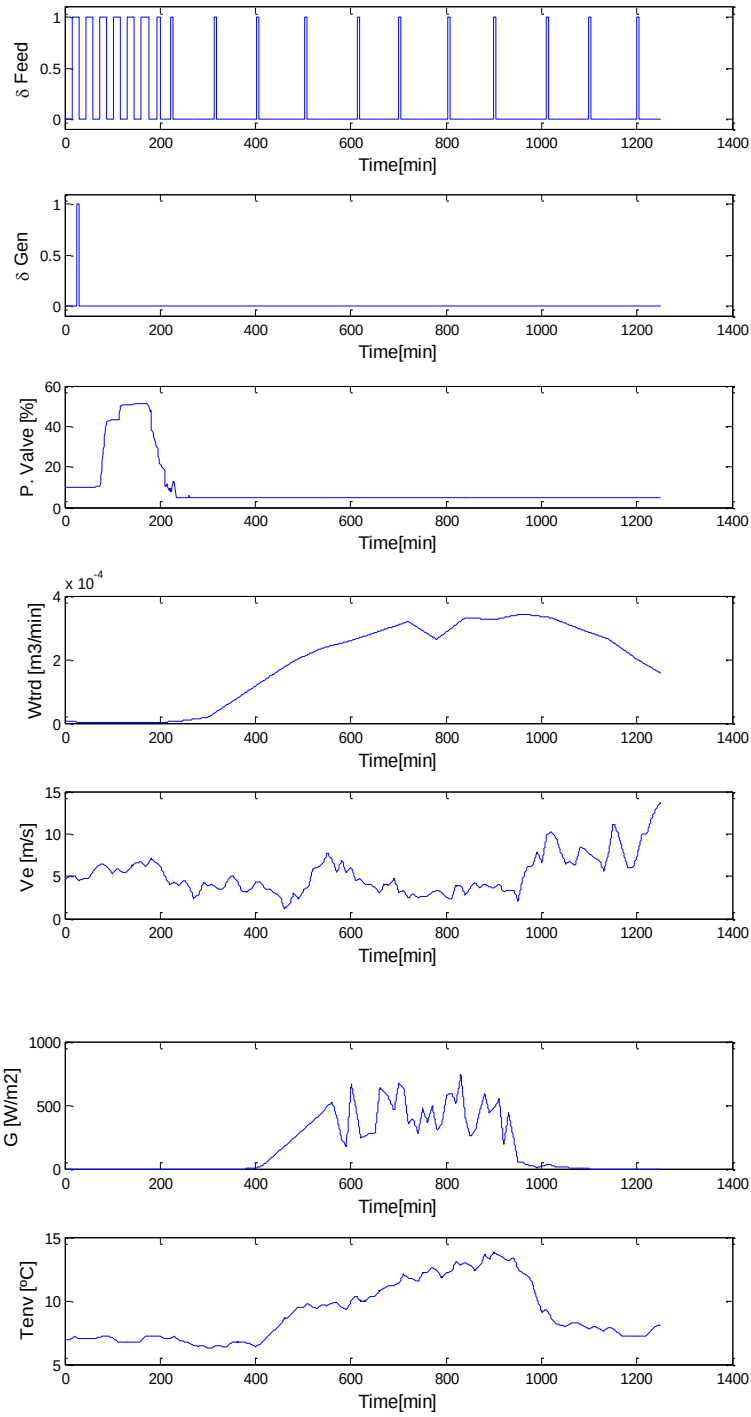
δ Feed
Time[min]
δ Gen
Time[min]
P. Valve [%]
Time[min]
x 10^-4
Wtrd [m3/min]
Time[min]
Ve [m/s]
Time[min]
G [W/m2]
Time[min]
Tenv [ºC]
Time[min]

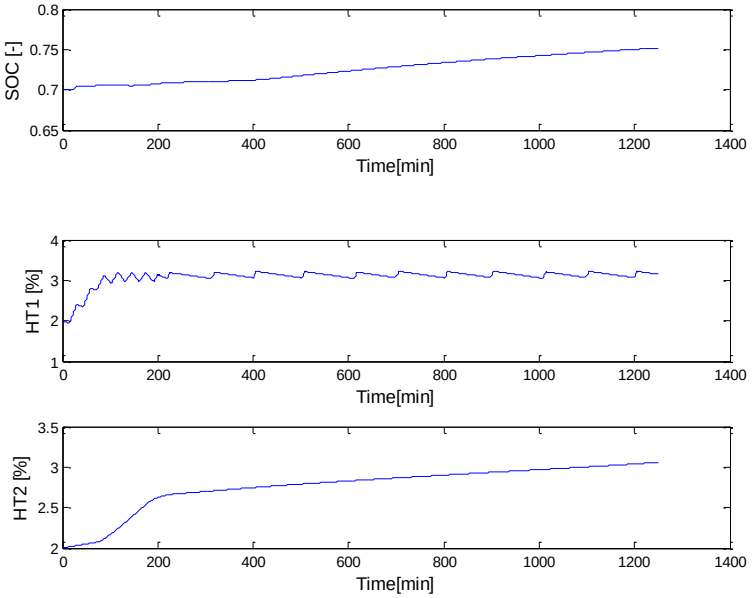

Figure 3.37.- Hybrid controller over solar/wind-based microgrid

3.11.- Conclusions

An energy supply system for small reverse osmosis plants has been proposed in remote locations, where all energy needs are produced locally using mainly renewable energies. The proposed approach is devised to improve efficiency, extend the life of the components and reduce installation and operation costs. The developed algorithms are based on predictions to adequately schedule the use of the non-renewable or temporally stored energies. These predictions are based on the use of models and previous measured values of water demand, and climatic variable.

CHAPTER 4

Solar/Gas Climatization Plant

Nowadays, energy consumption in buildings represents approximately 40% of total energy consumption around the world, more than half being used by climatization systems (Morosan et al., [93]) (Lombard et al., [96]) (Yang et al., [97]). Hence, energy efficiency, the integration of renewable energies, and the suitable use of energy inside buildings, are topics that are being widely studied from both scientific and technical points of view. Therefore, it is necessary to look for control strategies that can optimize the use of this kind of systems and, at the same time, reduce the energy consumption and its associated economic costs (Castilla et al., [94]) (Castilla et al., [95]).

Considered the air conditioning system is integrated by a refrigeration system, an absorption machine and a solar heat supply system, its main function is to provide chilled water to fan coil units by manipulating the inlet temperature of the generator of the absorption machine. Thanks to the support given by Proyecto Singular Estratégico sobre Arquitectura Bio-Climática y Frío Solar (PSE_Arfrisol PS-120000-2005-1), the Predictive Control strategy proposed for the solar heat supply system in order to keep the inlet temperature of the generator of the absorption machine in a range was included at the solar energy research centre, the CIESOL building.

The predictive controller calculates the process inputs by optimization of the predicted evolution of the different variables using a model. The difficulty of solving the optimization problem increases when binary variables appear in the models and constraints have to be taken into account.

4.1.- Process Description

The solar/gas air conditioning plant is located in southern Spain (Almeria) in a region with a Mediterranean climate (The temperatures are moderate with a small range of variation between winter and summer) and about 3000 hours of sunshine a year. During hot season, the typical daily temperature is around 33ºC. However, the

Levante wind, a hot dry easterly wind that blows from the Tabernas desert, might increase temperatures to 38ºC or higher.

The solar/gas air conditioning plant (Rosiek et al., 2009 2012 [98][99]) (Pasamontes et al. 2007, 2009 [100][102]) is integrated by three main sections: the refrigeration system, the single – effect LiBr-H2O absorption machine and the solar heat supply system. The mean function is to provide suitable temperature to a building for the hot season (from May to September). For this, it is required to provide chilled water in the range $\left[\underline{T_{eo}}, \overline{T_{eo}}\right]$ to fan coil units by keeping the inlet temperature of the generator of the absorption machine in the range $\left[\underline{T_{gi}}, \overline{T_{gi}}\right]$.

The solar/gas heat supply system provides a hot water flow to the generator and it is composed of three main elements: a solar collector field, an ON/OFF gas heater and two thermally isolated accumulation tanks. The hot water is obtained by an adequate combination of the water from solar collectors, the storage tanks and the gas heater (this last one, only if additional energy is temporally needed). A general scheme of the system is shown in Figure 4.1 while the prototype of the solar/gas heat supply system built at Almeria is presented in Figure 4.2

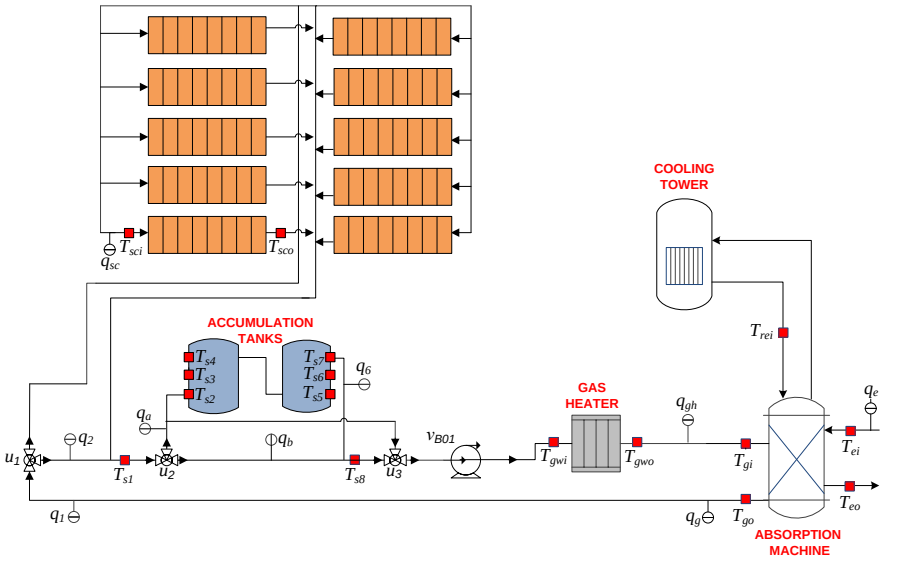

Figure 4.1.- Scheme of the Solar Heat Supply System

Figure 4.2.- Solar/gas heat supply system prototype built at Almeria

Measured Variables

The measured variables include flows and temperatures in the different elements that comprise the system:

- The temperature at the inlet and outlet of the solar collector: T_{sci} , T_{sco}
- The temperature at the inlet and outlet of the gas heater:T_{gwi}, T_{gwo}
- The temperature at the inlet and outlet of the generator:T_{gi}, T_{go}
- The temperature at the inlet and outlet of the evaporator:T_{ei}, T_{eo}
- The inlet temperature of the storage tanks: T_{s4}, T_{s50}, T_{s3}, T_{s6}, T_{s51}, T_{s5}
- The flow circulated through the solar collectors: q_{sc}
- The flow circulated through the gas heater: q_{gh}
- The flow circulated through the storage tanks: q_a, q_b
- The flow circulated through the generator: q_g
- The flow circulated through the evaporator: q_e

The measured temperature and water flow of the main components is related to the nomenclature used in the modeling.

Manipulated Variables

The solar heat supply system has the following manipulated variables that allow the control of the whole system:

1) The speed of the pump B01 (v_{B01}) which circulates the hot water flow between the absorption machine and solar collector field.

2) The three-ways valve u_1, which is used as a binary variable δ_{v1}. When the solar irradiation is above 400W/m^2, the water flows through the solar collectors, that is $\delta_{v1} = 1$. When the solar irradiation is below 400W/m^2, water flow is bloqued, which means $\delta_{v1} = 0$. With these policies, the safety request of maximum allowed temperature in the solar collectors $\overline{T_{sco}}$ is fulfilled.

3) The continuous valves u_2 and u_3 that form the bypasses of the storage tanks. These tanks are always full of water, so that no real mass accumulation takes place in them. Figure 4.3 shows a general scheme of the storage tanks configuration:

a) When the valves u_2 and u_3 are 100% open, the tanks are bypassed.
b) When the position of u_2 is 100% and u_3 is smaller, hot water could be stored in the tanks (from the solar collector field or from the return of the generator of the absorption machine) depending on u_3.
c) When u_3 is 100% and u_2 is smaller, hot water could be extracted from the storage tanks depending on u_2. u_2 and u_3 cannot be different from 100% simultaneously.

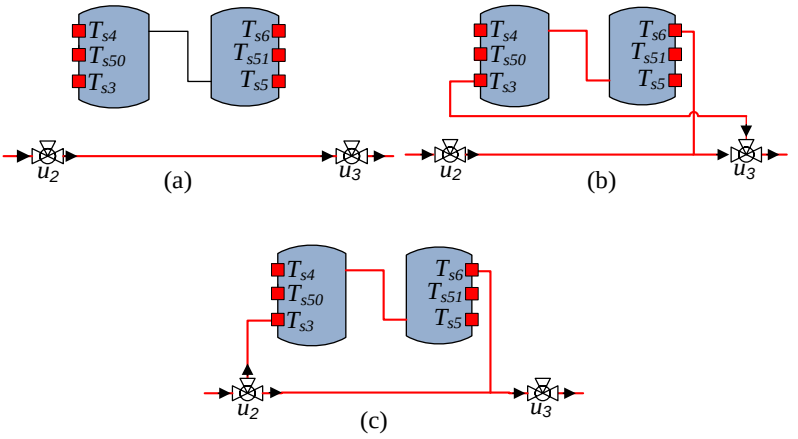

Figure 4.3.- Continuous valves configuration of the storage tanks

Due to the fact that the position of the valves u_2 and u_3 connected to the tanks cannot change simultaneously, the controller only manipulates the value of one of the valves, based on the current state:

- When the inlet temperature of the storage tanks is below the average temperature of the tanks, the valve u_3 is fixed to be fully open, so the controller regulates u_2.
- When the inlet temperature of the storage tanks is above the average temperature of the tanks, the valve u_2 is fixed to be fully open, so the controller regulates u_3.

Thus, a new variable u_{tan} has been defined to modify the value of the valves which is operating in a specific time. (u_2 and u_3 depends on the operating mode)

4) The solar/gas air conditioning plant also includes a binary actuator which regulates the gas heater is turned ON/OFF (δ_{gh}).

Operation Modes

A total of 11 operation modes results for the combination of the different ON/OFF actuators of the plants, together with the variability of the continuous manipulated variable. Therefore, a brief description of the different modes is now given:

Mode 1 (Recirculation): The water circulates in closed loop through the solar collectors without interaction of the other elements: gas heater and storage tanks. For this, u_1, u_2, and u_3 are at 100%, the gas heater and the absorption machine are turned off; and the water flow can be modified by the speed of the pump B01.

Mode 2 (Storing hot water): The storage tanks are filled with hot water from the solar collector, with u_1 and u_2 at 100%; the gas heater and the absorption machine are turned off; the water flow is regulated by the opening of the valve u_3 and the speed of the pump B01.

Mode 3 (Absorption machine operated with water from the solar collectors): With valves u_1, u_2, and u_3 at 100% and the gas heater OFF, the water from the solar collectors flows directly to the absorption machine. Notice that the water flow is regulated by the speed of the pump B01.

Mode 4 (Absorption machine operated with water from the solar collectors and the gas heater): The water from the solar collectors and the gas heater flows to the absorption machine. For this, u_1, u_2, and u_3 are at 100%, the gas heater and the absorption machine are on; and the water flow is modified by the speed of the pump B01.

Mode 5 (Absorption machine operated from the gas heater): The water through the gas heater flows to the absorption machine with u_1 at 0%, u_2 and u_3 at 100% and the gas heater and the absorption machine turned on. The water flow is regulated by the speed of the pump B01.

Mode 6 (Absorption machine operated with water from storage tanks and gas heater): With valve u_1 at 0%, valve u_3 at 100%, the gas heater and the absorption machine are turned on; the water is controlled using the valve u_2 and the speed of the pump B01.

Mode 7 (Absorption machine operated with water from the storage tanks): With valve u_1 at 0%, valve u_3 at 100%, the gas heater is off and the absorption machine is on; the water flow is modified using the valve u_2 and the speed of the pump B01.

Mode 8 (Absorption machine operated from the gas heater and the solar collectors. Moreover, the storage tanks are loaded simultaneously): Using u_1, u_2 are at 100%, the gas heater and the absorption machine are on; and the water flow is modified using the speed of the pump B01 and the valve u_3, the water through the gas heater will flow to the absorption machine and the water from the solar collectors will store energy in the storage tanks simultaneously.

Mode 9 (The solar collectors load the storage tanks and the resulting flow at the outlet of tank is used to feed the absorption machine simultaneously): Using u_1, u_2 at 100%, the gas heater is turned off, the absorption machine is turned on; and the water flow is controlled using the speed of the pump B01 and the valve u_3.

Mode 10 (Absorption machine operated with water from storage tanks and the gas heater while the solar collectors load the storage tanks simultaneously): With valves u_1, u_3 at 100%, the gas heater and the absorption machine are turned on; and the water flow is regulated by the valve u_2 and the speed of the pump B01.

Mode 11 (Absorption machine operated with water from storage tanks while the solar collectors load the storage tanks simultaneously): With valves u_1, u_3 at 100%, the gas heater is turned off, the absorption machine is turned on; and the water flow is controlled using the valve u_2 and the speed of the pump B01.

4.2.- Solar Air Conditioning Model

A hybrid dynamic model for the solar air conditioning plant is presented. The model takes into account the hybrid behavior of components, including the selection of different operating modes, the behavior of the plant components which are out of operation and the dynamic of the flow for each operating mode. The models are designed as simple as possible with regard to fast simulations, but without compromising the accuracy of results.

The solar gas air conditioning model was developed using mass and energy balances and further some experiments were carried out in the real plant. The model was designed as a modular and parametrized structure which can be adapted to another solar gas air conditioning plant by adjusting parameters or replacing each of its main elements such as solar collectors, gas heater, hot water storage tanks and absorption machine. The model is used for the development and implementation of

control strategies and the simulation of its behavior under different weather and component conditions.

The evolution of the temperatures in the different components depends on the value of the flow circulating through them, which is a function of the discrete and continuous manipulated variables. As a result, flow dynamic are needed for the modeling of temperature dynamic.

Notice the coupling between components, since the solar/gas air conditioning plant is a closed circuit, where temperature variations in any of its components affect the operation of those that are also in operation at that time. The interconnections of these components define the operating mode, considering the continuous and discrete manipulated variables.

After presenting models of the different components, this section shows also some results of experiments performed to validate them.

4.2.1.- Solar Collector Model

A solar collector can be considered as a heat exchanger, which absorbs solar irradiation to heat the flow circulating through it. The proposed model includes two energy balances: one corresponds to the flat plate and the other to the water pipes, following Figure 4.4. The first energy balance is given by equation (4.1) and considers the solar irradiation, the heat flow to the water and the thermal losses to the atmosphere. The second one is defined by equation (4.2) and involves the overall energy balance carried out by the water. The variables and parameters involved in the equations (4.1) and (4.2) are described in Table 4.1 and Table 4.2.

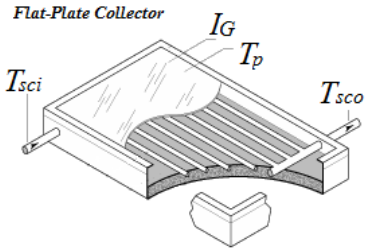

Figure 4.4.- Scheme of the solar collector subsystem

$$C_{ps}\frac{dT_p}{dt} = \eta A_{sc} I_G - K_a\left(T_m - T_{amb}\right) + U_{ps}A_{sc}\left(T_{amb} - T_p\right) + U_{pw}A_t\left(T_{sco} - T_p\right) \qquad (4.1)$$

$$C_{wc}\frac{dT_{sco}}{dt} = C_w q_{sc}\left(T_{sci} - T_{sco}\right) + U_{pw}A_t\left(T_p - T_{sco}\right) \qquad (4.2)$$

Variable	Unit	Description
T_p	ºC	Flat-plate temperature
T_{sco}	ºC	Outlet water temperature of the solar collector
T_{sci}	ºC	Inlet water temperature of the solar collector
T_{amb}	ºC	Ambient temperature
I_G	W/m^2	Solar irradiance
q_{sc}	m^3/s	Water flow though the solar collector
T_m	ºC	Average temperature inside the solar collector

Table 4.1.- Variables for solar collector model

Variable	Unit	Description
A_{sc}	m^2	Solar collector surface
A_t	m^2	Surface of the inner tubes which are inside the solar collectors
C_{ps}	J/ºC	Heat capacity of the flat-plate
C_{wc}	J/ºC	Heat capacity of the water inside the tubes
U_{pw}	W/m^{2}ºC	Heat transfer coefficient between the flat-plate and the water
U_{ps}	W/m^{2}ºC	Heat transfer coefficient between the flat-plate and the ambient
C_w	J/m^{3}ºC	Specific heat of the water
η	-	Efficiency of the solar collectors
K_a	W	Parameter which is defined considering the efficiency curves of the solar collector

Table 4.2.- Parameters for solar collector model

The equations (4.1) and (4.2) include unknown parameters that are estimated so that the model responses are close to the solar collector plant. For this purpose, data collected on the process were used together with an optimization approach as schematized Figure 4.5, based on minimizing the error between the measured outlet temperature ($\overline{T}_{sco}$) and the model output (T_{sco}).

The simplex search method of (Lagarias et al., [101]) is using as an optimization algorithm to estimate the model parameters. This is a direct search method that does not use numerical or analytic gradients. In order to execute the simplex search method in MATLAB, the function *fminsearch* have to be chosen.

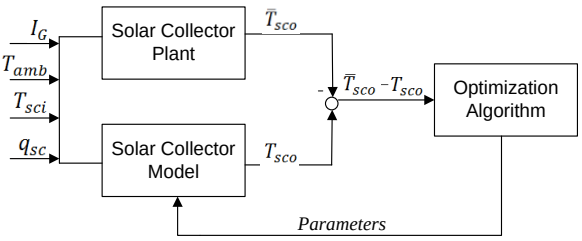

Figure 4.5.- Schematic for parameter estimation

The function minimized corresponds to the accumulated squared error between the model output and its measurements when the same experimental values were applied to the inputs of the simulation. The value of this cost function depends on the unknown parameters of the model so that an optimization algorithm can compute the value of the parameters that minimizes the cost function.

In order to validate the model obtained by minimizing accumulated squared error between the model output and its measurements, the inputs given in Figure 4.6 were used to compare the system measurements and model results.

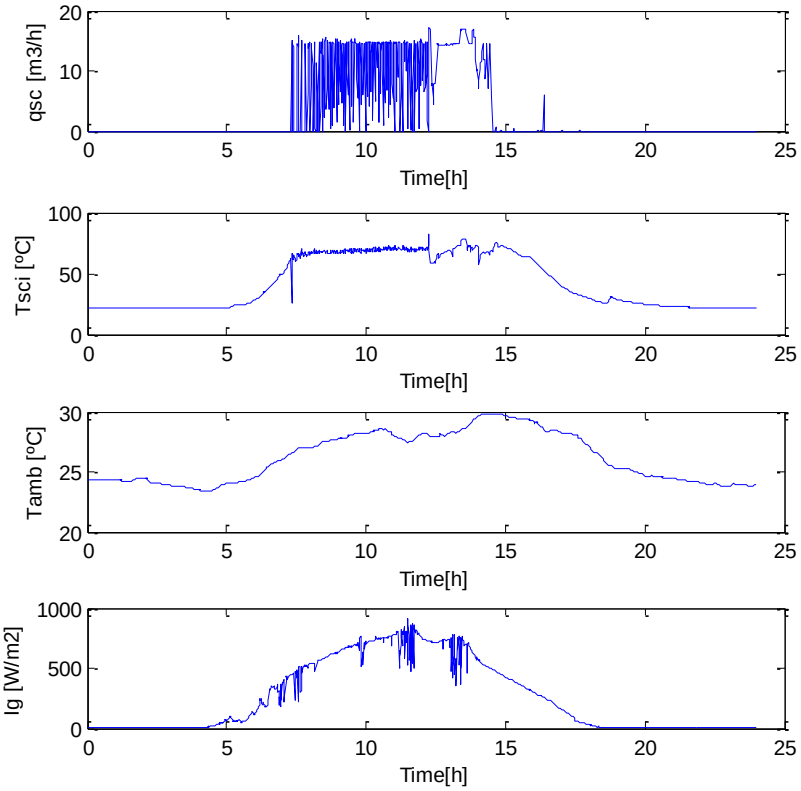

Figure 4.6.- Inputs values for solar collector validation

A comparison between the model response with the optimized parameters and the process responses can be seen in Figure 4.7. It suggests that the results produced by the model are close to those obtained from the system, then the implemented model is assumed to be a valid representation of the system.

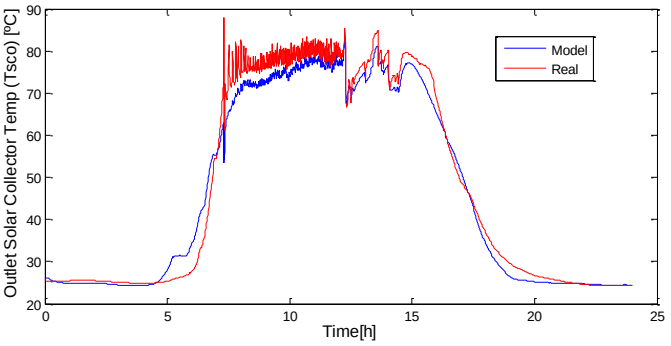

Figure 4.7.- Validation of solar collector model

4.2.2.- Gas Heater Model

The gas heater is connected in series between the second storage tank and the absorption machine. It can be used to increase temperature of the water from the solar collector field or hot water storage tanks, or even to fulfill the entire heat demand.

A detailed gas heater model can be found in Zambrano et al. [103]. The model considers the heat supplied, the one transported by the water and the ambient losses as given by (4.3). Figure 4.8 presents the schematic used: T_{gwi} and T_{gwo} are the inlet and outlet temperatures of the water circulating through the gas heater q_{gh} (l/s), respectively (ºC); C_{tg} is the heat capacity of the water (J/ºC), C_{gh} is the specific heat of the water (J/lºC), U_{aw} the heat losses to the ambient per unit difference of temperature between the water and the ambient when the heater is on and off respectively (W/ºC). Finally, E_{gh} is the power that can be supplied from the burning gas to the water (W) which depends on the flow circulating through the gas heater as is shown in Figure 4.9.

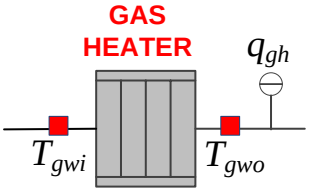

Figure 4.8.- Scheme of the gas heater subsystem

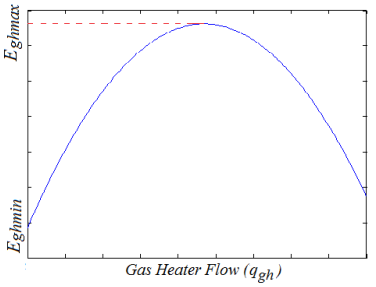

Figure 4.9.- Power supplied by the burning gas

$$C_{tg}\frac{dT_{gwo}}{dt} = E_{gh} + C_{gh}q_{gh}\left(T_{gwi} - T_{gwo}\right) + U_{aw}\left(T_{amb} - T_{gwo}\right) \tag{4.3}$$

The equations from the gas heater model include a set of unknown parameters that are specific of each device. They were estimated in the case study based on experimental response, so that the model responses are close to the gas heater plant. For this purpose, data collected on the process were used together with an optimization approach as shown in Figure 4.10.

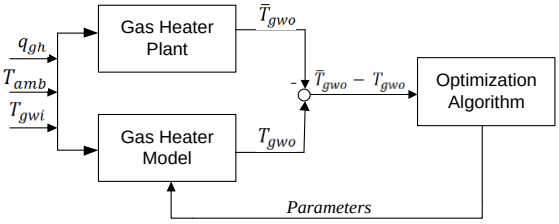

Figure 4.10.- Schematic for parameter estimation

The cost function used is the accumulated squared error between the model output and its measurements. The value of this cost function depends on the unknown parameters of the model so that an optimization algorithm is used to compute the values that minimize the cost function.

In order to validate the model obtained by minimizing accumulated squared error between the model output and its measurements, the inputs given in Figure 4.11 and Figure 4.12 were used to compare the system measurements and model results.

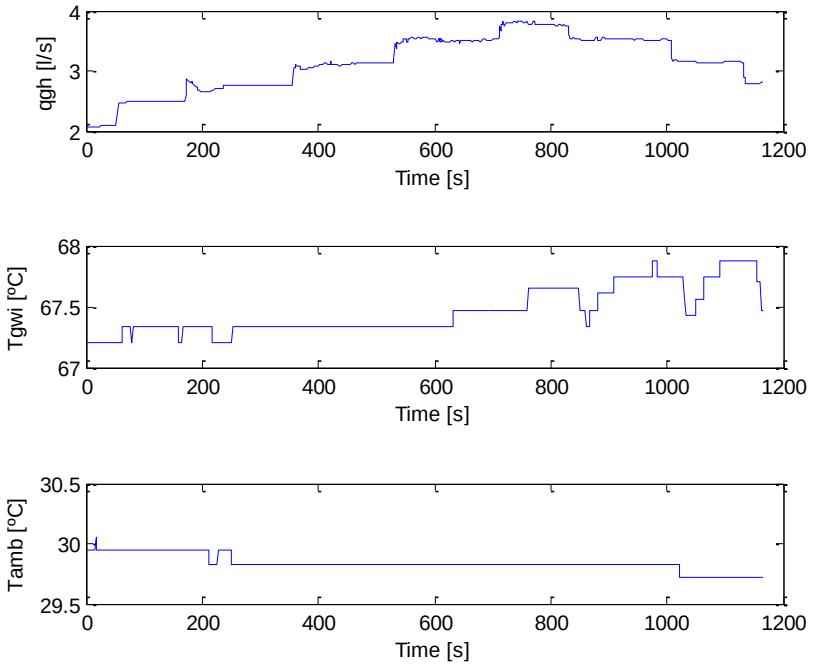

Figure 4.11.- Inputs values for Gas Heater (ON Mode)

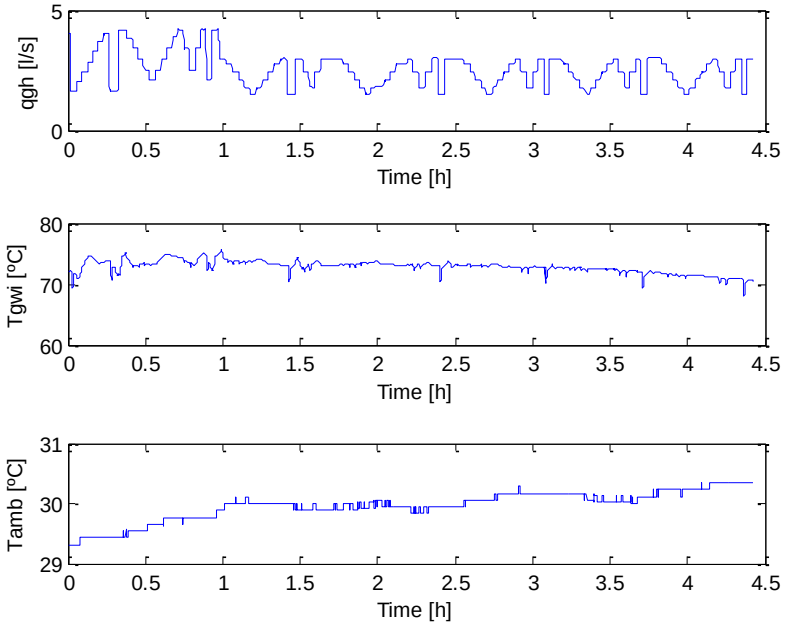

Figure 4.12.- Inputs values for Gas Heater (OFF Mode)

A comparison between the model responses and the process responses can be seen in Figure 4.13 and Figure 4.14 for two experiments: when the heater is connected or disconnected, respectively. As a result, a good agreement can be obtained between the model output and the experimental data.

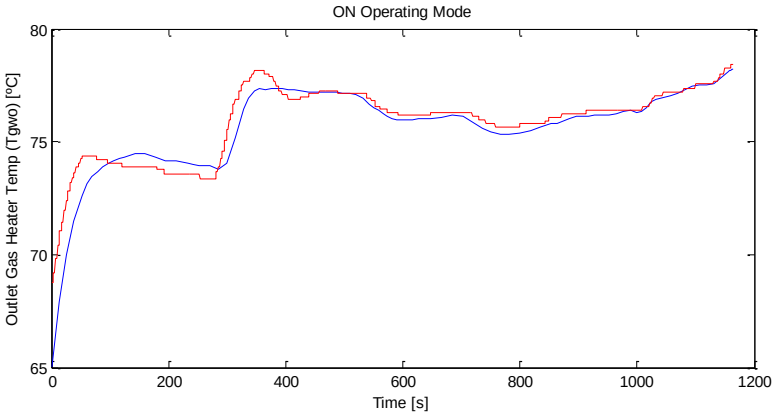

Figure 4.13.- Validation of Gas Heater (ON Mode)

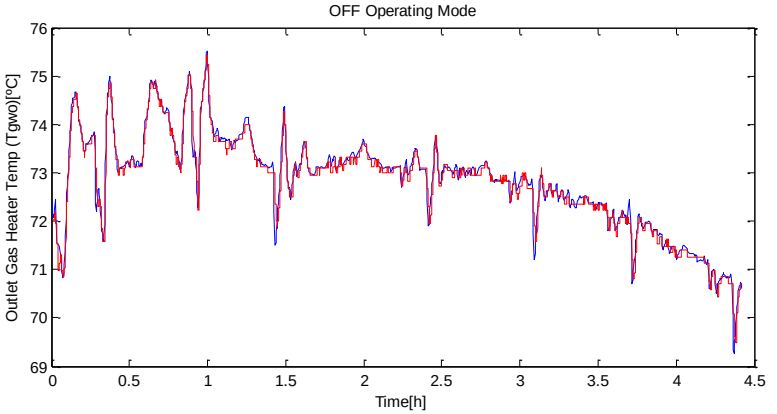

Figure 4.14.- Validation of Gas Heater (OFF Mode)

4.2.3.- Storage Tanks Model

Unfortunately, the short-term variability of the solar collector field temperature is well known. As it has mentioned, two storage tanks connected in series store temporarily the extra energy generated by the solar collectors. They act as a buffer, so they are always full of water. Hot water can be stored for later use when solar irradiation is not enough. The tanks can receive hot water from generator or solar collectors, and its output can be connected to the gas heater, or they can be isolated from the energy supply subsystem, following the control algorithm.

A stratified model as the suggested by Kleinbach et al. [104] has been considered, which includes six thermal layers (three in each tank at the top -T_{S4}, T_{S7}-, bottom -T_{S2}, T_{S5}- and middle side -T_{S3}, T_{S6}-). It is assumed that the water in each layer has uniform temperature, as shown in Figure 4.15.

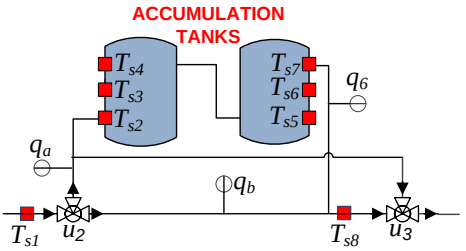

Figure 4.15.- Scheme of the accumulation subsystem

The equations used are based on energy balances, considering a heat transfer coefficient proportional to the water flow and the ambient losses. The equations are given by (4.4), (4.4), (4.5), (4.6), (4.7) and (4.8), where V is the tank volume in each layer (l), C_p is the specific heat of the water (J/Kg°C), ρ is the density of the water (Kg/l), U_{st} is the heat losses coefficient to the ambient per unit difference of temperature between the water and the ambient (W/°C), q_a and q_b are the water flow through the tanks which circulates from one side or the other respectively. The transport delays have been estimated based on data collected from different experiments.

$$C_p V\rho\frac{dT_{S2}}{dt} = K_a q_a C_p \rho\left(T_{S1}\left(t-T_{d1}\right)-T_{S2}\left(t\right)\right)+ K_b q_b C_p \rho\left(T_{S3}\left(t-T_{d2}\right)-T_{S2}\left(t\right)\right)+U_{st}\left(T_{amb}\left(t\right)-T_{S2}\left(t\right)\right) \tag{4.4}$$

$$C_p V\rho\frac{dT_{S3}}{dt} = K_a q_a C_p \rho\left(T_{S2}\left(t-T_{d3}\right)-T_{S3}\left(t\right)\right)+ K_b q_b C_p \rho\left(T_{S4}\left(t\right)-T_{S3}\left(t\right)\right)+U_{st}\left(T_{amb}\left(t\right)-T_{S3}\left(t\right)\right) \tag{4.5}$$

$$C_p V\rho\frac{dT_{S4}}{dt} = K_a q_a C_p \rho\left(T_{S3}\left(t-T_{d4}\right)-T_{S4}\left(t\right)\right)+ K_b q_b C_p \rho\left(T_{S5}\left(t-T_{d5}\right)-T_{S4}\left(t\right)\right)+U_{st}\left(T_{amb}\left(t\right)-T_{S4}\left(t\right)\right) \tag{4.6}$$

$$C_p V\rho\frac{dT_{S5}}{dt} = K_a q_a C_p \rho\left(T_{S4}\left(t-T_{d6}\right)-T_{S5}\left(t\right)\right)+ K_b q_b C_p \rho\left(T_{S6}\left(t\right)-T_{S5}\left(t\right)\right)+U_{st}\left(T_{amb}\left(t\right)-T_{S5}\left(t\right)\right) \tag{4.7}$$

$$C_p V\rho \frac{dT_{S6}}{dt} = K_a q_a C_p \rho\left(T_{S5}(t) - T_{S6}(t)\right) + K_b q_b C_p \rho\left(T_{S7}(t - T_{d7}) - T_{S6}(t)\right) + U_{st}\left(T_{amb}(t) - T_{S6}(t)\right) \quad (4.8)$$

$$C_p V\rho \frac{dT_{S7}}{dt} = K_a q_a C_p \rho\left(T_{S6}(t - T_{d8}) - T_{S7}(t)\right) + K_b q_b C_p \rho\left(T_{S8}(t) - T_{S7}(t)\right) + U_{st}\left(T_{amb}(t) - T_{S7}(t)\right) \quad (4.9)$$

Each equation corresponds to one thermal layer, and includes parameters to be estimated so that the model responses are close to the corresponding thermal layer inside the storage tank. Considering the first thermal layer, data collected on the process were used together with an optimization approach to estimate the model parameters as is shown in Figure 4.16.

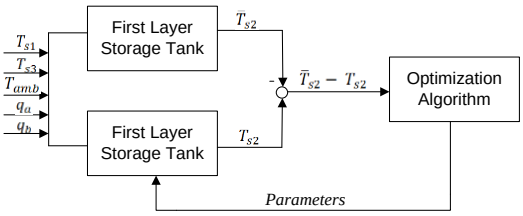

Figure 4.16.- Schematic for parameter estimation

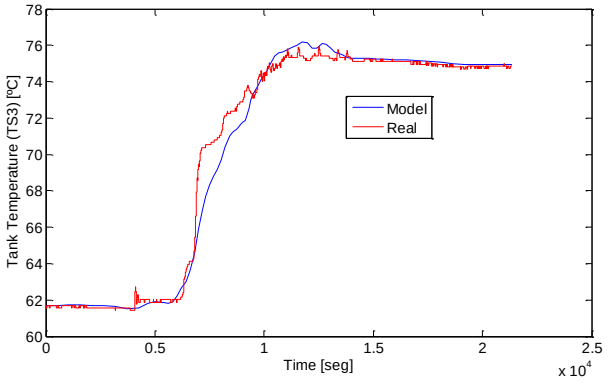

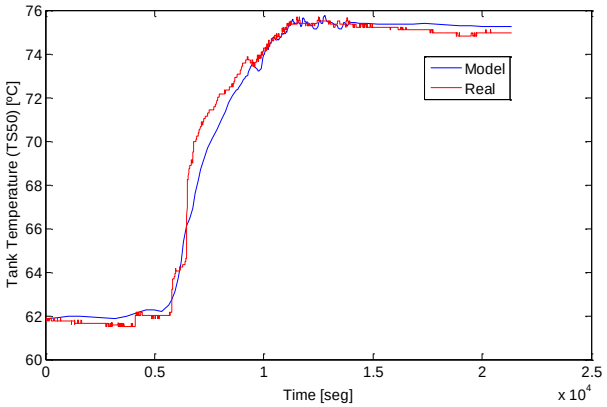
Tank Temperature (TS50) [ºC]
Time [seg]
x 10^4
Model
Real

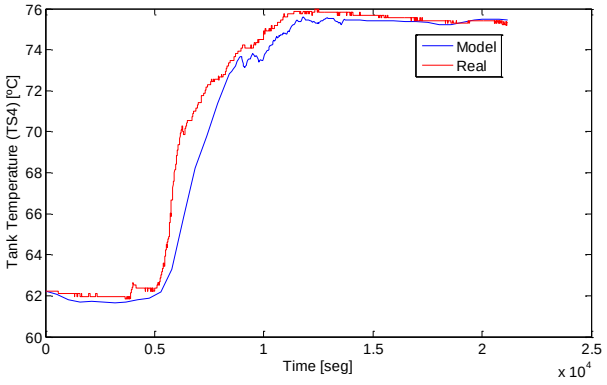
Tank Temperature (TS4) [ºC]
Time [seg]
x 10^4
Model
Real

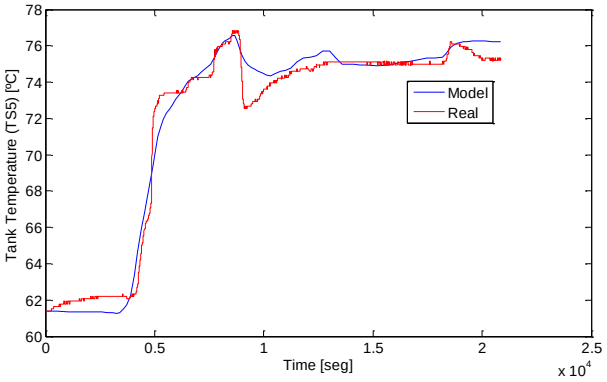
Tank Temperature (TS5) [ºC]
Time [seg]
x 10^4
Model
Real

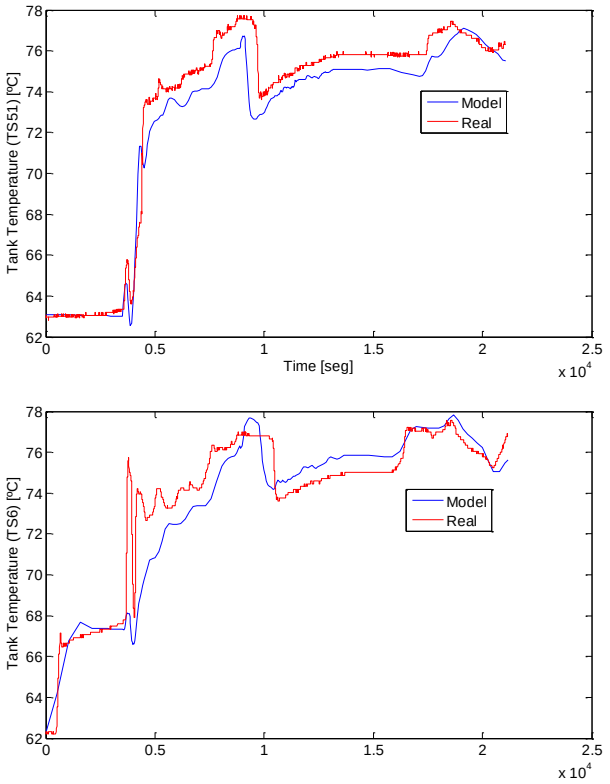

Figure 4.17.- Validation of Storage Tanks Model

The cost function was computed as accumulated squared difference between the model output and its measurements when the same experimental values were applied to the inputs of the simulation. An optimization algorithm can compute the value of the parameters that minimizes the cost function.

A comparison between the model response and the process responses for 6 thermal layers can be seen in Figure 4.17. As a result, a good agreement can be obtained between the model output and the experimental data.

4.2.4.- Absorption Machine Model

The absorption machine is a single – effect LiBr-H2O absorption device. The refrigerant used is water, and the absorbent lithium bromide (LiBr). The machine has four circuits: evaporator, generator, condenser and absorber (here the energy exchange that produces chilled water takes place). The entire process is shown in Figure 4.18. The components are now presented:

1. *Generator*: After exiting the heat exchanger, the dilute solution moves into the upper shell, where the generator (GE) is located. As a result of the heat supplied, the water from dilute solution boils and the vapor formed flows to the condenser (CO). The remaining solution is concentrated up to 56% LiBr. This solution flows through the heat exchanger (H), where it is cooled by the dilute solution being pumped up to the generator.

2. *Condenser*: The vapor is condensed to a liquid stated by transfer of heat to the cooling water from an external cooling tower. The cooling capacity depends on the inlet temperature of the generator and the condenser.

3. *Evaporator*: The refrigerant is introduced into the evaporator (E) where it boils at low pressure, taking the heat from the chilled water circulating through the evaporator, decreasing its temperature.

4. *Absorber*: The 56% concentrated solution of LiBr from generator (GE) flows to the absorber and shares space and pressure with the evaporator (E), where the refrigerant vapour is absorbed by the LiBr thanks to its affinity for water. The absorption generates heat which is removed by cooling water. The resulting dilute lithium bromide solution collects in the bottom of the lower shell, where it flows down to the solution pump (SP). The whole process is then repeated.

5. *Heat Exchanger*: A hermetic solution pump (SP) moves the dilute lithium bromide solution, collected in the bottom of the absorber shell, through a tube heat exchanger (H) for preheating.

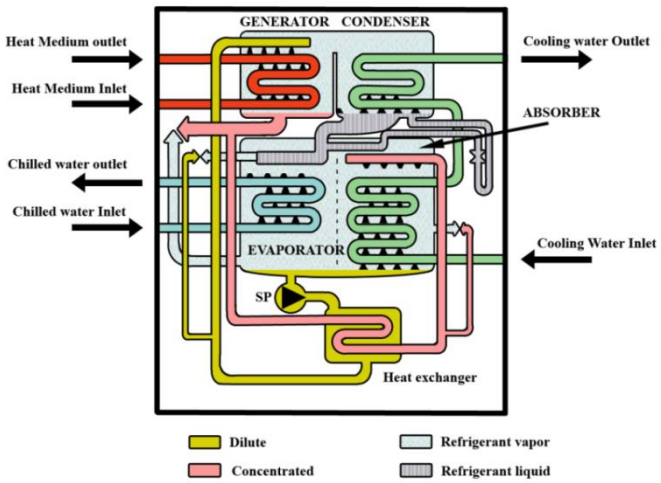

Figure 4.18.- Scheme of the Absorption Machine

For control purpose, the inlet temperature range of the generator mus be maintained in the range $\left[\overline{T_{gi}}, \underline{T_{gi}}\right]$; and of the condenser within $\left[\overline{T_{rei}}, \underline{T_{rei}}\right]$. A microprocessor embedded in the absorption machine control the evaporator circuit, the cooling tower fan as well as the water flow that circulates through the generator circuit. If the internal control of the absorption machine detects that the inlet temperature of the generator or condenser are not in the desired range, water flow is stopped.

In the literature there are complex thermodynamic models describing this kind of absorption machines, as the one presented in Grossman et al. [105]. However, for control purpose, a simplified model has been considered that includes one energy balance in the generator circuit (see Figure 4.19).

The model is then described by equation (4.10), where T_{gi} and the T_{go} are the input and the output temperatures of the generator circuit (ºC), T_{amb} is the ambient temperature (ºC), q_g is the water flow circulating through the generator circuit (m^3/s), C_g is the heat capacity of the flat plate (J/ºC), C_p is the specific heat of the water (J/m^3ºC), U_{st} is the heat losses to the ambient per unit difference of temperature between the water and the ambient (W/ºC) and Q_{gn} is the heat delivered to the generator that depends on the input water temperature of the generator T_{gi} and the condenser T_{rei} as shown in Figure 4.20 for the machine in the installation used as case study.

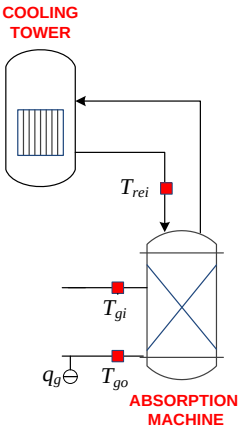

Figure 4.19.- Scheme of the absorption machine

$$C_g \frac{dT_{go}}{dt} = C_p q_g \left(T_{gi}(t) - T_{go}(t)\right) + U_{st}\left(T_{amb}(t) - T_{go}(t)\right) - Q_{gn}(T_{gi}, T_{rei}) \qquad (4.10)$$

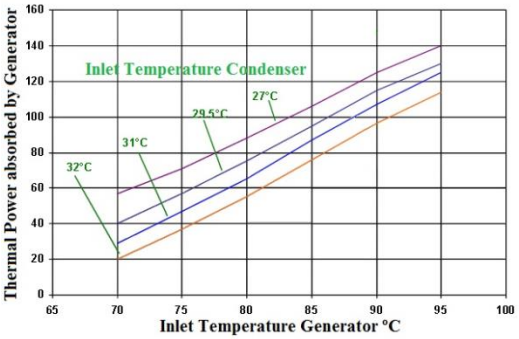

Figure 4.20.- Heat absorbed by the generator of the absorption machine

The equation from the generator model includes a set of unknown parameters that are estimated. For this purpose, data collected on the process were used together with an optimization approach as shown in Figure 4.21.

The cost function used is again as the accumulated squared difference between the model output and the measurements. The value of this cost function depends on the unknown parameters of the model so that the optimization algorithm can compute the value of the parameters that minimize this cost function.

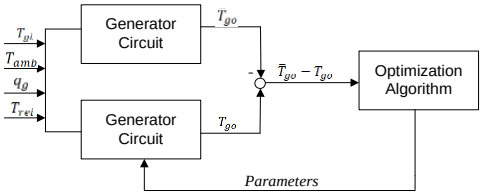

Figure 4.21.- Schematic for parameter estimation

A comparison between the model responses and the process responses is shown in Figure 4.22. Good agreement is obtained between the model output and the experimental data.

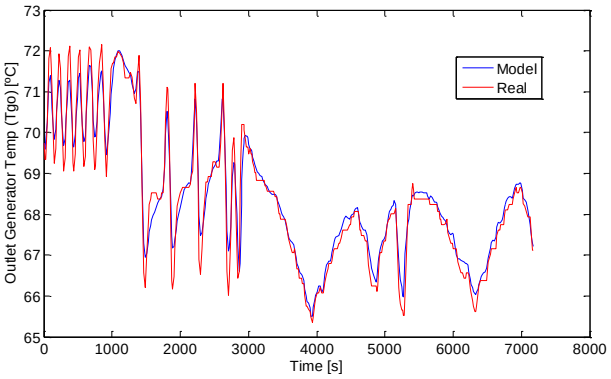

Figure 4.22.- Validation of the Generator Circuit Model

4.2.5.- Flow Model

The flows q_1, q_2, q_5 and q_6 shown in Figure 4.23 depend on the speed of the pump v_{B01} and the position of the valves u_1, u_2 and u_3 that are the main variables in our models. Dynamics have has been neglected considering that the dynamic response is much faster for the flow than for the temperature. As a result, the flow equations have been written as static nonlinear polynomial functions.

Parameters in these polynomial functions have been obtained by the identification, based on the data measured for q_1, q_2, q_5 and q_6, using an optimization approach. For instance, considering the first flow q_1 and the scheme shown in Figure 4.24, after fixing the position valve u_2, the speed of the pump v_{B01} is changed from 0% to 100% with increments of 10%, repeating this procedure for the entire range of u_2.

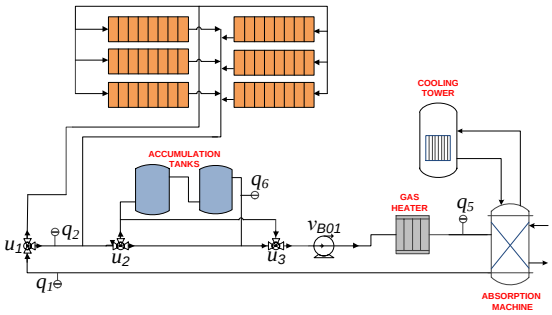

Figure 4.23.- Scheme of the Solar Heat Supply System

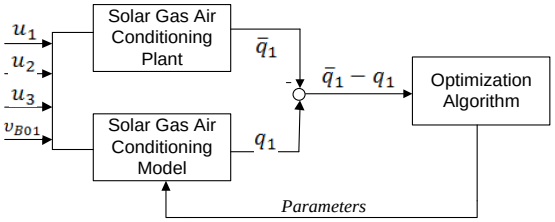

Figure 4.24.- Schematic for parameter estimation of flow model

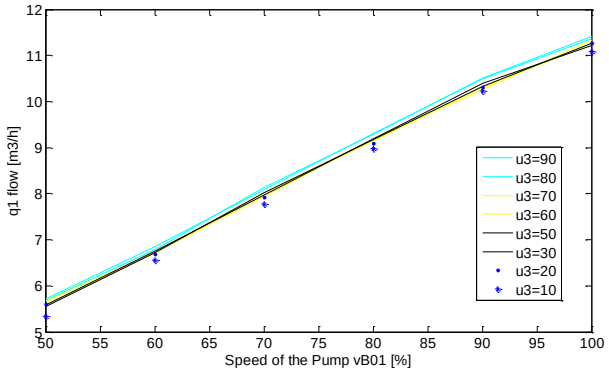

Figure 4.25.- Model for q_1

The results are presented in Figure 4.25: It can be seen that q_1 flows as a function of the speed of the pump v_{B01} with negligible dependence on the valve u_3. Meanwhile, q_6 is both function of the speed of the pump v_{B01} and the position valve u_3 (s. Figure 4.26).

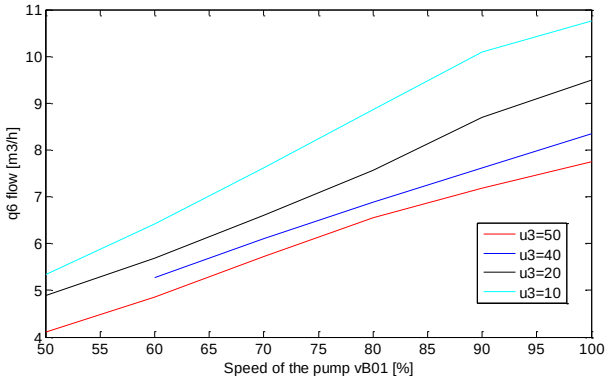

Figure 4.26.- Model pump nonlinearities for q_6

4.2.6.- Power Pump Model

From an energy consumption point of view, the pump v_{B01} is the most energy consuming component, hence, study of their power consumption is important. For this, the performance curve supplied by the manufacturer is shown in Figure 4.27. The curve shows the differential head H against the water flow q and is introduced in our model as a polynomial equation with parameters identified considering experimental results.

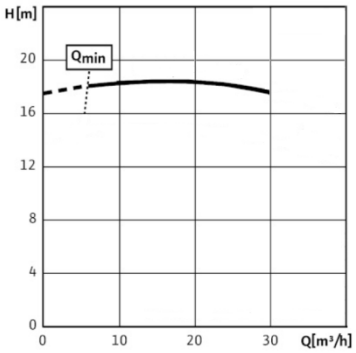

Figure 4.27.- Power pump performance curve

The ideal hydraulic power to drive a pump depends on the mass flow rate q, the liquid density ρ and the differential head H and can be calculated as presented in (4.11), where P_{hyd} is the ideal hydraulic power (W), q is the water flow through the pump (m^3/s), ρ is the density of the fluid (kg/m^3), g is the gravity (m/s^2) and H is the differential head (m). Additionally, the shaft power - the necessary power transfer from the motor to the shaft of the pump - depends on the efficiency of the pump η_{pump} and the motor η_{motor}. The shaft power P_1 is calculated as shown in (4.12). Finally, the pressure difference through the pump is given by the equation (4.13).

$$P_{hyd} = \rho g q H(q) \tag{4.11}$$

$$P_1 = \frac{P_{hyd}}{\eta_{pump}\eta_{motor}} \tag{4.12}$$

$$\Delta P_r = \rho g H \tag{4.13}$$

The polynomial relation $H(q)$ includes a set of unknown parameters that are estimated so that the model responses are close to the real pump. For this purpose, data collected on the process were used together with an optimization approach as shown in Figure 4.28.

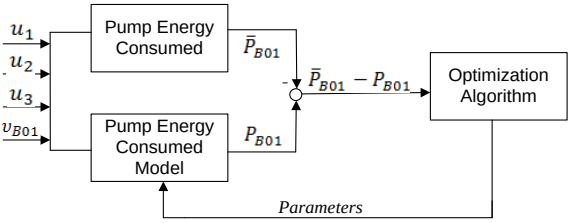

Figure 4.28.- Schematic for parameter estimation

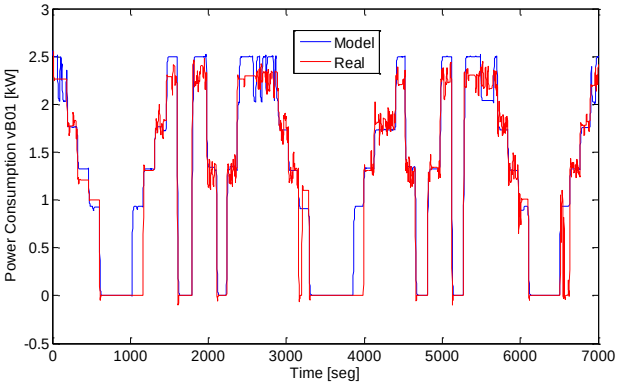

Figure 4.29.- Validation of the Power Pump Model

The cost function is again the accumulated squared difference between the model output and the measurements. The value of this cost function depends on the unknown parameters of the model so that an optimization algorithm computes the value of the parameters that minimize the cost function. A comparison between the measured data and the output model can be seen in Figure 4.29.

4.3.- Simulation Platform

The hybrid model, developed in Section 4.2, has been implemented in MATLAB Simulink. The implementation has been done as a modular structure which shown in Figure 4.30. The modular structure facilitates changes and the implementation of improvements in the model. The model is divided into six modules:

- One module for each components of the plant (solar collectors, gas heater, storage tanks, absorption machine);
- Other module related to the safety valve included in the whole system
- The last module for the water flow resulting from the position of the valves u_1, u_2, u_3 and the speed of the pump v_{B01}.

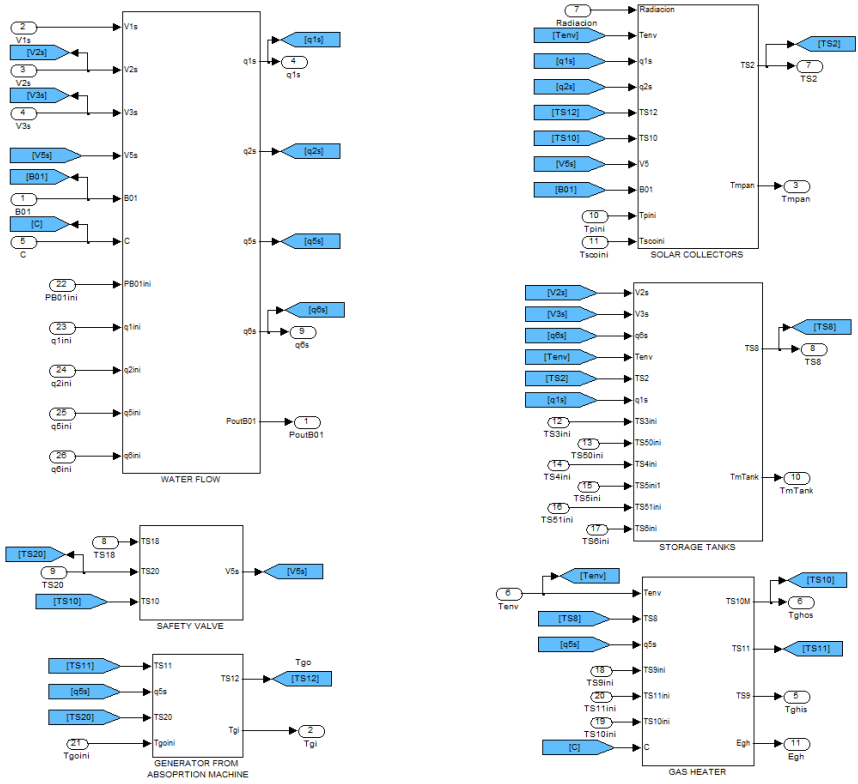

Figure 4.30.- Solar Gas Air Conditioning Platform

4.4.- Disturbance Prediction Model

Predictions of solar irradiation and ambient temperature are necessary for the control methodology proposed as energy management system. A simplified solar irradiation solar model for renewable energy applications was proposed in Myers [106]. More complex modeling methods based on empirical models were given in Li Danny et al. [107]. Methods for forecasting daily total solar irradiation based on adaptive wavelet network (Mellit et al., [108]) and fuzzy logic (Iqdour et al., [109]) have also been proposed. However, a reliable and simple model must be provided at the optimizer to obtain trustworthy results of the optimization due to the fact that the model must be evaluated by the optimizer several times each sample time to find a feasible solution. For this purpose, a model that predicts a time distribution of solar irradiation and ambient temperature described by Chaabene [110] was selected. Both solar irradiation and ambient temperature for each day (d) are estimated considering their measured evolution during the previous day (d-1).

4.4.1.- Irradiation Prediction Model

The proposed prediction model is based on a sinusoidal distribution and assumes that the maximum solar irradiation during the day (*d*) is the same as the previous day (*d*-1), as shown in (4.14), where *t* is the time, $\Delta L(d)$ is the day length for the day *d* and $I_{max}(d\text{-}1)$ is the value of $I(d\text{-}1,t)$ at $t = \Delta L(d\text{-}1)/2$, which can be expressed as (4.15), where $G(d\text{-}1)$ is the amount of solar irradiance of the previous day and is provided by a weather station (s. Figure 4.31).

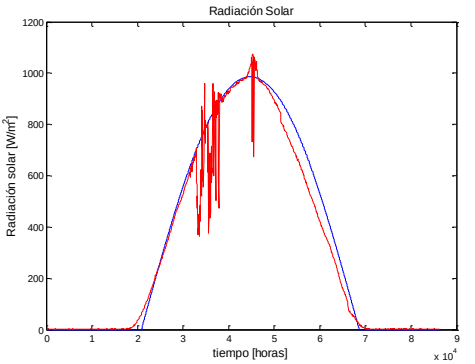

Figure 4.31.- Validation of the Irradiation Prediction Model

$$I(d,t) = I_{max}(d-1)\sin\left(\frac{\pi\,(t - GMT_{sunrise})}{\Delta L(d)}\right) \tag{4.14}$$

$$I_{max}(d-1) = \frac{\pi\, G(d\text{-}1)}{2\,\Delta L(d-1)} \tag{4.15}$$

Additionally, the day length $\Delta L(d)$ is computed by (4.16), (4.17), (4.18), (4.19) and (4.20), where GMT_{sunset} and $GMT_{sunrise}$ are the sunset and sunrise hours of the day *d* with $\varepsilon = +1$ for sunset and $\varepsilon = -1$ for sunrise, *L* is the longitude, ϕ the latitude, T_e the time equation (h), δ the declination (degree), *D* the day of the month, *m* the month number (January=1) and *N* the day of the year.

$$\Delta L(d) = GMT_{sunset}(d) - GMT_{sunrise}(d) \tag{4.16}$$

$$GMT(d) = 12 - T_e(d) + \frac{L + \varepsilon \cos^{-1}(tg\delta(d)\,tg\phi)}{15} \tag{4.17}$$

$$T_e(d) = 0.123\cos(N(d)+87) - \frac{\sin(2N(d)+20)}{6} \tag{4.18}$$

$$\delta(d) = 23.45\cos(N(d)+10) \tag{4.19}$$

$$N(d) = 0.988[D(d)+30.3(m(d)-1)] \tag{4.20}$$

4.4.2.- Ambient Temperature Prediction Model

The ambient temperature prediction model for the day *d* is computed using a sinusoidal distribution in combination with the minimum and maximum value of the ambient temperature registered during the previous day (*d-1*) (s. Figure 4.32). The equation is presented in (4.21), where T_{max} and T_{min} are the maximum and minimum value for the ambient temperature during the previous day (*d-1*).

$$T_{amb}(d,t) = \left(\frac{T_{max}(d-1)+T_{min}(d-1)}{2}\right) + \left(\frac{T_{max}(d-1)-T_{min}(d-1)}{2}\right)\sin\left(\frac{\pi(t-GMT_{sunrise})}{\Delta L(d)}\right) \tag{4.21}$$

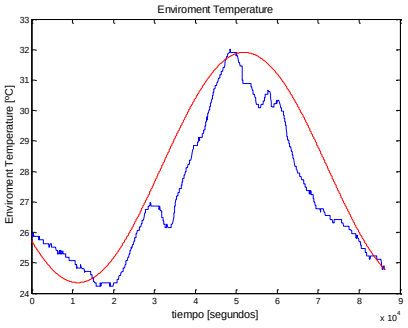

Figure 4.32.- Validation of the Ambient Temperature Prediction Model

4.5.- Hybrid Model Predictive Control

Model Predictive Control (MPC) offers a useful framework for solving problems of optimal decisions in real time under a set of constraints (Camacho et al., [25]). Thus, an MPC approach was selected for developing the controller, following previous experiences in renewable energy systems (s. Palacin et al., [111]) (Salazar et al., [112]).

The objectives of the proposed controller are:

- To maintain the inlet temperature of the absorption machine in the range $\left[\underline{T_{gi}}, \overline{T_{gi}} \right]$, in spite of possible disturbances
- To minimize the gas and electrical consumptions
- To guarantee the proper functioning of the equipment.

Notice the solar irradiation cannot be manipulated and has to be treated as a measurable disturbance while the decision variables are given by:

- The gas heater ON/OFF signal (δ_{gh}).
- The speed of the pump B01 (v_{B01}).
- The position of the mixing valve connected to the tanks (u_{tan}).

The proposed optimization minimizes the cost function J in each sampling time, considering the manipulated variables and the control objectives mentioned above, as described in (4.22).

$$
\begin{aligned}
J = {} & G_{\tan} V_{\tan} \left(T_{\tan}(N_{pb}) - T_{\tan}(0) \right) + \\
& \sum_{k=0}^{N_{pb}} \alpha_1 \left(\max\left(\left(T_g^{\min} - T_g(k) \right), 0 \right) \right)^2 + \\
& \sum_{k=0}^{N_{pb}} \alpha_2 \left(\max\left(\left(T_g(k) - T_g^{\max} \right), 0 \right) \right)^2 + \\
& \sum_{k=0}^{N_{pb}} G_{el} P_{B01}(k) + \\
& \sum_{k=0}^{N_{pb}} G_{oth} \frac{E_{gh}(k)}{C_{gh} Eff}
\end{aligned}
\tag{4.22}
$$

This function is integrated by five terms:

- The first (J_1) evaluates the variation of the thermal energy stored in the tank (final less initial value).

- The second and third terms (J_2 and J_3) penalize tank levels below a minimal value $T_{gi}^{\min}$ or over a maximum level $T_{gi}^{\max}$, respectively, with α_1 and α_2 tuning parameters.

- The fourth term (J_4) penalizes the electrical consumption of the pump v_{B01} (P_{B01}(k)). G_{el} (€/kWh) is the cost of a kWh imported from the main grid.

- The last term (J_5) penalizes the cost of the energy generated by the gas heater, to minimize the gas consumption. G_{oth} (€/kWh) is the cost of a thermal kWh generated by the gas heater.

Several constraints that must be fulfilled are as follows:

1) Time limitations between gas heater startups and shutdowns, to avoid excessive intermittent operation, as described in (4.23):

$$\begin{aligned} T^{k}_{on,i} &\geq \underline{T_{on,i}} \\ T^{k}_{off,i} &\geq \underline{T_{off,i}} \end{aligned} \tag{4.23}$$

2) The speed of the pump v_{B01} is limited by a minimum and a maximum value, as presented in (4.24):

$$\underline{v_{B01}} \leq v_{B01} \leq \overline{v_{B01}} \tag{4.24}$$

3) The position of the mixing valve connected to the tanks u_{tan} responsible for controlling the water flow circulating through the storage tanks is limited by a minimum and a maximum value given by expression (4.25):

$$\underline{u_{\tan}} \leq u_{\tan} \leq \overline{u_{\tan}} \tag{4.25}$$

Initially, as the proposed model predictive control proposed includes one binary variable δ_{gh}, the MPC problem corresponds to a problem of mixed integer optimization which is known to be computationally complex, see for instance Bemporad et al. [113] and Prada et al. [114]). In order to transform the optimization problem into a nonlinear one, but with continuous variables (NMPC), two new continuous manipulated variables are defined $T^{k}_{on,i}$ and $T^{k}_{off,i}$ which correspond to the duration of each activation/deactivation of the binary variable δ_{gh} respectively.

Regarding the MPC tuning parameters, the control horizon N_c and the prediction horizons N_p are the most important: In this case, these horizons are influenced by the gas heater dynamic. To compute the cost function J, the internal model will be integrated until the binary variables δ_{gh} has made at least one pulse (N_{pb}=1) Thus, the control and prediction horizons will depend on the time required by the binary variables δ_{gh} to generate a pulse.

For the continuous manipulated variable, a control horizon of two is considered as is shown in Figure 4.33. As a result, the optimization algorithm will provide three values for each continuous variable: two values for manipulating the speed of the pump B01 and the position of the mixing valve connected to the tanks ($v_{B01}(1)$, $v_{B01}(2)$, $u_{tan}(1)$, $u_{tan}(2)$) and one value of the duration (Tv_{B01}, Tu_{tan}) of the application of the first prediction ($v_{B01}(1)$, $u_{tan}(1)$). The second prediction ($v_{B01}(2)$, $u_{tan}(2)$) is not necessary, since the sign is held until the end of the prediction horizon. In summary, the optimizer will provide three optimal signals for the control of the speed of the pump B01 and the position of the mixing valve connected to the tanks.

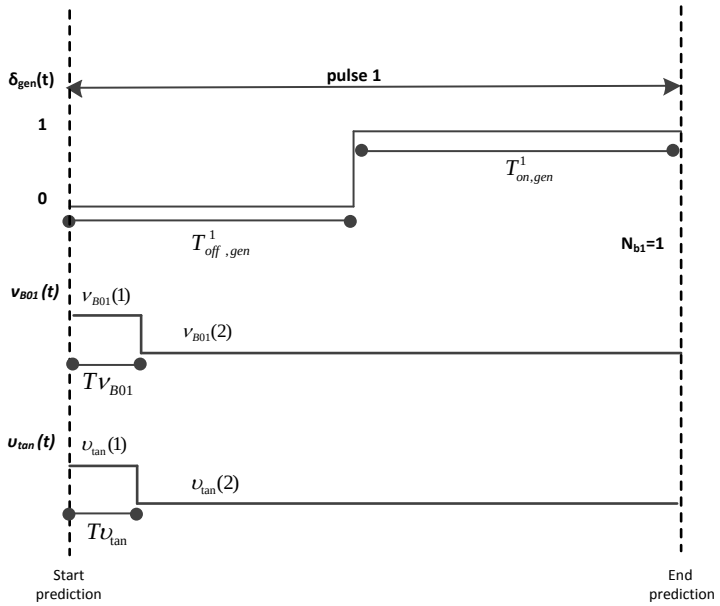

Figure 4.33.- Structure of the prediction and control horizons

The nonlinear optimization problem proposed in equation (4.22) is solved periodically, with a sampling period T_s, using the scheme presented in Figure 4.34. This diagram shows a sequential approach where the cost function J is calculated by integrating the internal dynamic model over the prediction horizon N_{pb}, taking the current state of the system as initial condition and evaluating the cost function at the end of the integration. Following a horizon approach, the optimization produces an optimal control sequence but only the first control signal is applied to the process. At the next control instant, the horizon is displaced towards the future and the controller using new measurements solves and updates the optimal control.

The internal model must represent the process dynamic to predict the output signal quite accurately as well as being simple because the future control actions computed by the optimizer takes into account the integration each sampling time of

the model along the prediction horizon. The dynamic model correspond to the Solar Gar Air Conditioning Plant is given by equations from (4.1) to (4.15).

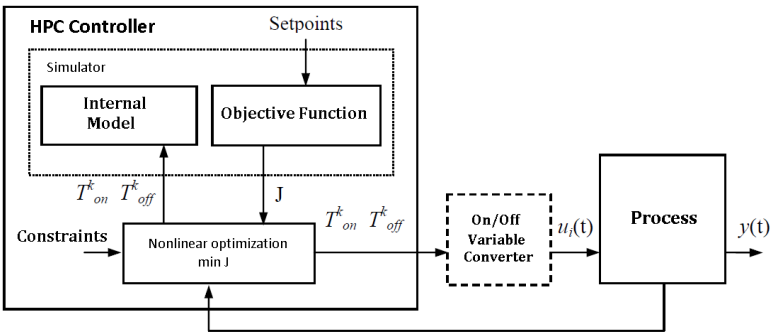

Figure 4.34.- Implementation of the Nonlinear Controller

From a technical point of view, it is necessary to add a converter between the predictive controller and the process. The Predictive Controller computes the times $T^k_{on,i}$ and $T^k_{off,i}$, then the converter transforms these continuous manipulated variables into ON/OFF signals corresponding to each binary manipulated variable. The use of the converter, together with the use of a continuous internal model, allows the ON/OFF variables to be decoupled from the sampling period.

4.6.- Validation

4.6.1.- Validation by simulation

A fundamental feature of a solar power plant is that the primary energy source cannot be manipulated. The intensity of the solar radiation, its seasonal and daily cyclic variations depends on atmospheric conditions such as cloud cover, humidity and air transparency. Thus, the control system was first tested in simulation using meteorological measurements at the target location. Some results of the application of the proposed methodology to a simulation of the process are presented from Figure 4.35 to Figure 4.41.

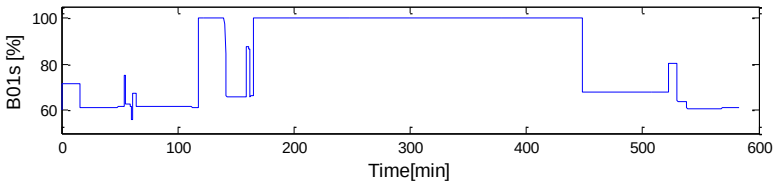

Figure 4.35.- Working point of the pump P_{B01}

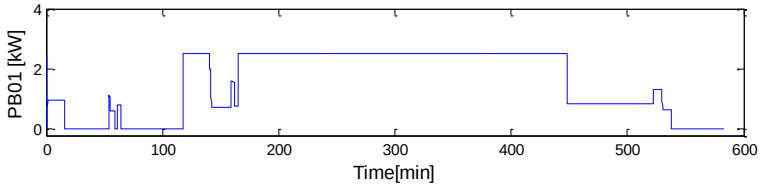

Figure 4.36.- Power consumed by the pump P_{B01}

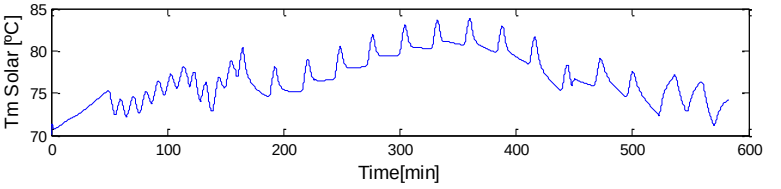

Figure 4.37.- Water temperature from solar collector field

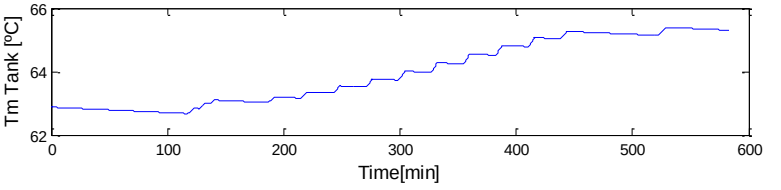

Figure 4.38.- Temperature of stored water in the tanks

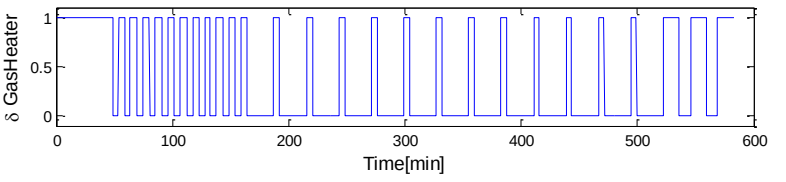

Figure 4.39.- Connection/Disconnection of gas heater

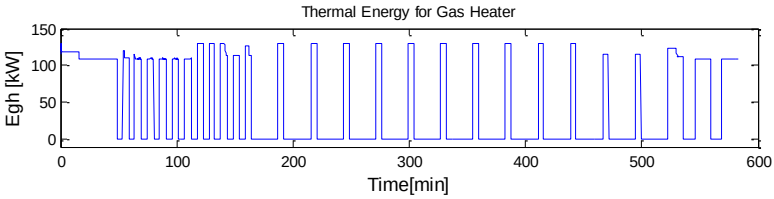

Figure 4.40.- Thermal Energy produced by gas heater.

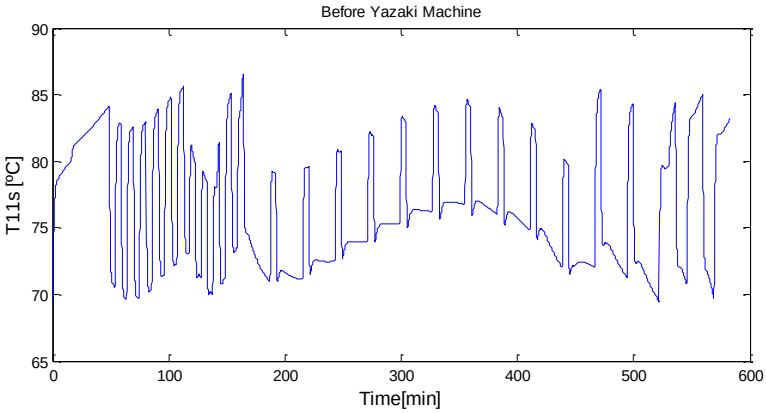

Figure 4.41.- Water temperature at the inlet of the absorption machine.

The main objective is to supply chilled water in the range [7ºC, 12ºC] to fan-coil units which is achieved by maintaining the inlet temperature of the absorption machine in the range [70º, 85º]. This is achieved by the proposed controller, as shown Figure 4.41. For this, the adjustment by the proposed controller of the flow (that is proportional to the pump consumption presented in Figure 4.36) and the thermal energy provided by the gas heater (presented in Figure 4.40) to maintain the inlet temperature inside a range considering the solar conditions change.

As it can be seen in Figure 4.37, in the morning (approximately time t=0 min to t=130 min), the thermal input from the solar collector field is not enough for keeping the inlet temperature of the absorption machine inside the range, as a consequence, the control system uses extensively the thermal energy provided by the gas heater. Since no extra thermal energy is available to be stored inside the tanks, the temperature of the stored water is not increased.

From time t=200 min to t=400 min, the outlet water temperature of the solar collector is well above 78º, so it is possible to minimize the consumption generated by the gas heater: the flow is used as a mean to maintain the inlet temperature inside the range. The average temperature of the storage tanks increases since some thermal energy provided by the solar collectors can be stored.

4.6.2.- Experimental validation

The proposed controller has been tested at CIESOL, Almería (Spain). Some results obtained are shown from Figure 4.42 to Figure 4.48. It can be seen that the main control objective is achieved: the inlet temperature of the absorption machine is maintained inside the range [70º, 85º] as shown in Figure 4.48.

From time t=0 to time t=1200, the solar energy is enough to supply the thermal energy necessary to maintain the inlet temperature of the absorption machine inside the range considering the adjustment of the fluid flow. There is no an excess of energy by the renewable source which could be stored inside the storage tanks. From time t=1200, the average temperature of the storage tanks since some extra thermal energy is available to be stored inside the tanks.

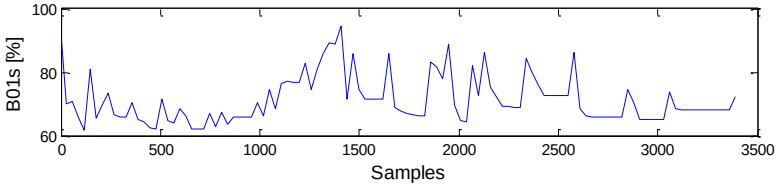

Figure 4.42.- Working point of the pump P_{B01}

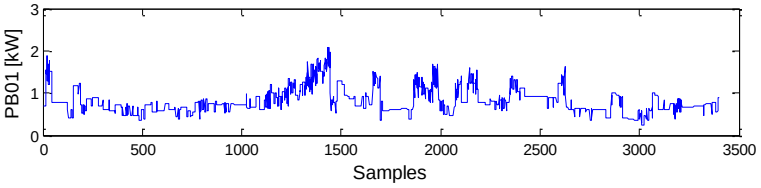

Figure 4.43.- Power consumed by the pump P_{B01}

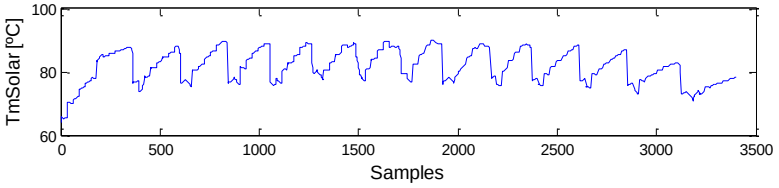

Figure 4.44.- Water temperature from solar collector field

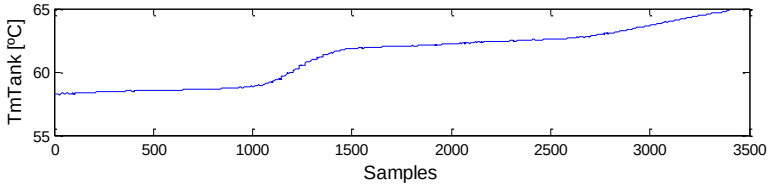

Figure 4.45.- Temperature of stored water in the tanks

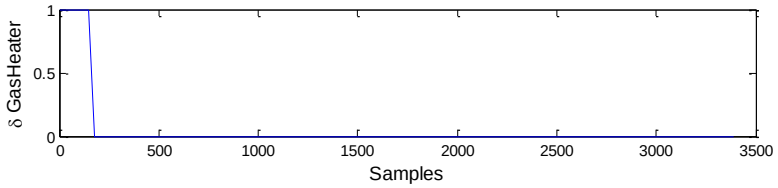

Figure 4.46.- Connection/Disconnection of gas heater

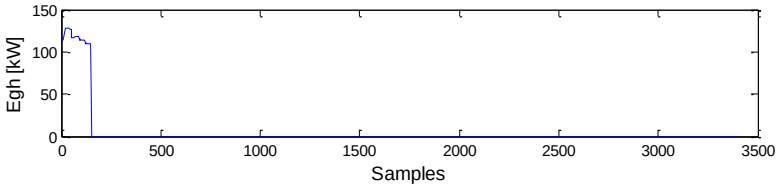

Figure 4.47.- Thermal energy produced by gas heater

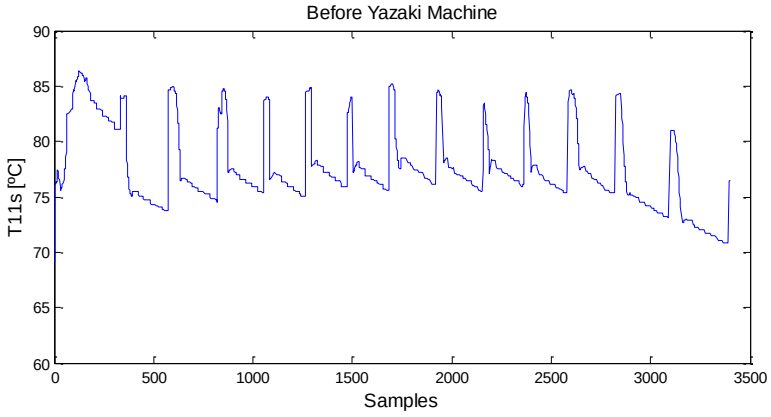

Figure 4.48.- Water temperature at the inlet of the absorption machine

4.7.- Hybrid Model Predictive Control Platform

The proposed predictive control was simulated and programmed with MATLAB. A real-time communication between the process devices and the MATLAB platform was carried out using OPC technology for a real time implementation. OPC, known as Open Process Control, is a series of several specifications defined by the OPC Foundation for supporting open connectivity in industrial automation based on Client/Server architecture (Zamarreño, [115]).

The real-time data exchange and remote communication was implemented thanks to the MATLAB OPC toolbox. This toolbox is an OPC Data Access client application, capable of connecting to any OPC Data Access compliant server. For this, configuring the OPC server object, the group objects and the items objects is required.

The OPC server object is defined by using the Host (computer on which the server is installed) and Server ID properties. In the OPC server object, OPC group objects can be created to manage OPC item objects. Each OPC server object can contains many OPC group objects. The direct data exchange with process data source is realized with OPC item objects. An OPC item object has a Value, a Quality, and a Timestamp, representing the information collected by the server from a process devices or a data point in SCADA system (s. Figure 4.49).

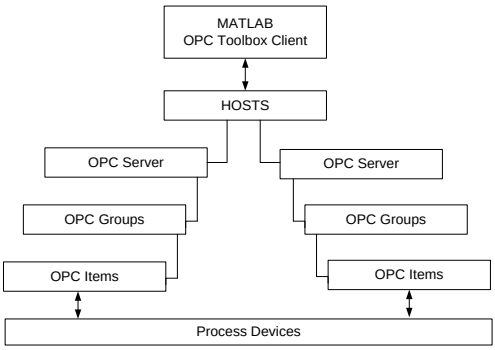

Figure 4.49.- OPC Exchange Data Diagram

There are three methods for data exchange between OPC client and OPC server:

- ***Synchronous operation***: MATLAB waits for the server to return data from a previous request.
- ***Asynchronous operation***: The OPC client sends a request to the server. Once the request has been accepted, MATLAB continues processing the next instruction without waiting for the server. MATLAB handles the read/write event as soon as it is able to perform that task.

- ***Subscription operation***: The OPC server will notify the OPC client automatically when the data changes. The update-rate and dead-band to deal with each OPC group can be configured.

Additionally, there are two communication modes for the OPC Server/Client:

- ***Local access***: The MATLAB client toolbox and the server are on the same PC (local host)
- ***Remote access***: The MATLAB client toolbox and the server are on separate PC connected via TCP-IP.

In our case, the local access was chosen as the communication modes and the Synchronous operation as the method for data exchange between OPC client and OPC server. In Figure 4.50, the OPC toolbox configuration used in our application is shown.

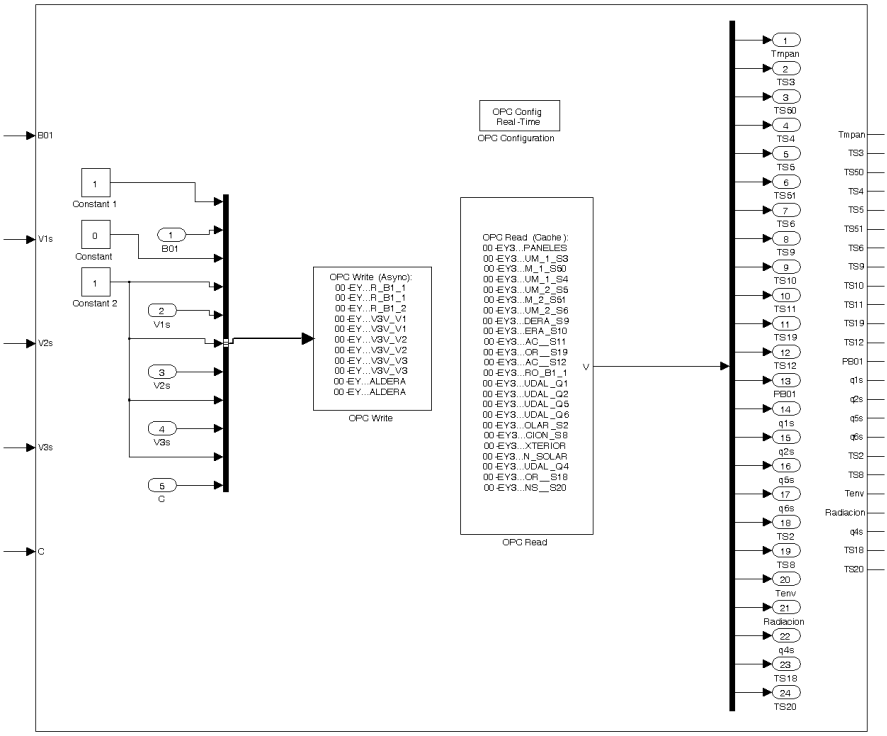

Figure 4.50.- Solar Gas Air Conditioning OPC Configuration

4.8.- Conclusions

A prediction-based control approach has been proposed to improve the operation of a solar gas air-conditioning system. Its performance has been demonstrated through simulation and experimental results on an installation integrated by a refrigeration system, a single – effect LiBr-H2O absorption machine and an auxiliary heat source. A specific predictive controller that takes into account the efficient use of the energy under the operational constraints is developed. Using the duration of the states as the main optimization variables make possible to transform the initial mixed integer optimization problem into a simpler problem that can be solved online. A central aspect of the controller is the models of the difference components used within the MPC to provide predictions, so they have been presented in detail.

CHAPTER 5

Hydrogen Based Microgrid

A Microgrid implies the interconnection of small, modular generation sources (microsource) to a low voltage distribution system (Lasseter et al., [116]). They can be connected to the national grid or be operated islanded. The supply sources may include reciprocating engine generator sets, microturbines, fuel cells, photovoltaic and other small-scale renewable generators, storage devices, and controllable end-use loads.

In off-grid installations, some energy storage is required to balance the mismatch between generation and consumption. In grid-connected installations, they make it possible to store the excess energy for later use.

This chapter concentrates on the use of hydrogen as energy storage. For this, a sophisticated system is required, made up of an electrolyzer, hydrogen storage and a fuel cell. The main objective of the electrolyzer is to produce pure hydrogen and oxygen. The bonds between the hydrogen and oxygen in the H_2O are broken by electromotive force and the catalytic action of the platinum when DC voltage is supplied. Among the other types of electrolyzer, PEM electrolyzers are very simple and compact and they ensure high purity and efficiency at high current density levels. Moreover, a PEM electrolyzer with small modifications can be used as a fuel cell to produce electricity from hydrogen and oxygen.

A variety of applications have already been accomplished by renewable microgrids in telecommunications, the military, tourism and industry, which makes them adequate for extensive storage (Chen et al., [117]). Demand response in different weather conditions is the main challenge in such systems. There is a great potential for improvement, especially in terms of control technology (Ulleberg, [118]).

Among these previous works, a Model Predicted control for a hydrogen-based microgrid has recently been proposed in Valverde et al. [119]), showing an excellent potential for optimal microgrid control. A more elaborated strategy is

presented here that directly takes into account the value of the energy generated, the storage costs and the aging of the components.

5.1.- Process Description

The system under study is presented in Figure 5.1. The main objective is to fulfill the local loads by keeping a balance between the consumed and the generated power. Solar is the available renewable energy source. However, the short-term unreliability of solar energy is well-known. Thus, the energy stored and/or the external grid is used when the production of renewable energies is low. The excess energy generated by the renewable source is temporally stored through the battery or the electrolyzer to produce hydrogen by electrolysis. The hydrogen is stored in the metal hydride and the fuel cell is used to supply power when the solar irradiation is low, using the hydrogen for the electromechanical reaction.

Basically, the hybrid energy storage will be employed to fulfill two different functions which are:

- To provide energy for short term requirements, such as meeting step load changes in energy demand. This is better carried out by the battery bank. This short term energy storage is required for the stable operation of the microgrid; this allows draw their energy from the microsources or the energy storage, as appropriate. The discharge time durations of the short term energy storage range from millisecond to a couple tens of seconds,

- Providing energy for long term requirements, such as shifting energy demand from on-peak hours to off-peak hours. This type of storage is responsibility of the hydrogen storage system. The long term energy storage is an enhancement which will add economic benefit to the microgrid. Long term energy storage can be used to shift energy to different times of day, or to shave peaks, to take advantage of economic incentives. Notice that there is no interdependency between the individual microsources and the long term energy storage.

A prototype was built at the University of Seville to gain real experience with the new system concept (Valverde et al., [120]). The prototype includes a Proton Exchange Membrane (PEM) electrolyzer and fuel cell for hydrogen and electricity production respectively, a metal hydride storage, a lead-acid battery bank, a photovoltaic array and an electronic load to emulate different demand profiles. Figure 5.1 shows a schematic diagram of the hydrogen-based microgrid, emphasizing the main variables. Converters are used as power interfaces allowing energy transfer between the different devices. All the units are connected through a DC bus whose voltage is held by the battery bank (directly connected to this DC bus).

This network, together with its MicroSources and loads, was transposed to a MATLAB® Simulink® simulation platform. It includes models for each source PV panels, batteries banks, electrolyzer and fuel cell; and the control of the whole system.

A central aspect is the automation of the overall system to improve reliability and ensure that the electricity demand is fulfilled. For this, the operational constraints related to the fuel cell and batteries must be fulfilled, the use of the photovoltaic arrays should be maximized and the energy extracted from the external grid should be reduced. As a result, a control system that correctly schedules the withdrawal of energy from the fuel cell, the batteries, the PV panels and the main grid is required. Additionally, variations in the supply of the solar panels are taken into account using short-term predictions.

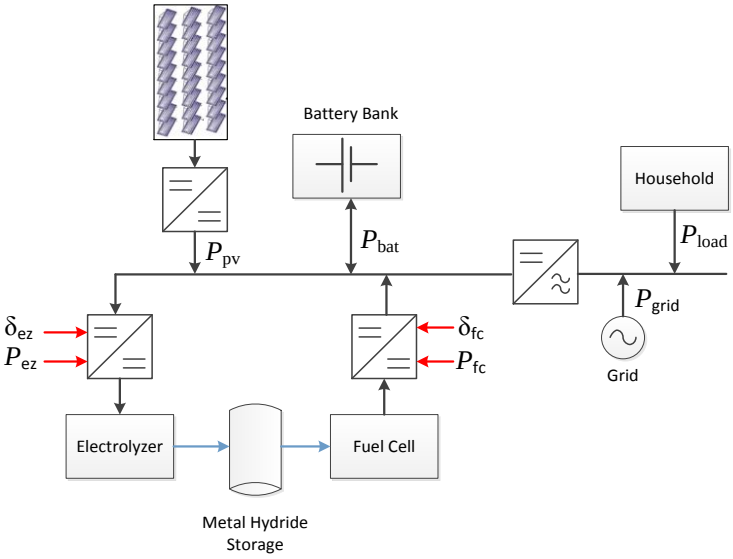

Figure 5.1.- A hydrogen-based microgrid system

Measured Variables

The variables measured in the system are the following:

- The electric power consumed or generated by the battery bank: P_{bat}
- The electric power generated by the solar panels: P_{pv}
- The electric power consumed by the load: P_{load}

- The state of charge of the battery bank: *SOC*
- The metal hybrid level: *MHL*

The measured variables are related to the nomenclature used in the modeling.

Manipulated Variables

The hydrogen-based microgrid has the following manipulated variables that allow the energy flow to be controlled:

- The binary variable (δ_{fc}) of the fuel cell controller: when the value of the variable δ_{fc} is 1, energy is extracted from the fuel cell; when it is 0, no energy flows from the fuel cell.
- The binary variable (δ_{ez}) of the electrolyzer controller: when the value of the variable δ_{ez} is 1, it is allowed to deliver energy to the electrolyzer; when it is 0, no energy flows to the electrolyzer.
- The reference power consumed by the electrolyzer (P_{ez}).
- The reference power produced by the fuel cell (P_{fc}).
- The reference power purchased from the grid (P_{grid}).

5.2.- Hydrogen-Based Microgrid Model

As it has mentioned before, the proposed model predictive control is based on an internal model to predict how performance depends on present and future control actions, which are then selected to optimize the performance.

To obtain trustworthy results of the optimization, we must provide a reliable model of the plant at the optimizer, but at the same time it must be simple, due to the fact that the model must be evaluated by the optimizer several times, and this must happen in every sampling period until a feasible solution is found. A simple model was thus implemented, and with very good reliability, inside the nonlinear model predictive control, NMPC.

5.2.1.- Hydrogen Energy Storage

The use of hydrogen for long-term energy storage is a new concept introduced for hybrid energy systems through a sophisticated system integrated by an electrolyzer, a hydrogen tank and a fuel cell as shown in Figure 5.2.

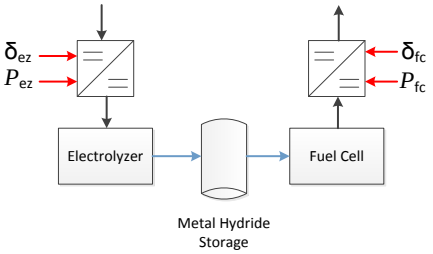

Figure 5.2.- A hydrogen energy storage Diagram

A proton exchange membrane is an electrochemical device that produces directly water, heat and electricity through the oxide-reduction reaction of hydrogen and oxygen. The decomposition of water into hydrogen and oxygen can be achieved by passing an electric current (DC) between two electrodes separated by an electrolyte membrane with good ionic conductivity. The total reaction is given by equation (5.1).

$$H_2O + Electrical\ \ Energy \rightarrow H_2 + \frac{1}{2}O_2 \qquad (5.1)$$

Mathematical models of this system are necessary for control system design. Up to now, many electrolysis cell models have been proposed; these models have been deduced from the thermal, the electrical and the fluid dynamics behaviors. Electrical model represents the relation between voltage U, current I and temperature T (Wang et al., [121]). Thermal model represents the temperature T variation and heat exchange (Ulleberg et al., [122]). The fluid dynamics model characterizes the chemical components movement, the pressure and the fluid volume (Srivastava et al., [123]). However, the model taken into account consists in a steady-state electrical model. The steady-state electric model represents algebra relations between electrical power and the hydrogen flow rate. For this, estimation of parameters using experimental data is required. The identification of the electrical model is developed using current I and voltage V step responses.

Proton Exchange Membrane (PEM) Electrolyzer

Almost for every device that produces energy, the main aim is how to achieve high efficiency in order to get the maximum output. The same applies for electrolysis and more specifically to the proton exchange membrane electrolyzer. In this case, the losses that create a drawback in achieving high efficiencies are activation, ohmic and concentration losses.

- *Activation losses*: they relate to the rate of the reactions that take place on the surface of the electrodes. During the chemical reactions in the electrodes, a proportion of the generated voltage is lost. This is called the

activation loss due to the activation energy required at both the anode and the cathode.

- *Ohmic losses:* They are due to the resistance of the wiring and the resistance of the imperfect electrodes. The ohmic loss of the PEM is slightly non-linear and variable due to the characteristics of the conduction at different conditions.

- *Concentration losses*: It relates to the reduction of the reactant's concentration in the gas channels. The fuel and the oxidant are used at the surface of the electrodes and then the incoming gas must take the place of the used reactant. The concentration of the fuel is therefore reduced.

Therefore, the overall voltage of the electrolyzer can be defined as is shown in (5.2):

$$V_{out} = V_{in} - V_{activation} - V_{ohmic} - V_{concentraton} \tag{5.2}$$

The polarization curve of losses is shown in Figure 5.3:

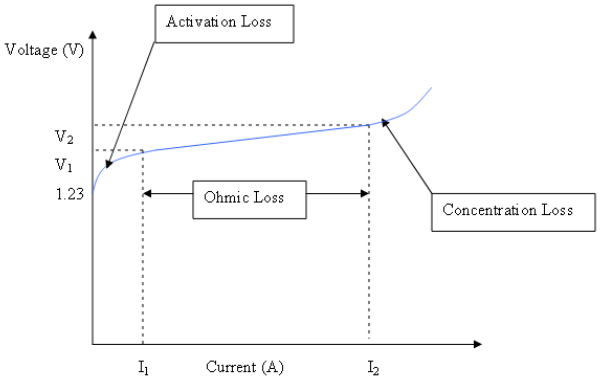

Figure 5.3.- Polarization curve of losses

Several empirical models have been suggested for the basic relationship of the I–V curve (Griesshaber et al. [124], Havre et al. [125], Vanhanen et al. [126] and Hug et al. [127]). However, the model used is based on the energy efficiency. This energy efficiency is defined as the ratio between the energy content of the hydrogen generated and the amount of electrical energy required. It expresses how efficient is the electrolyzer at different values of voltage and current and helps to establish the point where the electrolyzer produces the most.

The energy efficiency of the proton exchange membrane electrolyzer varies between 90.4% and 95.3%. Activation and concentration losses have different significant role at each point because the environment where the electrolyzer operates is a very important factor for achieving high efficiencies.

The energy efficiency can be expressed as (5.3).

$$\eta_{ez} = \frac{q_{ez} LCV}{P_{ez}} \tag{5.3}$$

The term *LCV* is the calorific value of hydrogen [kJ/m^3], q_{ez} is the hydrogen flow rate produced by the electrolyzer [m^3/s] and P_{ez} is the electrical power absorbed by the electrolyzer [kW].

Proton Exchange Membrane Fuel Cell

Considering that the efficiency of any energy conversion device is defined as the ratio between the useful output energy and the input energy. In a fuel cell, the useful output energy is the generated electrical energy and the input energy is the energy contained in the mass of hydrogen supplied. The electrical properties of the fuel cell are condensed in a current-voltage characteristic. As a result, the energy efficiency can be expressed as described in (5.4), where P_{fc} is the electrical power delivered by the fuel cell, q_{fc} is the flow rate of hydrogen consumed by the fuel cell and *LCV* is again the calorific value of the hydrogen.

$$\eta_{fc} = \frac{P_{fc}}{q_{fc} LCV} \tag{5.4}$$

The electrolyzer and the fuel cell are connected to the DC link through a DC/DC buck converter that controls the power flow. Only the static behavior (represented by the efficiency curves) will be used to model the DC converters, due to the fact that the dynamics of the DC converters are several orders of magnitude faster than the dynamics of the rest of the plant. The power converters between the PV array and the load are not modeled as the consumed and generated powers will be electronically simulated in the experiments.

Metal Hydride Storage

Basically, there are three main technologies for storing hydrogen: as a compressed gas, as a liquefied cryogenic fluid, and as a solid in a metal hydride (Ritter et al., [132]).

The technology considered here is metal hydrides. Storing hydrogen in metal hydrides has received a lot of attention because it can be stored reversibly in the

solid state at relatively low pressures and ambient temperatures (Güther et al. [133], Levesque et al. [134] and Heung et al. [135]). The storage typically contains a powdered metal that absorbs hydrogen exothermically with the concomitant release of energy as the tank is filled with hydrogen under pressure. The metal hydride desorbs the hydrogen endothermically by reducing the pressure and supplying some energy.

For modeling, the amount of hydrogen storage in the tank is simple computed considering the inlet and outlet hydrogen flow produced by the electrolyzer and the fuel cell, respectively:

$$MHL = \frac{100}{MHL_{nom}} \int_{t=0}^{T_p} q_{ez}(\tau) - q_{fc}(\tau) d\tau \tag{5.5}$$

5.2.2.- Solar Panels Model

The solar system shown in Figure 5.4 comprises a PV array and a DC/DC converter using Pulse Width Modulation (PWM), which controls the solar array operating point. The fast transients related to the commutation of the solid state switches due to the Pulse Width Modulation are not considered, so detailed modeling of the inverters is avoided, but can be in Santos et al [128].

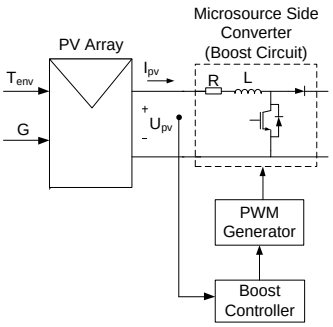

Figure 5.4.- Photovoltaic Panel control diagram

The main component of PV arrays is the solar cell, which is basically a p-n semiconductor junction that directly converts solar irradiation into DC current using the photovoltaic effect (Chaudhary et al., [129]). A simple equivalent circuit of a solar cell is used here: a current source I_L in parallel with a diode, shown in Figure 5.5 (Chouder et al., [68]).

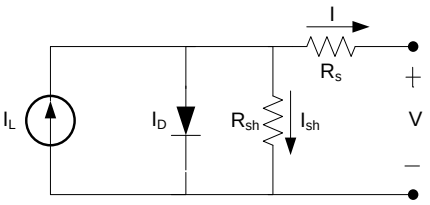

Figure 5.5.- Equivalent circuit of a solar cell

The characteristic equation describing the photovoltaic cell is described in (5.6).

$$I = I_L - I_{sc}\left(\exp\left(\frac{V + R_s I}{v_t}\right) - 1\right) - \frac{(V + R_s I)}{R_{sh}} \tag{5.6}$$

The series resistance R_s represents the internal losses due to the current flow. The shunt resistance R_{sh}, in parallel with the diode, corresponds to the leakage current to the ground. Here R_{sh} is assumed to be high enough to neglect the last term of (5.6), I_L is approximately equal to I_{sc} and $\exp((V+R_sI)/V_t)$ is assumed to be much greater than 1. Also, the open circuit voltage V_{oc} is included in the model to comply with the conditions $I(V_{oc})=0$ and $I(V=0)=I_{sc}$. The resulting characteristic equation is defined in (5.7).

$$I = I_{sc}\left[1 - \exp\left(\frac{V + R_s I - V_{oc}}{v_t}\right)\right] \tag{5.7}$$

PV cells are grouped together in PV arrays, which are combined in series and parallel to provide the desired output voltage and current. The mathematical model that predicts the power production of the PV array becomes an simple algebraically model which includes a nonlinear current-voltage characteristic defined in (5.8), where V_{pv} and I_{pv} are the output voltage and current of the PV array respectively, R_{sg} is the series resistance of the PV array, I_{scg} is the short circuit current, V_{ocg} is the open circuit voltage, N_{sc} is the number of cells in series within the PV module, N_{sm} is the number of modules in series within the PV array, and V_t is the thermal voltage.

$$I_{pv} = I_{scg}\left[1 - \exp\left(\frac{V_{pv} + R_{sg} I_{pv} - V_{ocg}}{v_t N_{sm} N_{sc}}\right)\right] \tag{5.8}$$

If the temperature and solar irradiation levels change, the voltage and current outputs of the PV array will follow this change. As a consequence, PV systems use a maximum power point tracking (MPPT) technique to continuously deliver the

highest possible power when variations in the irradiance and temperature occur. This maximum power point tracking (MPPT) control is critical for the success of a PV system (Chaudhary et al., [129]).

5.2.3.- Battery Bank Model

Nowadays, many dynamic models are available in literature for batteries with different degrees of complexity: (i) Electrochemical models are complex, time consuming and involve time-variant partial differential equations; (ii) Empirical models cannot offer dynamics description; (iii) Macroscopic model is based on micro-macroscopic description of the phenomena, (iv) Electrical model consider the battery behaviour as an equivalent electrical circuit (M'Sirdi et al, [131]).

The electrical model for an isolated microgrid shown in Figure 5.6 is used here: It consists of a variable voltage source V_g and a variable resistor R_g. This first generic model includes the main variables of the system: the battery state of charge SOC and the current flowing across the battery I_{bat}, following the equation (5.9).

$$V_{bat} = V_g + R_g I_{bat} \begin{cases} V_g = f(SOC) \\ R_g = g(SOC, I_{bat}) \end{cases} \tag{5.9}$$

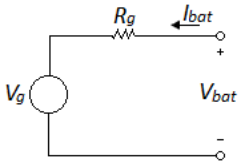

Figure 5.6.- Equivalent circuit of a battery

The voltage source V_g represents the voltage at open circuit between the battery terminals. This voltage is due to energy stored in the battery through the electrochemical reactions. Clearly, this term depends directly on the energy stored. On the other hand, R_g represents the resistance that the battery offers to the energy flow. This value includes the effects of the working point (I_{bat}, SOC) and the health of the battery.

The input is the battery power profile $P_{bat} = V_{bat}\, I_{bat}$, which is positive when power is extracted from the battery bank and negative when power is supplied to the battery bank. The battery current is defined in (5.10), where N_b is the number of batteries in series.

$$I_{bat}(t) = \frac{P_{bat}(t)}{V_{bat}(t) N_b} \tag{5.10}$$

An essential term is the state of charge of the battery SOC, which is defined as the relation between the energy stored and the capacity following (5.11). The integral term models the energy accepted over the battery's working life. Also, the outer integral term models the battery capacity due to the working point environment at any given time. Both terms are functions of time and are evolving continuously. The state of charge (SOC) ranges from 0 when the batteries are completely discharged to 1 when the batteries are completely charged as it is presented in (5.11), where C_{nom} is the rated battery capacity, η(t) is the charging efficiency and I_{bat}(t) the current flowing through it.

$$SOC(t_i) = \int_{i\,\infty}^{t} \frac{\eta(t) I_{bat}(t)}{C_{nom}} dt \tag{5.11}$$

Two working regions are defined depending on the battery current: charge and discharge.

Charge

The battery charges when P_{bat}<0. The energy is absorbed and causes V_{bat} to increase. A charge efficiency factor, η(t), reflects that only a fraction of the theoretical energy is really stored, as described in (5.12) and (5.12).

$$V_{bat}(t) = \left[V_{boc} - K_{boc} SOC(t)\right] - \frac{I_{bat}(t)}{C_{10}} \left(\frac{P_{1c}}{1 + I_{bat}(t)^{P_{2c}}} + \frac{P_{3c}}{\left(1 - SOC(t)\right)^{P_{4c}}} + P_{5c} \right) \tag{5.12}$$

$$\eta(t) = 1 - \exp\left(\frac{\alpha_{cmt}}{\left(\frac{I_{bat}(t)}{I_{10}} + b_{cmt} \right)} \left(SOC(t) - 1\right) \right) \tag{5.13}$$

Discharge

In this area the battery is delivering energy to the system: P_{bat}>0. The battery voltage is determined by the following equations:

$$V_{bat}(t) = \left[V_{bodc} - K_{bodc}\left(1 - SOC(t)\right)\right] - \frac{\left|I_{bat}(t)\right|}{C_{10}} \left(\frac{P_{1dc}}{1 + \left|I_{bat}(t)\right|^{P_{2dc}}} + \frac{P_{3dc}}{SOC(t)^{P_{4dc}}} + P_{5dc} \right) \tag{5.14}$$

5.3.- Case Study

A hydrogen-based microgrid has been installed and tested at the University of Seville (Valverde et al., [120]). The system's main components are:

- A 1 kW Proton Exchange Membrane (PEM) electrolyzer for hydrogen production.
- A 7 Nm^3 metal hydride storage. The hydrogen storage is based on LaNi5 metal hydrides alloy with a measured capacity of 6625.5 Nl.
- A 1.5 kW Proton Exchange Membrane (PEM) fuel cell, which uses the stored hydrogen to produce electricity.
- A lead-acid battery bank with a total capacity of C_{120}=367Ah. The battery bank includes 24 mono-blocks of 2 V each one which are connected in series to achieve the bus voltage of 48V. The battery internal resistance R_{int}=0.0838 while the time constant is 31 sec at 95% of the final value.
- A photovoltaic array emulated by an electronic power source array with a maximum power around 6kWp, controlled by a PLC.
- A 2.5 kW electronic load to emulate different demand profiles, controlled by a PLC.

All the units are connected through a DC bus whose voltage is held around 48Volts, defined by the battery bank.

5.3.1.- Electrolyzer

The PEM electrolyzer was designed for automatic operation at 690kPa hydrogen gas pressure. The energy efficiency reaches 74% for low current values and 69% for high current values. The controller allows operation at current up to 80A. At 80A, the electrolyzer produces 3.6 liters of hydrogen per minute. The V-I characteristic curve of electrolyzer is shown in Figure 5.7.

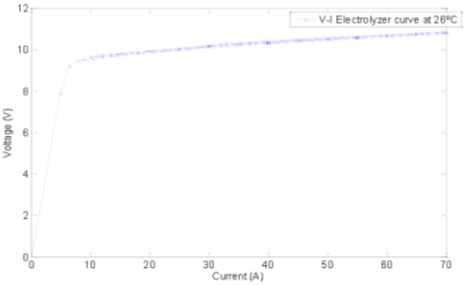

Figure 5.7.- V-I characteristic curve of PEM electrolyzer at 26ºC

5.3.2.- Fuel Cell

The PEM fuel cell has 60 cells and can generate a voltage between 36V and 57V with a current up to 55A. Hydrogen consumption is 20Nl/min and the energy efficiency reaches 45% at full load. The V-I characteristic curve of fuel cell is shown in Figure 5.8.

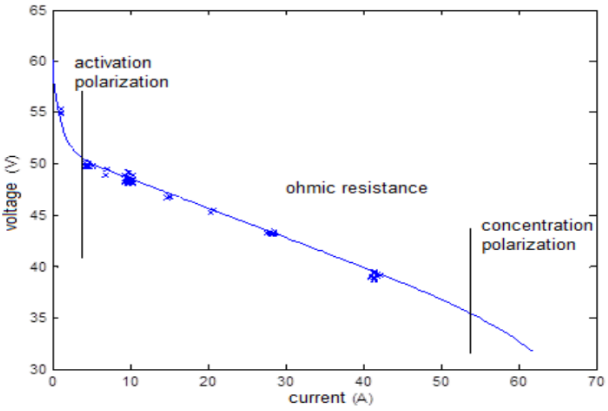

Figure 5.8.- V-I characteristic curve of PEM fuel cell

5.4.- Hybrid Model Predictive Control

In this section, the Energy Management System for the hydrogen microgrid hybrid controller is presented. It takes into account the operational constraints and optimizes the operational costs by considering the value of the energy generated and exchanged with the grid and the cost of storage using a predictive control strategy. Thanks to the selection of a proper structure of the controller and manipulated variables, the optimization problem obtained is transformed into a simple problem that can be solved online (Salazar et al., [136]).

5.4.1.- Cost function

The objective is to maximize the economic revenue and maintain a balance between the consumed and the generated power in spite of possible ambient disturbances. Considering the cost of energy, it is recommended minimizing the energy delivered or consumed by the external grid and maximizing the energy stored in the battery bank and the hydride storage without reducing the lifetime of the components (mainly the hydrogen circuit) due to excessive intermittent operation.

To achieve these objectives, the optimization problem to be solved at each sample time is based on calculating the value of the manipulated variables that fulfill the operational constraints given and maximize (at each sampling time) the revenue function J (5.15), where E_{bat} is the amount of energy consumed or provided by the battery bank during the prediction horizon N_{pb} (kWh), E_H is the amount of energy absorbed by the electrolyzer or delivered by the fuel cell (kWh), E_{grid} is the amount of energy generated or consumed by the external grid (kWh), J_{bat} is the economic value of the energy stored at the battery, J_H is the economic value of the energy stored as hydrogen, J_{grid} is the economic value for the energy exchanged with the external grid.

$$J = J_{bat}\left(E_{bat\_in}, E_{bat\_out}\right) + J_H\left(E_{H\_in}, E_{H\_out}\right) + J_{grid}\left(E_{grid\_in}, E_{grid\_out}\right) \tag{5.15}$$

If the cost function is evaluated during a prediction horizon N_{pb}, then the following is the proposed cost function to be minimized:

$$\begin{aligned} J = {} & \gamma_{bat,out}\left(\sum_{t=0}^{N_{pb}} \max\left(P_{bat}(t),0\right)\right) - \gamma_{bat,\text{int}}\left(\sum_{t=0}^{N_{pb}} \min\left(P_{bat}(t),0\right)\right) \\ & + \gamma_{H,in}\left(\sum_{t=0}^{N_{pb}} P_{fc}(t)\right) + \gamma_{H,out}\left(\sum_{t=0}^{N_{pb}} P_{ez}(t)\right) \\ & + G_{in}\left(\sum_{t=0}^{N_{Pb}} \max\left(P_{grid}(t),0\right)\right) - G_{out}\left(\sum_{t=0}^{N_{Pb}} \min\left(P_{grid}(t),0\right)\right) \end{aligned} \tag{5.16}$$

Where the following parameters are fixed a priori:

- G_{in} (€/kWh) is the cost of a kWh imported from the external grid,
- G_{out} (€/kWh) is the revenue obtained from each kWh supplied to the external grid,
- $\gamma_{bat,in}$ is the cost of the energy provided by the battery,
- $\gamma_{bat,out}$ is the cost of the energy transferred to the battery,
- $\gamma_{H,in}$ is the cost of the energy delivered by the fuel cell,
- $\gamma_{H,out}$ is the cost of the energy consumed by the electrolyzer.

5.4.2.- Constraints

Some constraints which have to be fulfilled are as follows:

C1) The electrolyzer power consumption is limited to $\overline{P_{ez}}$ due to manufacturer recommendations. Moreover, a minimum power of $\underline{P_{ez}}$ is required to ensure safe electrolysis operation:

$$\delta_{ez}(k)\underline{P_{ez}} \leq P_{ez}(k) \leq \overline{P_{ez}}\delta_{ez}(k) \tag{5.17}$$

C2) Minimum duration of the electrolyzer startups and shutdowns to avoid fast switching:

$$\begin{aligned} T^{k}_{on,ez} &\geq \underline{T_{on,ez}} \\ T^{k}_{off,ez} &\geq \underline{T_{off,ez}} \end{aligned} \tag{5.18}$$

C3) The power delivered by the fuel cell is limited by a minimum $\underline{P_{fc}}$ and a maximum $\overline{P_{fc}}$ in order this equipment from intensive use.

$$\delta_{fc}(k)\underline{P_{fc}} \leq P_{fc}(k) \leq \overline{P_{fc}}\delta_{fc}(k) \tag{5.19}$$

C4) Minimum duration of the fuel cell startups and shutdowns to avoid excessive intermittent operation are also taken into account:

$$\begin{aligned} T^{k}_{on,\,fc} &\geq \underline{T_{on,\,fc}} \\ T^{k}_{off,\,fc} &\geq \underline{T_{off,\,fc}} \end{aligned} \tag{5.20}$$

C5) The state of charge for the battery is also limited by a minimum $\underline{SOC}$ and a maximum $\overline{SOC}$ value in order to avoid overcharging or undercharging, which can reduce the capacity and lifetime of the batteries:

$$\underline{SOC} \leq SOC(k) \leq \overline{SOC} \tag{5.21}$$

C6) Additionally, a smooth operation is recommended for the batteries; so the current to the batteries is limited:

$$\left|I_{bat}(k)\right| \leq \overline{I_{bat}} \tag{5.22}$$

C7) The metal hybrid level (MHL) is limited by a minimum $\underline{MHL}$ and a maximum $\overline{MHL}$ value considering specifications for the metal hydride storage, as described in (5.23).

$$\underline{MHL} \leq MHL(k) \leq \overline{MHL} \tag{5.23}$$

5.4.3.- Transformation into a solvable optimization

As the Model Predictive Control proposed in this work includes a combination of binary and continuous manipulated variables, it gives a problem of mixed integer optimization, which is computationally complex to be solved online. To overcome this optimization was turned into a problem of nonlinear optimization with continuous variables (NMPC). For this, two new continuous manipulated variables are defined for each binary manipulated variable $T_{on,i}^{k}$ and $T_{off,i}^{k}$ which correspond to the duration of the activation/deactivation of the binary variable δ at each pulse k. In our case, four new continuous manipulated variables are defined $T_{on,fc}^{k}$, $T_{off,fc}^{k}$, $T_{on,ez}^{k}$ and $T_{off,ez}^{k}$ which correspond to the binary variables δ_{fc} and δ_{ez}, respectively. The nonlinear optimization can easily be solved using sequential programing SQP.

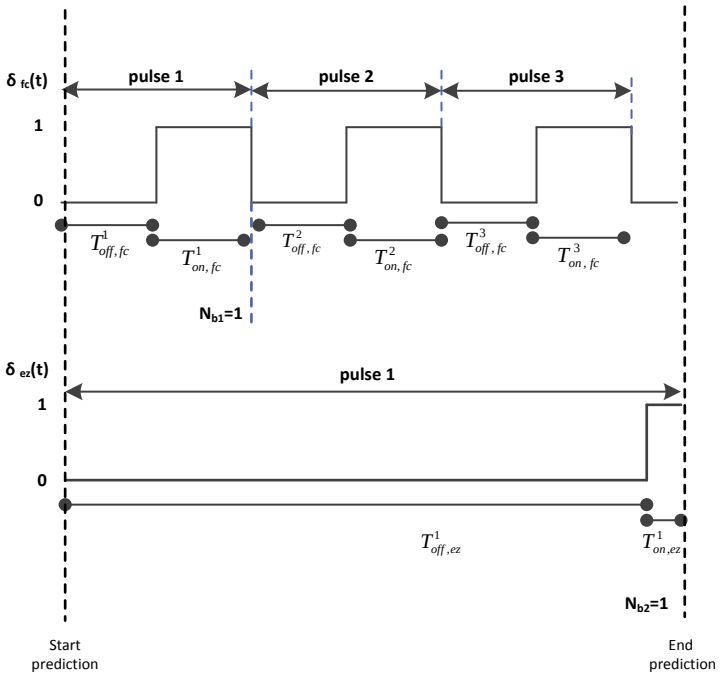

Figure 5.9.- Structure of the variables δ_{fc} and δ_{ez} during the Prediction and Control Horizons

Regarding the MPC tuning parameters, the control horizons N_c and the prediction horizons N_p are central parameters. In this case, influenced by the fuel cell process and the electrolyzer dynamics, the prediction horizon will depend on the number of pulses N_{pb} required for the binary variables to reach a stable

operation pattern. To compute the cost function J in equation (5.15), the internal model will be integrated until the binary variables δ_{fc} and δ_{ez} have made at least N_{pb} pulses (taking into account that in the same prediction period T_p, each manipulated variable can make different numbers of pulses).

As is shown in Figure 5.9, the prediction horizon is defined as the time required by the binary variables δ_{fc} and δ_{ez} to make at least one pulse (N_{pb}=1). Both binary variables have a prediction control of $N_b=1$; therefore, the instants corresponding to the first pulse will be calculated $T^1_{on,fc}$, $T^1_{off,fc}$, $T^1_{on,ez}$ and $T^1_{off,ez}$ and the same pattern is applied for future pulses, i.e., $T^k_{on,fc} = T^1_{on,fc}$, $T^k_{off,fc} = T^1_{off,fc}$, $T^k_{on,ez} = T^1_{on,ez}$ and $T^k_{off,ez} = T^1_{off,ez}$.

Regarding the continuous manipulated variable P_{grid}, the control actions applied in each sampling period will be defined, and the duration in which every action has to be applied must be computed. For example, considering a control horizon of 2, the optimization algorithm will provide two values for manipulating the grid power ($P_{grid}(1)$, $P_{grid}(2)$) and one value of the duration TP_{grid} for the application of the first prediction $P_{grid}(1)$. A value of the duration is not necessary for the second prediction $P_{grid}(2)$, since the sign is held until the end of the prediction horizon. In summary, the optimizer will provide three optimal signs for the control of the grid power (s. Figure 5.10).

Finally, if the continuous manipulated variables P_{ez} and P_{fc} have control horizons of 2. The optimization algorithm will provide two values for manipulating the power generated by the fuel cell ($P_{fc}(1)$, $P_{fc}(2)$) and one value of the duration TP_{fc} for the application of the first prediction $P_{fc}(1)$. A value of the duration for the second prediction $P_{fc}(2)$ is not necessary, since the sign is held until the end of the prediction horizon. Therefore, the optimizer will provide in this case three optimal signs for the control of power generated by the fuel cell. This procedure is repeated for the continuous manipulated variables P_{ez} related to the electrolyzer (s. Figure 5.11).

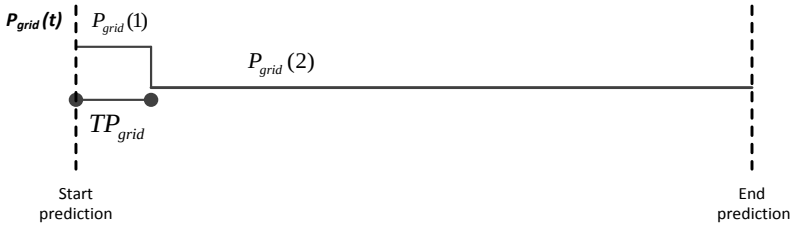

Figure 5.10.- Parameterization of the grid power P_{grid}

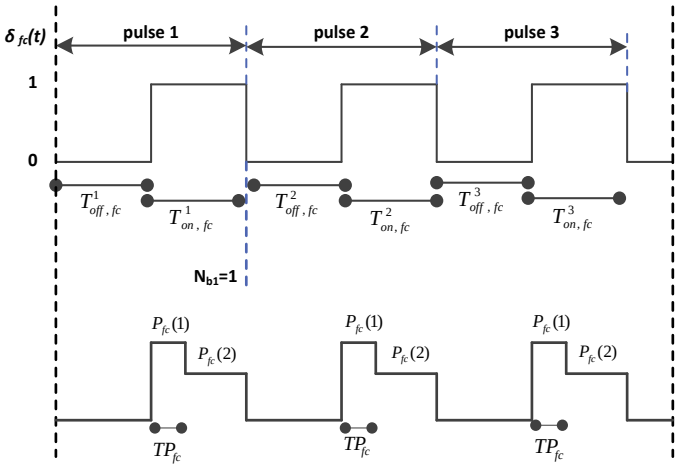

Figure 5.11.- Parameterization of the fuel cell power P_{fc}

The nonlinear optimization problem proposed in equation (5.16) is then solved periodically, with a sampling period T_s, using the scheme presented in Figure 5.12. This diagram shows a sequential approach where the cost function J is calculated by integrating the internal dynamic model over the prediction horizon N_{pb}, taking the current state of the system as initial condition and evaluating the cost function at the end of the integration. The optimization produces an optimal control sequence, although, following moving horizon ideas, only the first control signal is applied to the process, while the remaining signals serve the purpose of preventing control actions with poor long-term effects. At the next control instant, the horizon is displaced towards the future and the controller with new measurements solves and updates the optimal control.

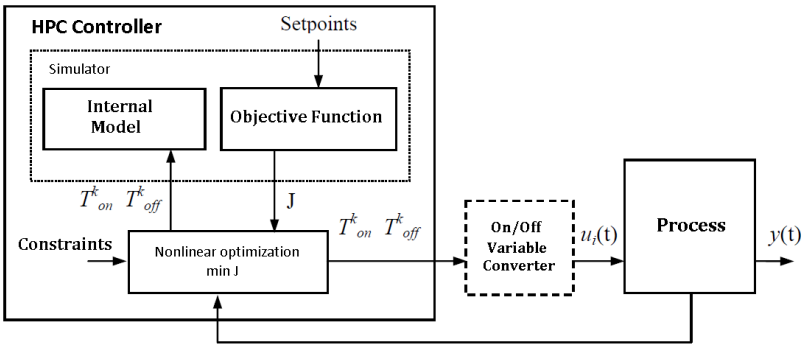

Figure 5.12.- Implementation of the Nonlinear Controller

The internal model must represent the process dynamic; to make possible to predict the output signals accurately, but it must be simple because of the integration of the model. The dynamic model for the hydrogen-based microgrid is given by equations (5.1) to (5.14).

From the point of view of the software implementation, it is necessary to add a simple converter between the predictive controller and the process, that converts $T_{on,i}^{k}$ and $T_{off,i}^{k}$ into ON/OFF signals corresponding to each binary manipulated variable. The use of the converter allows the ON/OFF variables to be decoupled from the sampling period.

5.5.- Simulation Results

Some results obtained when applying the controller proposed in Section (5.4) to a detailed simulator of the system in MATLAB/Simulink are now discussed. The control objective is to minimize the power generated or consumed by the external grid and maximize the power stored in the battery bank and the metal hydride storage, without reducing the lifetime of the battery and the hydrogen circuit.

The evolution of the solar radiation during a typical test can be seen in Figure 5.23. Solar energy is not available until t=320 min. Since this time, the solar radiation increases until 700W/m2 at t=600min.

The power generated or consumed by the external grid is minimized, thus, the external grid power is close to cero as shown in Figure 5.19.

When there is no photovoltaic energy, the fuel cell (P_{fc}) is activated to supply the load. Notice that the maximum power delivered by the fuel cell is around 900W, so if the power consumption were higher than 900W, it would be complemented by the battery bank (See Figure 5.17 and Figure 5.20).

As soon as the power provided by the photovoltaic array is higher than the power consumption of the load, the electrolyzer (Pez) will be activated to store the extra energy in the metal hydride storage. The battery bank starts to save energy when the difference between the solar power and the power consumption of the load is higher than the maximum power consumption by the electrolyzer (900W).

In Figure 5.22 and Figure 5.23, the dynamic of the state of charge of battery (SOC) and the metal hybrid level (NHM) is shown. The state of charge depends on the power generated or consumed by the battery bank, while the metal hybrid level depends on the power delivered by the fuel cell and consumed by the electrolyzer.

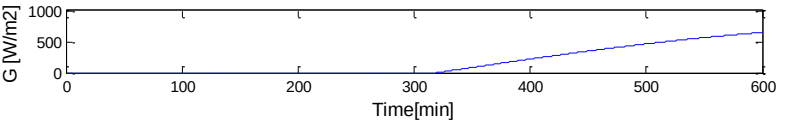

Figure 5.13.- Solar Radiation

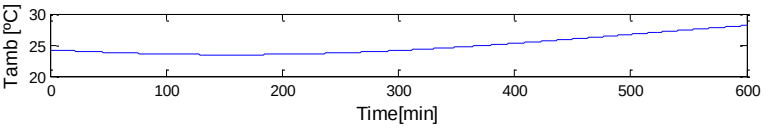

Figure 5.14.- Ambient Temperature

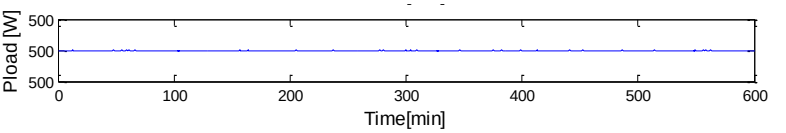

Figure 5.15.- Power consumed by the load

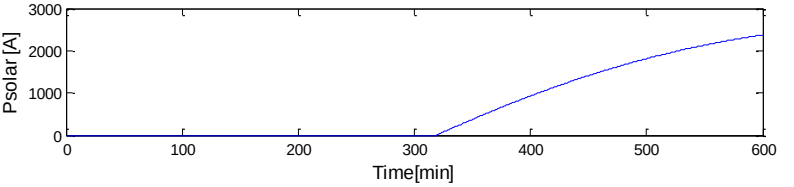

Figure 5.16.- Power produced by the solar panels

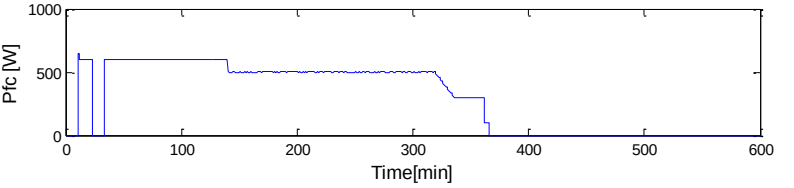

Figure 5.17.-Power delivered by the fuel cell

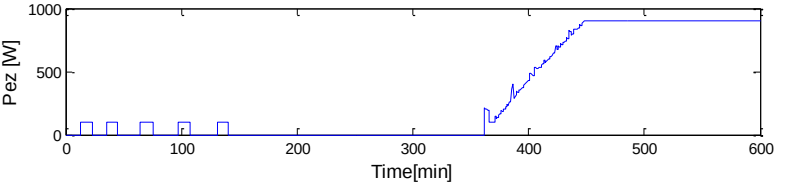

Figure 5.18.- Power consumed by the electrolyzer

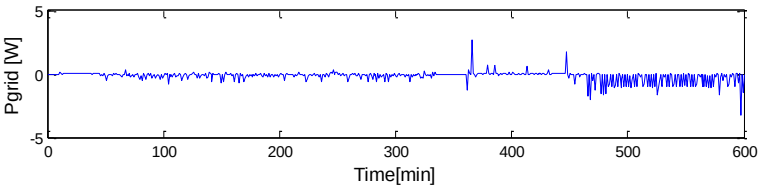

Figure 5.19.- Power generated or consumed by the main grid

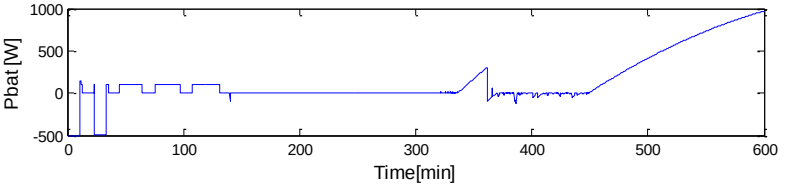

Figure 5.20.- Power delivered or consumed by the battery bank

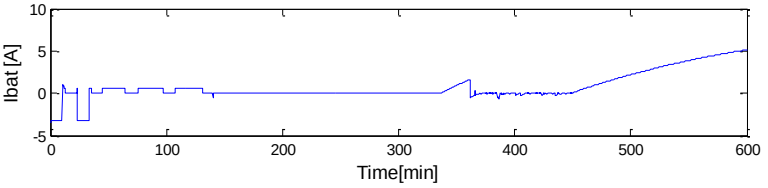

Figure 5.21.- Current of the battery bank

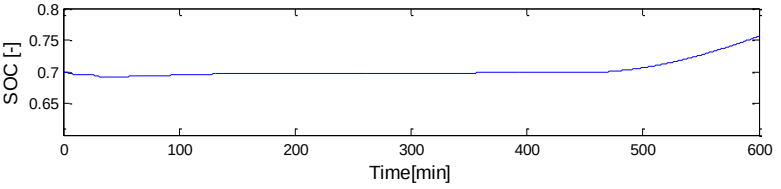

Figure 5.22.- State of charge of the battery bank

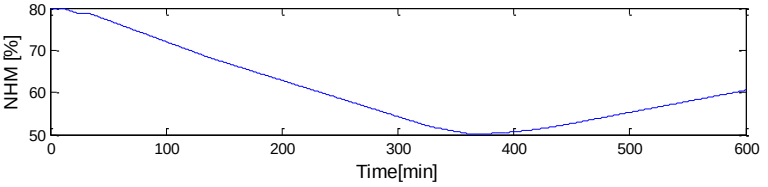

Figure 5.23.- Metal hybrid level

5.6.- Conclusions

With the objective of improving the operation of a solar-powered microgrid with mixed storage systems (hydrogen and batteries), a prediction-based energy management system has been proposed and tested using simulation. As novelty, predictive control is incorporated for efficient use of the energy generated, stored and exchanged with the grid, under strict operational constraints. The initial mixed integer optimization problem obtained is transformed into a simpler problem that can be solved online, by using durations as optimization variables. Some simulations have been presented to test the control strategies. Further work will be done to implement the controller on the real plant and get some experimental results.

APPENDIX A

Renewable Energy Library

As part of the work developed in this thesis, models of different components of microgrid have been developed in a library of EcosimPro© named ***RENEWABLE_ENERGY***, as EcosimPro© is a powerful modeling and simulation tool that follows an advanced methodology for modeling and dynamic simulation. This ***RENEWABLE_ENERGY*** library includes a set of models which represent the dynamics of typical components in a microgrid that is an energy supply system equipped with renewable and conventional sources, such as: wind turbine, solar panels, battery banks and diesel generator. The process models are selected to be simple and represent the dynamic of the components quiet accurately. Additionally, it is developed so that new components are easy to integrate into the library, since the implementation has been done as a modular structure.

A.1.- General Components

The following groups will be defined and included in the ***RENEWABLE_ENERGY*** library:

1) *Renewable Sources*: It includes the mathematical model of the renewable power generation: In the initial version photovoltaic panels and wind turbines are given by ***SolarPanelsModel*** and ***WindTurbineModel*** components (See Sections A.3.1and A.3.3).

2) *Conventional Sources*: In off-grid microgrid, a backup system is required to guarantee energy source when the production source of renewable energies is low and the energy stored is not enough to fulfill the load. For this, a simple model of a Diesel Generator is described in ***DieselGenerator*** component (See Section A.3.6).

3) *Storage Devices*: When the production of renewable energies is higher than the local demand, the extra energy is saved into storage devices to be used when the production source of renewable energies is not enough to

fulfill the load. The mathematical model of the batteries bank is included into the ***BatteryBank*** Component. (See Section A.3.5).

4) *Electrical Loads*: In the first version a desalination plant has been considered as electrical load as it is a typical controllable load in off grid microgrid (Bognar et al., [130]). From an electrical power point of view, a simple mathematical model is included: the ***DesalinationPlant*** component (See Section A.3.10).

5) *Inverters*: Each renewable source is connected to an inverter which controls the withdrawal of energy which is injected to the grid considering weather and demand conditions. For this, a mathematical model of a wind and a solar inverter is described in ***InversorSolar*** and ***InversorWind*** component respectively. Additionally, a battery inverter is responsible for charging and discharging of the battery which is represented by ***InversorBattery*** component.

6) *Controllers*: All the controllers associated to the diesel generator, wind turbine, solar panels and the grid are described in ***ControlGenerator***, ***ControlTurbine***, ***ControlSolar***, ***BatteryCtrl***, and ***SecondFreqCtrl*** component. The simple controllers included in this library are used to test the different components incorporated in this library and can be replaced by more complex controllers.

7) *Grid*: The relation between the production source of energies and the local load connected to the grid is defined in ***LocalGrid*** component.

8) *Experimental Data*: Experimental data is included to test the different components for solar radiation, wind speed, water demand and temperature: ***DataSolar***, ***DataViento***, ***DataWater*** and ***DataTemperature***.

9) *Forecast Data*: Some prediction models for solar radiation, wind speed, water demand and temperature are given to test the different components designed in the actual library such as: ***ForecastSolar***, ***ForecastWater*** and ***ForecastTemperature*** component.

A.2.- Ports

A port encapsulates the variables that represent the actual physical exchange among components, thus, the components are connected by ports which greatly facilitates the modeling of complex systems. The ports of the ***RENEWABLE_ENERGY*** library can be divided into controlled ports, manipulated ports and disturbance ports.

Controlled port associated to controlled variables are those conditions such as state of charge, frequency, power, speed, etc. that must be maintained at some desired value. For this, manipulated variables including in the manipulated port must be adjusted so that the desired value of the controlled variable is maintained despite any disturbance. Finally, the disturbance port comprises all the disturbances which affect the process and tend to drive the controlled variables away from their desired value or set point condition.

Port Name	Variables	Description
OutputGrid	P_{grid}	Resulting Grid Power
PGenOutput	P_{Gen}	Generator Output Power
OutputSolar	P_{max}	Solar Output Power
OutSolarInv	$P_{InvSolar}$	Solar Inverter Output Power
OutputWind	P_{max}	Wind Output Power
OutWindInv	$P_{InvWind}$	Wind Inverter Output Power
PLoadOutput	P_{load}	Load Consumed Power
OutputBatt	$P_{InvBatt}$	Battery Output Power
InputBatt	SOC	State of Charge
OutputBattInv	f_{grid}	Grid Frequency
WTsOutput	w_t	Rotor Rotational Speed

Table A.1.- Controlled Variables belong to Controlled Port

Port Name	Variables	Description
Efficiency	n_{Ctrl}	Control signal given by secondary local controller
WindController	T_{eref}, B_{etaref}	Torque and Pitch Angle
OutputGenCtrl	FlagGen	Activation/Deactivation Diesel Generator

Table A.2.- Manipulated Variables belong to Manipulated Port

Port Name	Variables	Description
DisturbanceSolar	T_{env}, G	Ambient Temperature and Solar Radiation
WindData	V_e	Wind Speed
DataAgua	q_{wd}	Water Demand

Table A.3.- Disturbance Variables belong to Disturbance Port

A.3.- Componets Description

A library on microsources of renewable energies integrated to form low voltage microgrids has been developed in EcosimPro to supply electrical power to remote areas that the main or national grid cannot reach on account of the typology or weather. A briefly description of all the components which integrated the library will be expressed as follow.

A.3.1.- Wind Turbine Component

The component responsible for modeling a three-blade, variable speed wind turbine equipped with permanent magnet synchronous generator (PMSG) is known as ***WindTurbineModel***. The symbol associated to this component is shown in Figure A.1, the modifiable parameters are described in Table A.4 and the input and output ports are given by Table A.5. The model is described in Section 2.2.

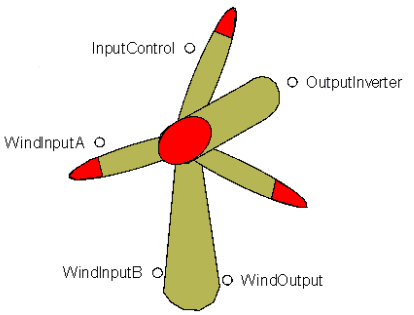

Figure A.1.- Symbol of ***WindTurbineModel*** Component

Variable	**Default Value**	**Unit**	**Description**
R	4.5	m	Rotor radio
F_r	0	$Kg.m^2/seg$	Friction force
T_{servo}	0.5	seg	Time constant of the pitch actuator
J_t	156.95	$Kg.m^2$	Whole drive train inertia
ω_{T_max}	13.09	rad/seg	Maximum rotor rotational speed
A	0.258	-	Estimated parameter for power coefficient curve
B	100	-	Estimated parameter for power coefficient curve
C	0.4	-	Estimated parameter for power coefficient curve
D	2.164	-	Estimated parameter for power coefficient curve
E	15.21	-	Estimated parameter for power coefficient curve
F	0.00571	-	Estimated parameter for power coefficient curve

Table A.4.- Wind Turbine Component Attributes

Variable	**Port**	**Name associated**	**Type**	**Unit**	**Description**
V_e	WindData	WindInputA	REAL	m/seg	Wind Speed
T_{eref}	WindControler	WindInputB	REAL	Nm	Torque Reference
B_{etaref}	WindControler	WindInputB	REAL	degree	Pitch Angle Reference
n_{Ctrl}	Efficiency	InputControl	REAL	-	Efficiency by controller

ω_T	WtsOutput	WindOutput	REAL	rad/seg	Rotor Rotational Speed
P_{out}	OutputWind	OutputInverter	REAL	W	Output power

Table A.5.- Ports associated to ***WindTurbineModel*** Component

The component is comprised of the blades which take a part of the wind energy available, a hydraulic actuator of the pitch angle, a drive train where energy is transferred from the blades to a synchronous generator (PMSG) and a synchronous generator which converts mechanical to electrical energy considering its associated current controller. The mathematical models related with blades, hydraulic actuator, drive train and synchronous generator will be given in the following sections.

A.3.2.- Wind Controller Component

The controller responsible for obtaining the maximum power from a three-blade, variable speed wind turbine equipped with permanent magnet synchronous generator (PMSG) is given by the component: ***ControlTurbine***. The symbol associated to this component is shown in Figure A.2, the modifiable parameters are described in Table A.6 and the input and output ports related with the component are given by Table A.7. Finally, the procedure implies in the design of the controller is given in the section 2.4.

Variable	**Default Value**	**Unit**	**Description**
λ_{op}	8	rad	Optimum Tip Speed Ratio
C_{pmax}	0.49	-	Optimum Power Coefficient
T_{erefop}	410.4531	Nm	Operate Point for torque
K_p	6.629	-	PI controller constant
K_i	7.627	-	PI controller constant
R	4.5	m	Radio
n_p	10	-	Number of poles
Eff_{Mech}	1.15	-	Mechanical Efficiency
GenSpeedTrans2	850	rpm	Generator Speed for Transition 2
GenSpeedAux2	900	rpm	Generator Speed for Transition 2
TorqueRated	143.24	Nm	Rated Torque
TorqOpInt2	52.60	Nm	Torque Optimum Interpolation 2
RatedGenSpeed	1000	rpm	Rated Gen Speed
HhystGenSpeed	100	rpm	Hysteresis Gen Speed
GenSpeedAux1	980	rpm	Generator Speed for Transition 1
GenSpeedTorqueRef1	950	rpm	Generator Speed for Transition 1
TorqOpInt1	65.71	Nm	Torque Optimum Interpolation 1
RatedGenSpeedInt1	980	rpm	Generator Speed for Transition

Table A.6.- Wind Turbine Control Component Attributes

Variable	**Port**	**Name associated**	**Type**	**Unit**	**Description**
V_e	WindData	WindCtrlInputA	REAL	m/s	Wind Speed
ω_T	WTsOutput	WindCtrlInputB	REAL	rad/s	Rotor Rotational

					Speed
T_{eref}	WindControler	WindCtrlOutput	REAL	Nm	Torque Reference
B_{etaref}	WindControler	WindCtrlOutput	REAL	Degrees	Pitch Angle Reference

Table A.7.- Ports associated to ***ControlTurbine*** Component

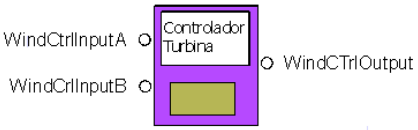

Figure A.2.- Symbol of the Component ***ControlTurbine***

A.3.3.- Solar Panels Component

The component responsible for modeling a solar panel is known as ***SolarPanelsModel***. The symbol associated to this component is shown in Figure A.3, the modifiable parameters are described in Table A.8 and the input and output ports related with the component are given by Table A.9. The model is presented in detail in section 3.2.2.

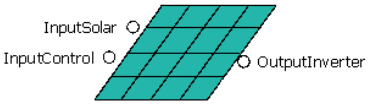

Figure A.3.- Symbol of ***SolarPanelsModel*** Component

Variable	Default Value	Unit	Description
$V_{ocm,stc}$	44.8	Volts	Open Circuit Voltage
$I_{scm,stc}$	5.51	Amps	Short Circuit Current
$NOCT$	46	ºC	Normal Operating Cell Temperature
$V_{mpm,stc}$	36.2	Volts	Voltage at maximum power
$I_{mpm,stc}$	5.11	Amps	Current at maximum power
$P_{maxm,stc}$	185	Wp	Maximum Power
T_{ref}	25	ºC	Reference Temperature
G_{stc}	1000	Wm^{-2}	Standard Solar Radiation
B	-0.38	% $ºC^{-1}$	Sensitivity of Open Circuit voltage to temperature
A	0.10	% $ºC^{-1}$	Sensitivity of Short Circuit Current to temperature
Γ	-0.47	% $ºC^{-1}$	Sensitivity of Maximum Power to temperature
S_{urface}	1.277	m^2	Module Surface
N_{SC}	12	-	Number of cells in series within PV module

N_{pc}	6	-	Number of cells in parallel within PV module
$E_{fficiency}$	14.8	%	Modules efficiency
N_{pm}	3	-	Number of modules in parallel within the PV array
N_{sm}	9	-	Number of modules in series within PV array
V_t	0.0248	Volts	Thermal voltage

Table A.8.- Solar Panels Component Attributes

Variable	Port	Name associated	Type	Unit	Description
T_{env}	DisturbanceSolar	InputSolar	REAL	Degree	Ambient Temperature
G	DisturbanceSolar	InputSolar	REAL	W/m^2	Solar Radiation
n_{Ctrl}	Efficiency	InputControl	REAL	-	Signal control
P_{out}	OutputSolar	OutputInverter	REAL	W	Output Power

Table A.9.- Ports associated to ***WindTurbineModel*** Component

A.3.4.- Solar Control Component

The controller responsible for obtaining the maximum power from solar panels is given by the component: ***ControlSolar***. The symbol associated to this component is shown in Figure A.4, the modifiable parameters are described in Table A.10 and the input and output ports are given by Table A.11. Finally, the procedure implies in the design of the controller is described in section 3.2.2.

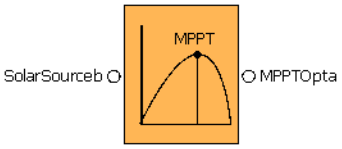

Figure A.4.- Symbol of the Component ***ControlSolar***

Variable	Default Value	Unit	Description
$V_{ocm,stc}$	44.8	Volts	Open Circuit Voltage
$I_{scm,stc}$	5.51	Amps	Short Circuit Current
$NOCT$	46	ºC	Normal Operating Cell Temperature
$V_{mpm,stc}$	36.2	Volts	Voltage at maximum power
$I_{mpm,stc}$	5.11	Amps	Current at maximum power
$P_{maxm,stc}$	185	Wp	Maximum Power
T_{ref}	25	ºC	Reference Temperature
G_{stc}	1000	Wm^{-2}	Standard Solar Radiation
B	-0.38	% ºC^{-1}	Sensitivity of Open Circuit voltage to temperature
A	0.10	% ºC^{-1}	Sensitivity of Short Circuit Current to temperature
Γ	-0.47	% ºC^{-1}	Sensitivity of Maximum Power to temperature
S_{urface}	1.277	m^2	Module Surface
N_{SC}	12	-	Number of cells in series within PV module

N_{pc}	6	-	Number of cells in parallel within PV module
$E_{fficiency}$	14.8	%	Modules efficiency
N_{pm}	3	-	Number of modules in parallel within the PV array
N_{sm}	9	-	Number of modules in series within PV array
V_t	0.0248	Volts	Thermal voltage

Table A.10.- Solar Panels Control Component Attributes

Variable	Port	Name associated	Type	Unit	Description
T_{env}	DisturbanceSolar	InputSolar	REAL	Degree	Ambient Temperature
G	DisturbanceSolar	InputSolar	REAL	W/m^2	Solar Radiation
V_{max}		SolarPanels	REAL	Volt	Voltage at maximum power tracking

Table A.11.- Ports associated to ***ControlSolar*** Component

A.3.5.- Battery Bank Component

The component responsible for modeling a batteries bank is known as ***BatteryBank***. The symbol associated to this component is shown in Figure A.5, the modifiable parameters are described in Table A.12 and the input and output ports related with the component are given by Table A.13. The model is presented in detail in section 3.2.3

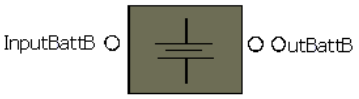

Figure A.5.- Symbol of ***BatteryBank*** Component

Variables	Deafult Value	Unit	Description
N_b	4	-	Number of batteries in series
C_{nom}	5000	Ah	Rated Battery Capacity
V_{boc}	2	Volts	Extra voltage when the battery is charged
K_{boc}	0.16	Volts	Constant which relates open circuit voltage to state of charge
P_{1c}	6	VAh	First Loss coefficients associated with the internal resistance
P_{2c}	0.86	-	Second Loss coefficients associated with the internal resistance
P_{3c}	0.48	Vh	Third Loss coefficients associated with the internal resistance
P_{4c}	1.2	-	Fourth Loss coefficients associated with the internal resistance
P_{5c}	0.036	Vh	Fifth Loss coefficients associated with the internal resistance
α_{cmt}	20.73	-	Model Parameter to be estimated
b_{cmt}	0.55	-	Model Parameter to be estimated
V_{bodc}	2.085	Volts	Residual voltage when the battery is discharged
K_{bodc}	0.12	Volts	Constant which relates open circuit voltage to state of charge

P_{1dc}	4	VAh	Loss coefficients associated with the internal resistance
P_{2dc}	1.3	-	Loss coefficients associated with the internal resistance
P_{3dc}	0.27	Vh	Loss coefficients associated with the internal resistance
P_{4dc}	1.5	-	Loss coefficients associated with the internal resistance
P_{5dc}	0.02	Vh	Loss coefficients associated with the internal resistance

Table A.12.- Batteries Bank Component Attributes

Variable	Port	Name associated	Type	Unit	Description
P_{Batt}	OutputBatt	OutBatt	REAL	W	Output Battery Power
SOC	InputBatt	InputBattB	REAL	-	State of Charge

Table A.13.- Ports associated to ***BatteryBank*** Component

A.3.6.- Diesel Generator Component

The component responsible for modeling a diesel generator is known as ***DieselGenerator***. The symbol associated to this component is shown in Figure A.6, the modifiable parameters are described in Table A.14 and the input and output ports related with the component are given by Table A.15. The model is described in Appendix B.

Variable	Default Value	Unit	Description
K_3	1	pu	Mechanical torque obtained per unit of fuel flow
K_2	1	pu	Actuator gain
K_1	1.15	pu	Engine torque constant
A,C	-0.085	-	Parameter for delay variation
B	0.08	-	Parameter for delay variation
τ_2	0.125	s	Actuator time constant
H	1	s	Inertia Constant
K_D	0.1	pu	Damping factor
X_d	1.57	pu	Synchronous d-axis reactances
X'_d	0.21	pu	Transient d-axis reactances
X''_d	0.076	pu	Subtransient d-axis reactances
X_q	1.35	pu	Synchronous q-axis reactances
τ'_{d0}	0.4	s	Transient d-axis open circuit time constant
τ'_d	0.053	s	Transient d-axis short circuit time constant
τ''_{d0}	0.0064	s	Subtransient d-axis open circuit time constant
J_{gen}	0.083	Kgm^2	Moment of inertia of Generator
K_A	187	-	Gain for amplifiers
T_A	0.89	s	Time constant for amplifiers
T_E	1.15	s	Time constant exciter
A_{EX}	0.014	-	Parameter for exciter saturation function
B_{EX}	1.55	-	Parameter for exciter saturation function
K_F	0.058	-	Gain for excitation circuit
T_F	0.62	s	Time constant for excitation system
T_B	0.06	s	Voltage Regulator
T_C	0.173	s	Voltage Regulator
T_R	0.05	s	Time constant for voltage transducer
V_{RMAX}	1.7	-	Amplifier limitation

V_{RMIN}	-1.7	-	Amplifier limitation

Table A.14.- DieselGenerator Component Attributes

Variable	Port	Name associated	Type	Unit	Description
δ_{Gen}	OutputGenCtrl	InputGen	BOOL	-	Activation of Diesel Generator
P_{Gen}	PGenOutput	GenPower	REAL	W	Diesel Generator Output Power

Table A.15.- Ports associated to ***DieselGenerator*** Component

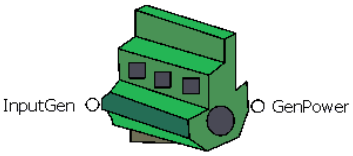

Figure A.6.- Symbol of DieselGenerator Component

A.3.7.- Diesel Generator Controller Component

The component responsible for controlling a diesel generator is represented using the ***ControlGenerator*** component. The symbol associated to this component is shown in Figure A.7, the modifiable parameters are described in Table A.16 and the input and output ports are given by Table A.17. The design of the controller is presented in detaild in Appendix B.

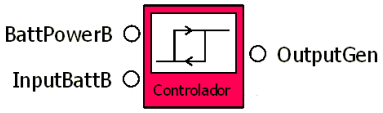

Figure A.7.- Symbol of ***ControlGenerator*** Component

Variable	Default Value	Unit	Description
SOC_{min}	0.3	-	Minimum SOC for diesel activation
SOC_{max}	0.8	-	Maximum SOC for diesel deactivation
$PBatt_{min}$	2000	W	Minimum power of a imbalance microgrid for diesel deactivation
$PBatt_{max}$	4000	W	Maximum power of an imbalance microgrid for diesel activation
ΔGen_{ON}	900	s	Minimum duration of diesel activation
ΔGen_{OFF}	900	s	Minimum duration of diesel deactivation

Table A.16.- ControlGenerator Component Attributes

Variable	Port	Name associated	Type	Unit	Description
δ_{Gen}	OutputGenCtrl	OutputGen	BOOL	-	Activation of Diesel Generator
P_{Grid}	OutputGrid	BattPowerB	REAL	W	Balanced Grid Power
SOC	InputBatt	InputBattB	REAL	-	State of Battery

Table A.17.- Ports associated to ***ControlGenerator*** Component

The approach is to define the ON/OFF switching of the diesel engine based on the battery SOC and the balanced grid power using a hysteresis band with a specific width. This control algorithm is known as "hysteresis band control"..

A.3.8.- Microgrid Component

The component responsible for modeling the inverters associated to the solar panel, wind turbine and batteries are known as ***InversorSolar, InversorWind*** and ***InversorBattery*** respectively. Notice, the symbol associated to these components are shown in Figure A.8, Figure A.9 and Figure A.10, all the modifiable parameters are described in Table A.18, Table A.20 and Table A.22; and all the input and output ports related with these components are given by Table A.19, Table A.21 and Table A.23.

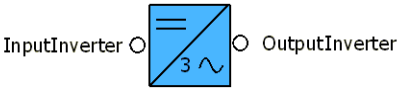

Figure A.8.- Symbol of ***InversorSolar*** Component

Variable	Default Value	Unit	Description
τ	1	s	Inverter Time Constant
η_{inv}	0.95	-	Inverter Efficiency

Table A.18.- ***InversorSolar*** Component Attributes

Variable	Port	Name associated	Type	Unit	Description
P_{Solar}	OutputSolar	InputInverter	REAL	W	Output Solar Power
$P_{InvSolar}$	OutSolarInv	OutputInverter	REAL	W	Output Solar Inverter Power

Table A.19.- Ports associated to ***InversorSolar*** Component

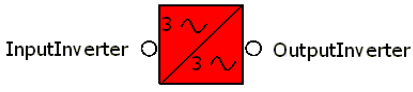

Figure A.9.- Symbol of ***InversorWind*** Component

Variable	Default Value	Unit	Description
T	1	s	Inverter Time Constant
η_{inv}	0.95	-	Inverter Efficiency

Table A.20.- InversorWind Component Attributes

Variable	Port	Name associated	Type	Unit	Description
P_{Wind}	OutputWind	InputInverter	REAL	W	Output Wind Power
$P_{InvWind}$	OutWindInv	OutputInverter	REAL	W	Output Wind Inverter Power

Table A.21.- Ports associated to ***InversorWind*** Component

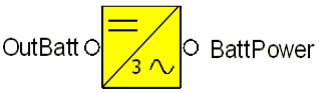

Figure A.10.- Symbol of ***InversorBattery*** Component

Variable	Default Value	Unit	Description
T	1	s	Inverter Time Constant
η_{inv}	0.95	-	Inverter Efficiency

Table A.22.- InversorBattery Component Attributes

Variable	Port	Name associated	Type	Unit	Description
P_{Batt}	OutputGrid	BattPower	REAL	W	Output Battery Power
$P_{InvBatt}$	OutputBatt	OutBatt	REAL	W	Output Battery Inverter Power

Table A.23.- Ports associated to ***InversorBattery*** Component

A.3.9.- Microgrid Control Component

Inverter control is the main concern in MicroGrid operation. In general, MicroGrid is intended to operate in two different operating conditions:

- *Connected mode:* The MicroGrid is connected to a small diesel engine. Frequency and voltage references are provided by the diesel engine. All inverters act as current sources (slaves), following the reference from the diesel engine.

- *Island mode:* The MicroGrid is not connected to a small diesel engine. Frequency and voltage references are provided by one inverter which acts as a voltage source (VSI – Voltage Source Inverter). In this case, one

inverter connected to batteries acts as a voltage source (master) and the other inverters act as current sources (slaves), following the reference from the VSI.

The component using for modeling a master and slave controllers are known as ***BatteryCtrl*** and ***SecondFreqCtrl***. Notice, the symbol associated to these components are shown in Figure A.11 and Figure A.12, all the modifiable parameters are described in Table A.24, Table A.26 and all the input and output ports related with these components are given by Table A.25, Table A.27.

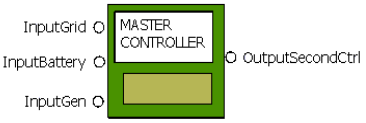

Figure A.11.- Symbol of ***InversorBattery*** Component

Variable	Defalut Value	Unit	Description
k_{pf}	-1	Hz/Pnom	Active Power/Frequency droop
P_{nom}	5000	W	Nominal Active Power
f_{gridop}	51	Hz	Fundamental Grid Frequency
SOC_{max}	1	-	Maximum State of Charge allowed
k_{bat}	-0.5	-	Penalized weight for state of battery
$f_{gridnom}$	50	Hz	Nominal Grid Frequency
T	0.1	seg	Time constant for Grid Frequency

Table A.24.- BatteryCtrl Component Attributes

Variable	Port	Name associated	Type	Unit	Description
P_{Grid}	OutputGrid	InputGrid	REAL	W	Output Grid Power
δ_{Gen}	OutputGenCtrl	InputGen	REAL	-	Activation of Diesel Generator
SOC	InputBatt	InputBattery		-	State of Charge
f_{Grid}	OutputBattInv	OutputSecondCtrl	REAL	Hz	Grid Frequency

Table A.25.- Ports associated to ***BatteryCtrl*** Component

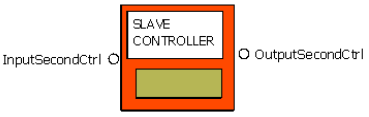

Figure A.12.- Symbol of ***SecondFreqCtrl*** Component

Variable	Default Value	Unit	Description
k_p	1	-	Proportional Gain for PI
k_i	0.0666	-	Derivative Gain for PI

f_{gridop}	51	Hz	Fundamental Grid Frequency

Table A.26.- SecondFreqCtrl Component Attributes

Variable	Port	Name associated	Type	Unit	Description
f_{Grid}	OutputBattInv	InputSecondCtrl	REAL	Hz	Grid Frequency
η_{Ctrl}	Efficiency	OutputSecondCTrl	REAL	-	Signal Control

Table A.27.- Ports associated to ***SecondFreqCtrl*** Component

A.3.10.- Desalination Component

The component used for modeling the desalination plant is ***DesalinationPlant***. The symbol associated to this component is shown in Figure A.13, the modifiable parameters are described in Table A.28; and the input and output ports related with these components are given by Table A.29. The mathematical model is described in section 3.4

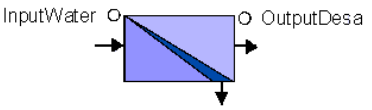

Figure A.13.- Symbol of ***DesalinationPlant*** Component

Variable	Default Value	Unit	Description
P	1000	Kg/m^3	Water density
$q_{FeedRef}$	3	m^3/h	Real flow
H_{Feed}	25.7	M	Resulting height
G	9.81	m/seg^2	Gravity acceleration
$\eta_{MotorFeed}$	54.97	%	Motor efficiency
$\eta_{PumpFeed}$	55.8	%	Pump efficiency
η_{MB01}	0.6895	%	Motor efficiency
η_{B01}	38.4	%	Pump efficiency
P_{atm}	1	bar	Atmospheric pressure
A_{T1}	1.5	m^2	Area of tank 1
q_{des}	2.5	m^3/h	Flow
$Cos\varphi_{B03}$	0.86	-	Power factor
η_{MB03}	0.886	-	Motor efficiency
η_{B03}	91.558	%	Pump efficiency
H_{T1max}	3.5	m	Maximum level tank
H_{T1min}	0.5	m	Minimum level tank
A_{T2}	2	m^2	Tank1 area
H_{T2max}	2.95	m	Maximum level tank
H_{T2min}	0.05	m	Minimum level tank
A	0.2	$m^3/hbar$	Water permeability
B	0.01	$m^3/hbar$	Salt permeability
N	5	-	Discretization
A	0.0750	m^2	Membrane Area
V_i	0.03	m^3	Volume in each discretization
k_{pd}	1.3	-	Difference Pressure

$Feed_C$	18	kg/m^3	Feed concentration
$Feed_T$	20	degrees	Feed temperature
$P_{permeate}$	1.5	bar	Permeate pressure

Table A.28.- DesalinationPlant Component Attributes

Variable	Port	Name associated	Type	Unit	Description
q_{wd}	DataAgua	InputWater	REAL	m^3/seg	Water demand
P_{load}	PLoadOutput	OutputDesa	REAL	W	Electrical demand

Table A.29.- Ports associated to ***DesalinationPlant***

A.3.11.- Water Demand Component

The component responsible for modeling the water demand is known as ***ForecastWater***. Notice, the symbol associated to this component is shown in Figure A.14, all the modifiable parameters are described in Table A.30 and all the input and output ports related with the component are given by Table A.31.

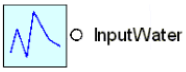

Figure A.14.- Symbol of ***ForecastWater*** Component

Variable	Type	Unit	Description
a_o	REAL	m^3/h	Modifiable Parameter
a_k	REAL	m^3/h	Modifiable Parameter
b_k	REAL	m^3/h	Modifiable Parameter
d_o	REAL	day	The initial day of the year in climate terms
Δ_w	REAL	m^3/h	Weekly corrector factor
Δ_h	REAL	m^3/h	Daily corrector factor

Table A.30.- ForecastWater Component Attributes

Variable	Port	Name associated	Type	Unit	Description
q_{wd}	DataAgua	InputWater	REAL	m^3/h	Water Demand

Table A.31.- Ports associated to ***ForecastWater*** Component

A.3.12.- Solar Irradiation Component

The component responsible for modeling solar radiation is known as ***ForecastSolar***. Notice, the symbol associated to this component is shown in Figure A.15, all the modifiable parameters are described in Table A.32 and all the input and output ports related with the component are given by Table A.33.

Figure A.15.- Symbol of ***ForecastSolar*** Component

Variable	Type	Unit	Description
I_{max}	REAL	W/m^2	Maximum solar radiation during (*d-1*) day
ΔL(d)	REAL	Hours	Day length for the day *d*
GMT_{sunset}	REAL	Hours	Sunset hours of the day *d*
$GMT_{sunrise}$	REAL	Hours	Sunrise hours of the day *d*
L	REAL	Degree	Longitude
ϕ	REAL	Degree	Latitude
Δ	REAL	Degree	Declination
D	REAL	Day	Day of the month
M	REAL	Month	Month number
N	REAL	Day	Day of the year

Table A.32.- ForecastSolar Component Attributes

Variable	Port	Name associated	Type	Unit	Description
G_e	DisturbanceSolar	InputSolar	REAL	W/m^2	Solar radiation

Table A.33.- Ports associated to ***ForecastSolar*** Component

A.3.13.- Ambient Temperature Component

The component responsible for modeling temperature is known as ***ForecastTemperature.*** Notice, the symbol associated to this component is shown in Figure A.16, all the modifiable parameters are described in Table A.34 and all the input and output ports related with the component are given by Table A.35.

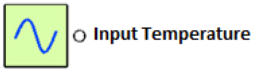

Figure A.16.- Symbol of ***ForecastTemperature*** Component

Variable	Type	Unit	Description
ΔL(d)	REAL	Hours	Day length for the day *d*
$GMT_{sunrise}$	REAL	Hours	Sunrise hours of the day d
T_{min}	REAL	Degree	Minimum Temperature
T_{max}	REAL	Degree	Maximum Temperature

Table A.34.- ForecastTemperature Component Attributes

Variable	Port	Name associated	Type	Unit	Description
T_{env}	DisturbanceSolar	InputSolar	REAL	degree	Ambient temperature

Table A.35.- Ports associated to ***ForecastTemperature*** Component

APPENDIX B

Diesel Generator Model

The modelling and simulation of the response of the diesel generator for start-up and load disturbances are presented. Considering generator will be used as a back up supply, it must possess good dynamic response at startup. The nonlinear dynamic model is developed using SIMULINK dynamic systems module of the MATLAB software package. Normally, the diesel generator consists of three main components: the diesel engine, the synchronous generator and the excitation system (see Figure B.1). Thus, models of the diesel engine, diesel engine governor, synchronous generator, excitation system, automatic voltage regulation (AVR) and the load are presented.

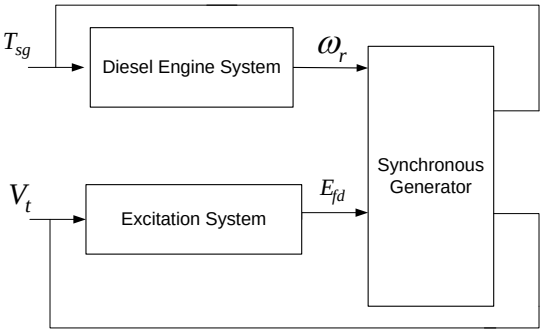

Figure B.1.- The overall block diagram of diesel generator

B.1.- Model of Diesel Engine System

Although detailed models are available to simulate the complete dynamics of a diesel engine (Wellstead et al., [137]), that include thermodynamic aspects, as the focus here is in electricity production as auxiliary system, it is sufficient to use a

much lower order model, so thermodynamic variables may be considered to be constant but unknown. This approach has been adopted in other internal-combustion engine simulation studies, such as in (Morris et al., [138]). The general structure of the plant is shown in Figure B.2. It can be seen that the plant consists of three parts: the actuator, the engine and the flywheel. The model of each component is now briefly described.

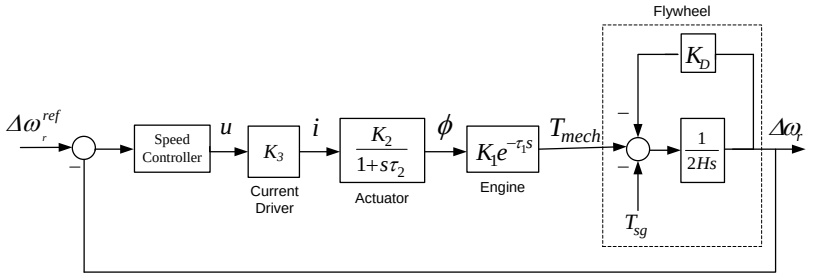

Figure B.2.- Block diagram of a typical diesel engine system

B.1.1.- Current Driver Model

The "current driver" block represents the amount of mechanical torque obtained per unit of fuel flow. It is represented by a constant K_3, which depends on the operating point of the prime mover.

B.1.2.- Actuator Model

The "actuator" block represents the governor (actuator) system of the diesel engine. A governor can be defined as a mechanical or electromechanical device for automatically controlling the speed of an engine by relating the intake of fuel. The input driving current (i) controls the fuel rack position, which in turn determines the amount of fuel (ϕ) to be injected into the combustion chamber. The actuator is usually represented by a first order phase lag function, which is characterized by a gain K_2 and a variable time constant (τ_2). Here, K_2 is the actuator constant, that is considered to be fixed, τ_2 is the actuator time constant, which is a complicated function of the temperature of the fuel. For simplicity, the variation of the parameters is ignored and τ_2 is assumed to be constant.

B.1.3.- Diesel Engine Model

The "Engine" block comprises the combustion system of the diesel engine. The injected fuel is ignited by the compressed hot air in the combustion chamber,

causing the movement of the piston during the power strokes. This action drives the crankshaft, so the mechanical torque T_{mech} is produced.

For modelling, this engine combustion system is represented as an engine torque constant with a dead time element τ_1, which is the result of having several cylinders. For each individual cylinder, this has essentially two components. The "ignition delay" represents the time taken by the fuel-air mixture to reach combustion point at the particular operating temperature and pressure; it can be shown to have a hyperbolic variation with speed deviation. The "power stroke delay" represents the time that elapses from a load disturbance to the time at which a particular engine cylinder responds to the disturbance. This delay is random and depends on the crank angle value at which a load disturbance is imposed. Its effect can be reduced by increasing the number of cylinders. Since for a particular load disturbance, the time after which the cylinders responds goes down inversely with speed, it may be approximated by an inverse function of speed.

The engine dead time (τ_1) is a function of the speed deviation $\Delta\omega_r$ (pu) through a nonlinear function. An adequate non-linear function to represent the dead time variation is (see Figure B.3):

$$\tau_1 = \frac{A\Delta\omega_r^2 + B\Delta\omega_r + C}{\Delta\omega_r^2} \tag{B.1}$$

Where A, B and C are parameters that are determined by curve fitting techniques to reproduce empirically determined curves, such as those in (Mina, [139]).

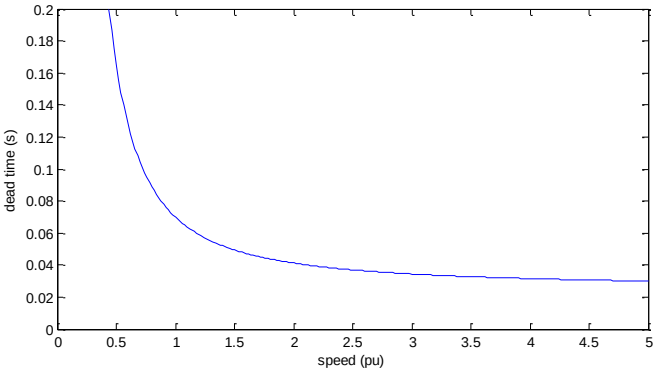

Figure B.3.- Typical variation of dead time with engine speed

B.1.4.- Flywheel Model

The "Flywheel" block comprises the rotating system, so it comprises the dynamics of the engine inertia, the flywheel, the damping factor (K_D) and the loaded alternator. The mechanical motion of equation is then:

$$2H\frac{d\Delta\omega_r}{dt} = T_{mech} - T_{sg} - K_D\Delta\omega_r \tag{B.2}$$

$$\frac{d\delta}{dt} = \omega_0\Delta\omega_r \tag{B.3}$$

$$\Delta\omega_r = \omega_r - 1 \tag{B.4}$$

Where time t is in seconds, rotor angle δ is in radians, rated generator speed ω_0 is in rad/s, $\Delta\omega_r$ is the speed deviation (pu), ω_r is the angular velocity of the rotor (pu), T_{sg} is the generator torque (pu), H is the per unit inertia constant (s).

B.2.- Synchronous Generator Model

The equations of synchronous generator are obtained from Park Transformation, after a per unit representation and some simplifications. The most important simplification is that stator transients are neglected because it is much faster compared to the rotor ones. Considering a salient pole synchronous generator, rotor consists of three windings. A field and a damping winding are considered on the direct axis in order to take into account the transient and subtransient behavior respectively in this axis. Meanwhile, a damping winding is considering on the quadrature axis.

The terminal voltage phasor is determined by, $V_t = V_d + jV_q$, that can be evaluated from:

$$V_d = E''_d - R_s I_d + X''_q I_q \tag{B.5}$$

$$V_q = E''_q - R_s I_q - X''_d I_d \tag{B.6}$$

where R_s is the armature resistance, I_q and I_d are the currents flowing in the stator winding, the $X''_{d,q}$ are the so-called subtransient d and q-axis reactances and $E''_{d,q}$ are given by (Krause, [140]).

$$E''_d = \frac{\left(X_q - X''_q\right)}{1+\tau''_{qo}s} I_q \tag{B.7}$$

$$E''_q = \frac{1}{1+\tau''_{do}s} E'_q - \frac{\left(X'_d - X''_d\right)}{1+\tau''_{do}s} I_d \tag{B.8}$$

Where $X_{d,q}$ and $X'_{d,q}$ are the synchronous and transient reactances, the $\tau''_{do,qo}$ are the open circuit subtransient time constants and E'_q is given by

$$E'_q = \frac{1}{\left(\frac{X_d - X''_d}{X'_d - X''_d}\right)+\tau'_{do}s} E_{fd} + \frac{\left(\frac{X_d - X'_d}{X'_d - X''_d}\right)}{\left(\frac{X_d - X''_d}{X'_d - X''_d}\right)+\tau'_{do}s} E''_q \tag{B.9}$$

Where E_{fd} is the exciter field voltage and τ'_{do} is the open circuit transient time constant.

As it can be seen in Figure B.1, there is an additional feedback term from the generator to the diesel engine given by the electromagnetic torque that in flywheel mode can be evaluated from:

$$T_{sg} = E''_d I_d + E''_q I_q - \left(X''_d - X''_q\right) I_d I_q \tag{B.10}$$

B.3.- Excitation System Model

The main function of an excitation system is to supply and automatically adjust the field current of the synchronous generator considering control and protective functions essential to the satisfactory performance of the system. The control functions include the control of voltage and the enhancement of system stability. The protective functions ensure that the capability limits of the synchronous machine, excitation system, and other equipment are not exceeded. The functional block diagram of a typical excitation control system is shown in Figure B.4.

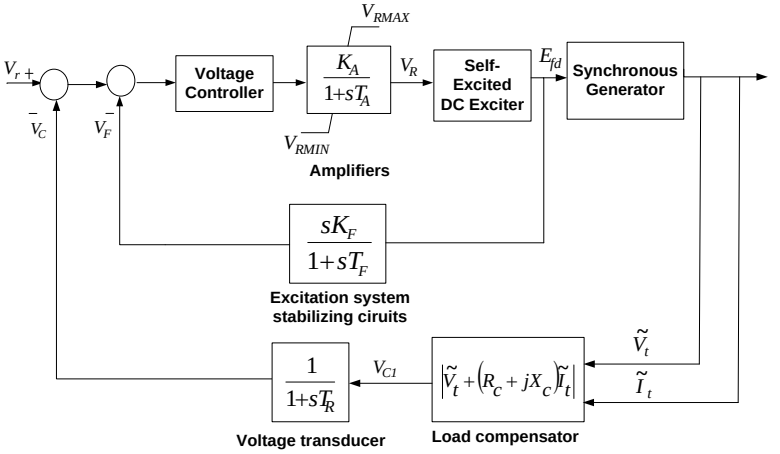

Figure B.4.- Funtional Block diagram of a synchronous generator excitation control system (Kundur, [141])

A.- Excitation system stabilizing circuits: Excitation systems comprised of elements with significant time delays have poor dynamic performance. Hence, excitation system stabilizing circuits is used to improve the dynamic performance of the control excitation control system. A derivative feedback is the most commonly used form of compensation. The aim of the compensation is to minimize the phase shift introduced by the time delays over a selected frequency range.

B.- Load compensation: The compensator has adjustable resistance (R_c) and inductive reactance (X_c) that simulate the impedance between the generator terminals and the point at which the voltage is being effectively controlled. Using this impedance and the measured armature current, a voltage drop is computed and added to or subtracted from the terminal voltage. The magnitude of the resulting compensated voltage (V_{c1}), which is fed to the AVR, is given by:

$$V_{c1} = \left|\tilde{V}_t + \left(R_c + jX_c\right)\tilde{I}_t\right| \tag{B.11}$$

This is used to ensure proper sharing of reactive power between generators placed together at their terminals, sharing a common step-up transformer. The compensator functions as a reactive current compensator by creating an artificial coupling between the generators. Without this provision, one of the generators would try to control the terminal voltage slightly higher than the other; hence, one generator would tend to supply all of the required reactive power while the other would absorb reactive power to the extent allowed. When load compensator is not used, R_c and X_c are set to zero.

C.- Voltage transducer: The time constant T_R represents rectification and filtering of the synchronous machine terminal voltage. The voltage transducer output (V_c) forms the principal control signal to the excitation system. If a load compensator is not used and V_c is negligible, $V_c = V_t$.

D.- Amplifiers: Amplifiers may be magnetic, rotating, or electronic type. Magnetic and electronic amplifiers are characterized by a gain and may also include a time constant.

B.3.1.- Self-Excited DC Exciter

The excitation systems of this category utilize dc generators as source of excitation power and provide current to the rotor of the synchronous machine through slip rings.

The self-excited DC exciter is represented in block diagram form as shown in Figure B.5. All variables are in per unit.

$$V_R = K_E E_{fd} + S_E\left(E_{fd}\right)E_{fd} + T_E \frac{dE_{fd}}{dt} \tag{B.12}$$

There are several mathematical expressions that may be used to approximate the effect of exciter saturation. A commonly used expression is the exponential function:

$$S_E\left(E_{fd}\right)E_{fd} = A_{EX} e^{B_{EX} E_{fd}} \tag{B.13}$$

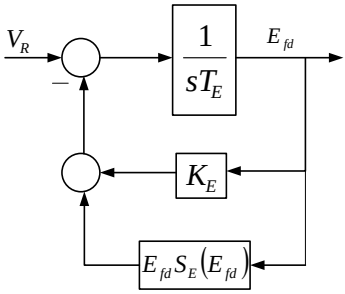

Figure B.5.- Block Diagram of a self- excited DC exciter

To establish initial conditions, K_E is often chosen such that it is equal in magnitude to the saturation function at the initial value of E_{fd}. At this value, the shunt field exactly compensates for exciter saturation and no regular output is

required to establish the initial value of E_{fd}. In other words, K_E is computed so that initially $V_R = 0$.

B.4.- Speed Control

The speed controller is designed to keep constant the internal combustion engine speed by changing the quantity of fuel consumed by the motor. The direct result of this speed controller is a stable frequency for the voltage at the generator terminals. A constant frequency requires good precision and a short response time from the speed controller.

Detailed models of diesel engines are characterized by nonlinear, time-varying parameters including a nonlinear input dead-time variation that introduces an unknown delay (τ_1) between the injection of fuel and the production of engine torque. The presence of this dead time together with some other system parameters gives rise to a serious control problem and significantly degrades the performance especially under varying loads. The dead time is an unknown time delay and is commonly considered as a complicated function of operating conditions and the engine speed (Haddad et al., [142]) (Choe et al., [143]).

Conventional PID controllers are widely employed in diesel engine speed control, which gives acceptable performance. However, PID schemes might not be able to handle large variations in the engine dead time. Here, several advanced control techniques for the speed control of the diesel engine systems have been reported in the literature, based on the methods of H∞ (Kuang et al., [144]), adaptive control (Roy et al., [145]) and neural network (Yacoub et al., [146]).

B.5.- Automatic Voltage Regulation

The Automatic voltage regulator (AVG) controls the exciter field to provide a constant terminal voltage. In the past, the generator response using an analog excitation system was a matter of adjusting potentiometers or adding or deleting capacitors and resistors in the control loops of the voltage regulator stability circuit. Adjustment could be very time consuming because changes would often involve turning the excitation system on and off many times in order to make modifications.

Today, the digital excitation system provides the means to easily access the challenging parameters of the analog system. The most important point of digital controllers is the embedded microprocessors that perform various control functions

for the excitation system. These control functions include the automatic voltage regulator, field current regulator, Var/Power factor control, and a host of excitation limiters to regulate and maintain the generator within safe operating limit of the machine (Schaefer et al., [147]). Conventional PID controllers are employed in digital AVG.

Bibliography

[1] P. Novak, T. Ekelund, I. Jovik, and B. Schmidtbauer, "Modeling and control of a variable-speed wind-turbine drive-system dynamics", *IEEE Control Syst. Mag.*, vol. 15, pp. 28-38, 1995.

[2] M. Chinchilla , S. Arnaltes and J. C. Burgos, "Control of permanent magnet generators applied to variable-speed wind-energy systems connected to the grid", *IEEE Trans. Energy Convers.*, vol. 21, no. 1, pp.130-135, 2006.

[3] M. S. Khan and M. R. Iravani, "Hybrid control of a grid-interactive wind energy conversion system", *IEEE Trans. Energy Convers.*, vol. 23, no. 3, pp.895-902, 2008.

[4] T. A. Johansen and C. Storaa, "Energy-based control of a distributed solar collector field", *Automatica*, vol. 38, no. 7, pp. 1191-1199, 2002.

[5] E. F. Camacho and M. Berenguel, "Robust adaptive model predictive control of a solar plant with bounded uncertainties", *Int. J. Adaptive Contr. Signal Processing*, vol. 11, no. 4, pp. 311-325, 1997.

[6] N. Hamrouni, M. Jraidi and A. Chief, "New control strategy for 2-stage grid-connected photovoltaic power system", *Renewable Energy*, vol. 33, pp. 2212-2221, 2008.

[7] Si, T., Jana, N.D., Sil, J.: "Particle Swarm Optimization with Adaptive Polynomial Mutation", *Proc. World Congress on Information and Communication Technologies (WICT 2011)*, Mumbai, India, pp. 143–147, 2011.

[8] Hiroaki Kakigano, Yushi Miura and Toshifumi Ise. "Distribution Voltage Control for DC Microgrids Using Fuzzy Control and Gain-Scheduling Technique". *IEEE Transactions on Power Electronics*, Vol. 28, No. 5, Mayo 2013.

[9] F. Keyrouz, M. Hamad and S. Georges, "A novel unified maximum power point tracker for controlling a hybrid wind-solar and fuel-cell system", *Eighth*

International Conference and Exhibition on Ecological Vehicles and Renewable Energies (EVER), 2013.

[10] H. Weiss, and Jian Xiao, "Fuzzy system control for combined wind and solar power distributed generation unit", *IEEE International Conference on Industrial Technology*, vol. 2, 2003.

[11] K. H. Hussein and I. Mota, "Maximum photovoltaic power tracking: An algorithm for rapidly changing atmospheric conditions," *in IEE Proc. Generation Transmiss. Distrib.,* 1995, pp. 59–64.

[12] Y. Zhang, H.J. Jia and L. Guo, "Energy Management Strategy of Islanded Microgrid Based on Power," *IEEE PES Innovative Smart Grid Tech*., pp. 1-8, 2012.

[13] W. Qi , J. Liu , X. Chen and P. D. Christofides "Supervisor predictive control ofstand-alone wind-solar energy generation systems", *IEEE Trans. Control Syst.Technol.,* vol. 19, no. 1, pp.199 -207 2011.

[14] W. Qi, J. Liu, and P. D. Christofides, "Distributed Supervisory Predictive Control of Distributed Wind and Solar Energy Systems", *IEEE Trans. Control Syst. Technol*., vol. 21, no. 2, pp. 504-512, 2013.

[15] E. F. Camacho, F. R. Rubio, and F. M. Hughes, "Self-tuning control of a solar power plant with distributed collector field", *IEEE Control Syst*., vol. 12, no. 2, pp.72 -78, 1992.

[16] R. Pickhardt and R. N. Silva, "Application of a nonlinear predictive controller to a solar power plant". *Proceedings of IEEE International Conference on Control Applications*, Trieste, 1998, pp. 6-10.

[17] J. Henriques, A. Cardoso and A. Dourado, "Supervision and c-Means clustering of PID controllers for a solar power plant", *International Journal of Approximate Reasoning*, vol. 22, pp. 73-91, 1999.

[18] T. A. Johansen, K. Hunt, and I. Petersen, "Gain-scheduled control of a solar power plant". *Control Engineering Practice*, vol. 8, pp. 1011-1022, 2000.

[19] R. Stirrup, D. Loebis, A. J. Chipperfield, K. S. Tang, S. Kwong and K. F. Man, "Gain-scheduled control of a solar power plant using a hierarchical MOGA-tuned fuzzy PI- controller". *Proceedings of the IEEE International Symposium on Industrial Electronics*, vol 1, pp. 25-29, 2001.

[20] R. Stirrup R. and A. J. Chipperfield A. J., "Improved MOGA-tuning and visualization for a hybrid control system". *Proceedings of the 16th IFAC World Congress*. Prague, Czech Republic, 2005.

[21] I. Farkas and I. Vajk, "Internal model-based controller for solar plant operation". *Computers and Electronics in Agriculture*, vol. 49, no. 3, pp. 407-418, 2005.

[22] S. Engell, "Feedback control for optimal process operation". *Journal of Process Control*, vol. 17, no. 3, pp. 203-219, 2007.

[23] D. Zambrano and W. García-Gabín, "Hierarchical control of a hybrid solar air conditioning plant" *European Journal of Control*, vol. 14, no. 6, pp 464-483, 2008.

[24] M. Rodriguez, C. De Prada, F. Capraro and S. Cristea "Logic embedded NMPC of a solar air conditioning plant", *European Journal of Control*, vol. 14, no. 6, pp. 484-500, 2008.

[25] E. F. Camacho and C. Bordons. "Model Predictive Control", Springer, 2nd ed., 2004.

[26] R. De Keyser, "A Gentle Introduction to Model Based Predictive Control", *In PADI2 International Conference on Control Engineering and Signal Processing*, Piura, Peru, 1998.

[27] C. R. Cutler and B. C. Ramaker. "Dynamic Matrix Control – A Computer Control Algorithm". *In Automatic Control Conference*, San Francisco, 1980.

[28] J. Richalet, A. Rault, J. L. Testud, and J. Papon. "Model Predictive Heuristic Control: Application to Industrial Processes". *Automatica*, 14(2): 413-428, 1978.

[29] J. Richalet, S. Abu el Ata-Doss, C. Arber, H. B. Kuntze, A. Jacubash, and W. Schill. "Predictive Functional Control. Application to fast and accurate robots". *In Proc. 10th IFAC Congress*, Munich, 1987.

[30] R.M.C. De Keyser and A. R. Van Cuawenberghe. "Extended Prediction Self-adaptive Control". *In IFAC Symp. on identification and System Parameter Estimation*, York, UK, pages 1317-1322, 1985.

[31] J.Richalet, "Pratique de la commande prédictive-Hermès", Paris, 1993.

[32] J. M. Maciejowski "Predictive control with constrains", Prentice-Hall, 2002.

[33] P. O. M. Scokaert, D. Q. Mayne, and J. B. Rawlings. "Suboptimal Model Predictive Control (Feasibility Implies Stability)". *IEEE Transactions on Automatic Control*, vol. 44, No. 3, March 1999.

[34] Chen, H. and Allgower, F. “A quasi-infinite horizon nonlinear model predictive control scheme with guaranteed stability”. *1997 European Control Conference (ECC)*, 1-4 July 1997, Brussels, Belgium.

[35] M. Rasila, "Torque- and Speed Control of a Pitch Regulated Wind Turbine", Master's Thesis, Department of Electric Power Engineering, Chalmers University of Technology, 2003.

[36] K. Raiambal and C. Chellamuthu, “Modeling and simulation of grid connected wind electric generating system”. *Proceedings of IEEE TENCON*, pp. 1847-1852, 2002.

[37] F. Mei and B. C. Pal, "Modelling and small-signal analysis of a grid connected doubly-fed induction generator", *Proceedings of IEEE Power Eng. Soc. General Meeting* 2005, 2005.

[38] F. Wua, X. Zhangb and P. Jua, "Small signal stability analysis and control of the wind turbine with the direct-drive permanent magnet generator integrated to the grid," *Electric Power Systems Research*, vol. 79, pp. 1661-1667, 2009.

[39] D. Svechkarenko, "Simulations and control of direct driven permanent magnet synchronous generator", *Project Report, Department of Electrical Engineering, Royal Institute of Technology*, Sweden, 2005.

[40] A. J. Mahdi, W. H. Tang, L Jiang, Q. H. Wu., “A Comparative Study on Variable-Speed Operations of a Wind Generation System Using Vector Control”. *International Conference on Renewable Energy and Power Quality (ICREPQ)*, Granada, Spain, 2010.

[41] I. Cataña, C. Safta and V. Panduru, “Power Optimisation Control System of Wind Turbines by changing the pitch angle”, *U. P. B. Sci Bull*., Series D, Vol. 72, Iss 1, 2010.

[42] J. Solsona and M. Valla. “Disturbance and Nonlinear Luenberger Observers for Estimating Mechanicals Variables in Permanent Magnet Synchronous Motors under Mechanicals Parameters Uncertainties” *Industrial Electronic IEEE*, Vol 50, Nº 4, August 2003.

[43] M. M. Hand and M. J. Balas, “Systematic Control Design Methodology for Variable-Speed Wind Turbine”, *Technical Report of National Renewable Energy Laboratory*, Colorado, USA, 2002.

[44] E .S. Abdin, W. Xu, “Control Design and Dynamic Performance Analysis of a Wind Turbine-Induction Generator Unit”, *IEEE Transactions on Energy Conversion*, vol. 15, no. 1, pp. 91-96, 2000.

[45] R. Chedid, F. Mrad, and M. Basma, "Intelligent control of class of wind energy conversion systems", *IEEE Transactions on Energy Conversion*, vol. 14, pp. 1597-1604, 1999.

[46] F. Lescher, J. Y. Zhao and P. Borne "Robust gain scheduling controller for pitch regulated variable speed wind turbine", *Stud. Inform. Control*, vol. 14, no. 12, pp. 299 -315, 2005.

[47] A. S. Yilmaz, and Z. Ozer, "Pitch angle control in wind turbines above the rated wind speed by multi-layer perceptron and radial function neural networks," *Expert Systems with Applications*, vol. 36, 2009, pp. 9767-9775, 2009.

[48] A. Kulka, "Pitch and Torque Control of Variable Speed Wind Turbines," *Master of Science, Department of Electric Power Engineering, Chalmers University of Technology*, Goteborg, Sweden, 2004.

[49] S. Postel, "Facing water scarcity. In: State of the world", *A Worldwatch Institute Report, W.W. Norton & Co.*, New York and London, 1993.

[50] C. Fritzmann, J. Löwenberg, T. Wintgens and T. Melin, "State-of-the-art of reverse osmosis desalination", *Desalination*, vol. 216, pp. 1-76, 2007.

[51] M. Wilf, "The Guidebook to Membrane Desalination Technology" *Balaban Desalination Publications*, L'Aquila, Italy, 2007.

[52] U. Seibert, G. Vogt, C. Brennig, R. Gebhard and F. Holz, "Autonomous, desalination system concepts for seawater and brackish water in rural areas with renewable energies". *Desalination*, 168, 29-37, 2004.

[53] M. Amer, A. Namaane and N. M'Sirdi, "Optimization of Hybrid Renewable Energy Systems (HRES) using PSO for Cost Reduction". *Mediterranean Green Energy*, Volume 42, 2013, pages 318-327.

[54] Soteris A. Kalogirou, "Effect of fuel cost on the price of desalination water: a case for renewables". *Desalination*, Vol. 138, Issues 1–3, 20 September 2001, Pages 137–144.

[55] Ahmad Agus Setiawan, Yu Zhao and Chem. V. Nayar. "Design, economic analysis and environmental considerations of mini-grid hybrid power system with reverse osmosis desalination plant for remote areas". *Renewable Energy*, Volume 34, Issue 2, February 2009, Pages 374–383.

[56] A. Gambier, A. Krasnik and E. Badreddin, "Dynamic Modeling of a Simple Reverse Osmosis Desalination Plant for Advanced Control Purposes", *Proc. of the American Control Conference*, New York, USA, 2007.

[57] R.W. Baker, “Membrane Technology and Applications”, John Wiley & Sons, Ltd, 2nd ed., New York, 2004.

[58] Donald J. Hammerstrom. “AC Versus DC Distribution Systems - Did We Get it Right?” *Power Engineering Society General Meeting, IEEE*, 24-28 June 2007.

[59] W. Kleinkauf, “Photovoltaic Power Conditioning / Inverter Technology”, *10th European Photovoltaic Solar Energy Conference*, Lisbon, Portugal, 1991.

[60] G. Cramer, J. Reekers, M. Rothert, and M. Wollny, "The future of village electrification - More than two years of experiences with AC-coupled hybrid systems", *Proceedings of the 2nd European PV-Hybrid and Mini-Grid Conference*, Kassel, Germany, 2003, pp. 1-6.

[61] G. Cramer, M. Ibrahim and W. Kleinkauf, “PV system technologies: State-of-the-art and trends in decentralized electrification", *Refocus Journal*, vol. 5, no. 1, pp. 38-42, 2004.

[62] J. Salazar, F. Tadeo, C. Prada. "Renewable Energy for Desalinization using Reverse Osmosis", *International Conference on Renewable Energies and Power Quality (ICREPQ'10)*, Granada, Spain, 2010.

[63] L. Palacin, F. Tadeo, C. de Prada and J. Salazar, “Operation of desalination plants using renewable energies and hybrid control”. *Desalination and Water Treatment*, vol. 25, pp. 119-126, 2011.

[64] J. Salazar, F. Tadeo, C. de Prada. “A Microgrid Library in a General Simulation Language”. The International Federation of Automatic Control, Cape Town, South Africa, Volume 19, August 2014, Pages 3599-3604.

[65] J. Salazar, F. Tadeo, C. de Prada and L. Palacin. “Modeling and control of a wind turbine equipped with a permanent magnet synchronous generator (PMSG)”, *22nd European Modeling & Simulation Symposium*, FES, Morocco, October 13-15, 2010.

[66] R.A. Ibrahim, M.S. Hamad, Y.G. Dessouky and B.W. Williams, “A review on recent low voltage ride-through solutions of wind farm for permanent magnet synchronous generator”, *SPEEDAM*, June 2012, Italy.

[67] R. Ibrahim, M. Hamad, Y.G. Dessouky and B.W. Williams, “A Novel Topology for Enhancing the Low Voltage Ride through Capability for Grid Connected Wind Turbine Generators”, Energy Conversion Congress and Exposition (ECCE), IEEE, September 2012, USA.

[68] A. Chouder, S. Silvestre and A. Malek, "Simulation of photovoltaic grid connected inverter in case of grid-failure", *Revue des Energies Renouvelables*, vol. 9, no. 4, pp. 285-296, 2006.

[69] J. Salazar, F. Tadeo, C. Prada and L. Palacin. "Simulation and Control of a PV System connected to a Low Voltage Network", *XXXI Jornadas de Automática*, Jaén, SPAIN, September 08-10, 2010.

[70] T. Esram and L. Chapman, "Comparison of Photovoltaic Array Maximum Power Point Tracking Techniques", *IEEE Transactions on Energy conversion*, vol. 22, no. 2, pp. 439-449, 2007.

[71] I. Yahyaoui, "Sizing and energy management for photovoltaic pumping", Tesis doctoral, Universidad de Valladolid, Valladolid, 2015.

[72] N. M'Sirdi, K. Rabhi and B. Nehme, "The VSAS approach gives the best MPPT for Solar Energy Sources (RES)", J*ournal of Renewable Energy and Sustainable Development (RESD)*, pages 60-71, June 2015.

[73] A. Zegaoui, P. Petit, P. Sawicki, J. P. Charles, M. Aillerie, M. DellaK and A. O. Belarbi, "Simulation of Photovoltaic Generators and Comparison of two common Maximum Power Point trackers", *International Conference on Renewable Energies and Power Quality (ICREPQ)*, 2010.

[74] Stefano Barsali and Massimo Ceraolo. "Dynamical Models of Lead-Acid Batteries: Implementation Issues". *IEEE Transactions On Energy Conversion*, Vol 17, No. 1, March 2002.

[75] James F. Manwell and Jon G. McGowan. "Lead acid battery storage model for hybrid energy systems". *Solar Energy*, Vol. 50, Issue 5, May 1993, Pages 399–405.

[76] D. Guasch and S. Silvestre. "Dynamic Battery Model for Photovoltaic Applications", *Progress in Photovoltacis: Research and Applications. Prog. Photovolt: Res. Appl. 2003*; 11:193–206 (DOI: 10.1002/pip.480).

[77] P. E. Wellstead and P. M. Zanker, "Application of self-tuning to engine control", Ch12 of "Self-tuning and adaptive control: theory and applications" (book, Eds: C. J. Harris ad S. A. Billings), *Instt. Of Electrical Engrs*., 1981.

[78] L. Palacin, F. Tadeo, J. Salazar and C. de Prada. "Initial validation of a reverse osmosis simulator" *Proc. of the 15th IEEE International Conference on Emerging Technologies and Factory Automation, ETFA*, 2010, Bilbao, Spain.

[79] A. Engler, "Applicability of droops in low voltage grids", *Int. J. Distrib. Energy Res*., vol. 1, no. 1, 2005.

[80] B. Burger, A. Engler, “Fast Signal Conditioning in Single Phase Systems”, *9th European Conference on Power Electronics and Applications*, 2001.

[81] J. A. Peças Lopes, C. L. Moreira, and A. G. Madureira. ‘Defining Control Strategies for MicroGrids Islanded Operation’, *IEEE Transactions on Power Systems*, Vol. 21, No. 2, MAY 2006.

[82] A. Madureira, C. Moreira, and J. A. P. Lopes, “Secondary load-frequency control for microgrids in islanded operation”, *in Proc. Int. Conf. Renewable Energy Power Quality*, Spain, 2005.

[83] A. Engler, “Vorrichtung zum gleichberechtigten Parallelbetreb von einoder dreiphasigen Spannungsquellen”, German patent Nº 101 40 783. 1 (pending), European patent Nº 02018526.26 (pending), US Patent Nº. US 6,693,809 B2, Feb. 17, 2004 (granted), Japanese patent Nº. 2002-240991 (pending).

[84] G. H. Riahy, and M. Abedi, “Short term wind speed forecasting for wind turbine applications using linear prediction method,” *Renewable Energy*, vol. 33, no. 1, pp. 35-41, January 2008.

[85] R. Bellman, “Dynamic Programming and modern control theory”, Princeton Univ. Press, 1957.

[86] A. E. Bryson and Y. Ho, “Applied Optimal Control”, Hemisphere Publ. Corp., 1975.

[87] R. W. H. Sargent, and G. R. Sullivan, "The development of an efficient optimal control package", *Proceedings of the 8th IFIP Conference on Optimization Techniques*, Heidelberg, Germany, pp. 158-168, 1978.

[88] C. P. Neuman and A. Sen "A Suboptimal Control Algorithm for Constrained Problems Using Cubic Splines", *Automatica*, vol. 9, pp.601-613, 1973.

[89] H. G. Bock and K. J. Plitt, "A multiple shooting algorithm for direct solution of optimal control problems", *Proc. 9th IFAC World Congress*, Budapest, Hungary, pp .243-247, 1984.

[90] S. Galán, W.F. Feehery, P.I. Barton, “Parametric sensitivity functions for hybrid discrete/continuous systems”. *Applied Numerical Mathematics*. Vol. 31, pp. 17-47, 1999.

[91] P. I. Barton, R. J. Allgor, W. F. Feehery, and S. Galan, "Dynamic optimization in a discontinuous world", *Industrial & Engineering Chemistry Research*, vol. 37, no. 3, pp. 966-981, 1998.

[92] P.I., Barton, C. K. Lee, "Design of process operations using hybrid dynamic optimization". *Computers and Chemical Engineering*. vol. 28, no. 6-7, pp. 955-969, 2004.

[93] D. Morosan, R. Bourdais, D. Dumur, and J. Buisson, "Building temperature regulation using a distributed model predictive control," *Energy and Buildings*, vol. 42, pp. 1445-1452, 2010.

[94] M. Castilla, J. D. Álvarez, M. Berenguel, M. Pérez, F. Rodríguez, J. L. Guzmán, "Técnicas de control del confort en edificios", *Revista Iberoamericana de Automática e Informatica Industrial* 7, pages 5-24, 2010.

[95] M. Castilla, J. D. Álvarez, M. Berenguel, M. Pérez, J. L. Guzmán, F. Rodríguez, "Comfort optimization in a solar energy research center", *in: Proceedings of the IFAC Conference on Control Methodologies and Technology for Energy Efficiency*, Vilamoura, Portugal, 2010.

[96] L. Lombard, J. Ortiz, and C. Pout, "A review on buildings energy consumption information" *Energy and Buildings*, vol. 40, pp. 394-398, 2008.

[97] I. H. Yang, M. S. Yeo, and K. W. Kim, "Application of artificial neural network to predict the optimal start time for heating system in building," *Energy Conversion and Management*, vol. 44, pp. 2791-2809, 2003.

[98] S. Rosiek and F. J. Batlles, "Integration of the solar thermal energy in the construction: Analysis of the solar-assisted air-conditioning system installed in CIESOL building" *Renewable Energy*, vol. 34, pp. 1423-1431, 2009.

[99] S. Rosiek and F. J. Batlles, "Shallow geothermal energy applied to a solar-assisted air-conditioning system in southern Spain: Two-year experience" *Applied Energy*, vol. 100, pp. 267-276, 2012.

[100] M. Pasamontes, J. L. Guzmán, F. Rodríguez, M. Berenguel and E. F. Camacho, "Modelo híbrido de una planta de frío solar". *Congreso CIATEA*, Gijón, España, 2007.

[101] Lagarias, J.C., J. A. Reeds, M. H. Wright, and P. E. Wright, "Convergence Properties of the Nelder-Mead Simplex Method in Low Dimensions," *SIAM Journal of Optimization*, Volume 9 Number 1, pp. 112-147, 1998.

[102] M. Pasamontes, J. D. Álvarez, J. L. Guzmán and M. Berenguel, "Hybrid Modeling of a Solar Cooling System". *3rd IFAC Conference on Analysis and Design of Hybrid Systems*, Zaragoza, Spain, 2009.

[103] D. Zambrano, C. Bordons, W. Garcia and E. Camacho, "Model development and validation of a solar cooling plant" *International Journal of Refrigeration*, vol. 31, pp. 315-327, 2008.

[104] E. M. Kleinbach, W. A. Beckman and S. A. Klein, "Performance study of one-dimensional models for stratified thermal storage tanks", *Solar energy*, pp. 155-166, 1993.

[105] G. Grossman and M. Wilk, "Advanced modular simulation of absorption systems", *International Journal of Refrigeration*, vol. 17, pp. 231-244, 1994.

[106] D. Myers, "Solar radiation modeling and measurements for renewable energy applicaions: data and model quality", *Energy*, pp. 1517-1531, 2005.

[107] D. H. W. Li and G. H. W. Cheung, "Study of models for predicting the diffuse irradiance on inclined surfaces," *Applied Energy*, vol. 81, no. 2, pp. 170-186, 2005.

[108] A. Mellit, M. Benghanem and S. A. Kalogirou, "An adaptive wavelet network model for forecasting daily solar radiation". *Applied Energy*, vol. 83, pp. 705-722, 2006.

[109] R. Iqdour and A. Zeroual, "A rule based fuzzy model for the prediction of solar radiation". *Revue des energies renouvelables*, vol. 9, pp. 113-120, 2006.

[110] M. Chaabene, "Measurements based dynamic climate observer". *Solar Energy*, vol. 82, pp. 763-771, 2008.

[111] L. Palacin, C. de Prada, F. Tadeo, and J. Salazar, "Operation of medium-size reverse osmosis plants with optimal energy consumption," *In Proceedings of the 9th International Symposium on Dynamics and Control of Process Systems (DYCOPS '10),* pp. 841–846, Leuven: Belgium, July 2010.

[112] J. Salazar, F. Tadeo, C. de Prada and L. Palacin, "Modeling and control of MicroGrids in Island Operation" *International Renewable Energy Congress*, Sousse, Tunisia, November 5-7, 2009.

[113] A. Bemporad and M. Morari, "Control of systems integrating logic, dynamics, and constraints", *Automatica*, vol. 35, pp. 407-428, 1999.

[114] C. de Prada, I. Grossmann, D. Sarabia and S. Cristea, "A strategy for predictive control of a mixed continuous batch process". *Journal of Process Control*, vol. 19, pp. 123-137, 2009.

[115] J. M. Zamarreño, "Acceso a Datos mediante OPC", Andavira, 2010.

[116] R. H. Lasseter, A Akhil, C. Marnay, J Stephens, J. Dagle, R. Guttromson, A. Meliopoulous, R. Yinger, and J. Eto, "The CERTS microgrid concept," *White paper for Transmission Reliability Program, Office of Power Technologies*, U.S. Department of Energy, 2002.

[117] H. Chen, T. N. Conga, W. Yang, C. Tan, Y. Li and Y. Ding, "Progress in electrical energy storage system: A critical review", *Progress in Natural Science*, vol. 19, no. 3, pp. 291-312, 2009.

[118] O. Ulleberg, "The importance of control strategies in PV–hydrogen systems", *Solar Energy*, vol. 76, no. 1, pp. 323-329, 2004.

[119] L. Valverde, C. Bordons and F. Rosa, "Power Management using Model Predictive Control in a hydrogen-based microgrid", *38th Annual Conference of the IEEE Industrial Electronics Society (IECON)*, Montreal, Canada, 2012.

[120] L. Valverde, F. Rosa, C. Bordons, "Design, planning and management of a hydrogen-based microgrid", *IEEE Transactions on Industrial Informatics*, vol. 9, no. 3, 2013.

[121] C. Wang, M. H. Nehrir and S. R. Shaw, "Dynamic models and model validation for PEM fuel cells using electrical circuits". *IEEE transactions on energy conversion*, vol. 20, no. 2, pp. 442-452, 2005.

[122] O. Ulleberg, "Modeling of advanced alkaline electrolyzers: a system simulation approach". *International Journal of Hydrogen Energy*, vol. 28, pp. 21-33, 2003.

[123] Q. Srivastava, A. K. Choe and W. Gao, "Improved modeling and control of a PEM fuel cell power system for vehicles". *Proceedings of the IEEE Southeast Conference*, pp. 331-336, 2006.

[124] W. Griesshaber and F. Sick, "Simulation of Hydrogen-Oxygen-Systems with PV for the Self-Sufficient Solar House". *FhG-ISE*, Freiburg im Breisgau, German, 1991.

[125] K. Havre, P. Borg and K. Tommerberg, "Modeling and control of pressurized electrolyzer for operation in stand alone power systems". *Second Nordic Symposium on Hydrogen and Fuel Cells for Energy Storage*, Helsinki, Finland, pp. 63-78, 1995.

[126] J. Vanhanen, "On the performance improvements of small-scale photovoltaic-hydrogen energy systems". *PhD thesis*, Helsinki University of Technology, Espoo, Finland, 1996.

[127] W. Hug, J. Divisek, J. Mergel, W. Seeger and H. Steeb, "Highly efficient advanced alkaline electrolyzer for solar operation". *Int. Journal Hydrogen Energy*, vol. 17, pp. 699-705, 1992.

[128] J. Santos, F. Antunes, A. Chehab and C. Cruz. "A maximum power point tracker for PV systems using a high performance boost converter". *Solar Energy*, Volume 80, Issue 7, pages 772-778, 2006.

[129] P. Chaudhary and R. Maheshwari. "A critical Review on Photovoltaic base Maximum Power Generation System". *International Journal of Recent Technology and Engineering (IJRTE)*, Volume 1, Issue 6, January 2013.

[130] K. Bognar, P. Blechinger and F. Behrendt. "Seawater desalination in micro grids: an integrated planning approach". *Energy, Sustainability and Society*, Volume 2, 2012.

[131] N. M'Sirdi, A. Belhani and A. Naamane. "Battery Models for Estimation of State of Charge by Sliding Mode Observer", *Sustainability in Energy and Buildings*, Volume 12, pages 133-149, 2012.

[132] J. A. Ritter, A. D. Ebner, J. Wang, R. Zidan, "Implementing a Hydrogen Economy," *Materials Today*, vol. 6, pp. 18-23, 2003.

[133] V. Güther and A. Otto, "Recent developments in hydrogen storage applications based on metal hydrides", *Journal of Alloys and Compounds*, vol. 293-295, pp. 889-892, 1999.

[134] S. Levesque, M. Ciureanu, R. Roberge and T. Motyka, "Hydrogen storage for fuel cell systems with stationary applications. Transient measurement technique for packed bed evaluation", *International Journal of. Hydrogen Energy*, vol. 25, pp. 1095-1105, 2000.

[135] L. K. Heung, "On-board hydrogen storage system using metal hydride, hydrogen power: theoretical and engineering solutions", *Proceedings of the HYPOTHESIS Symposium*, Grimstad, Norway, vol. 2, pp. 251-256, 1997.

[136] J. Salazar, L. Valverde, C. Bordons and F. Tadeo, "Predictive Control of a photovoltaic system with mixed battery and hydrogen storage". *39th Annual Conference of the IEEE Industrial Electronics Society (IECON)*, 2013.

[137] P. E. Wellstead and P. M. Zanker, "Application of self-tuning to engine control", Ch12 of "Self-tuning and adaptive control: theory and applications" (book, Eds: C. J. Harris ad S. A. Billings), *Instt. Of Electrical Engrs*. (1981).

[138] R. L. Morris, H. G. Hopkins and R. H. Borcherts, "An identification approach to throttle torque modeling", *Soc. Of Automotive Engrs*., paper # 810448.

[139] T. I. Mina, "A detailed study of the start and run-up behavior of a multi-cylinder direct injection diesel engine", *Insst. Of Mech. Engrs. Paper* # C372/011, 1989.

[140] Paul C. Krause, Analysis of Electric Machinery, McGrawHill, 1987.

[141] P. Kundur, "Power System Stability and Control", McGraw-Hill, Inc.

[142] S. Haddad and N. Watson, "Principles and Perfomance in Diesel Engineering", Chichester [West Sussex]: Ellis Horwood, 1984.

[143] Y. W. Choe and B. G. Jung, "An H∞ controller design for the speed control of large size and low speed diesel engine," *Proceedings of the SICE Annual Conference*, pp. 747-752, 1994.

[144] Bo Kuang, Youyi Wang, Yoke Lin Tan, "An H∞ controller design for Diesel Engine System", IEEE *Transactions on Energy Conversion*. 2000.

[145] S. Roy, O. P. Malik and G. S. Hope, "A Low Order Computer Model for Adaptive Speed Control of Diesel Driven Power-Plants*", IEEE Transactions on Energy Conversion*. 1991.

[146] Yasser Yacoub, "Mean Value Modeling and Control of A Diesel Engine Using Neural Networks", *Ph.D. Dissertation*, West Verginia University, 1999.

[147] Schaefer Richard and Kiyong Kim. "Excitation control of the synchronous generator", *IEEE Industry Applications Magazine*, March-April 2001.